UNIVERSIDADE DE LISBOA
INSTITUTO SUPERIOR TÉCNICO

Modeling Radiation Injury and Countermeasure Drug Responses in a Human Intestine Chip

Sasan Jalili Firoozinezhad

Supervisor: Doctor Joaquim Manuel Sampaio Cabral
Supervisor: Doctor Donald E. Ingber

Thesis approved in public session to obtain the PhD Degree in
Bioengineering

Jury final classification: Pass with Distinction

2019

TÉCNICO LISBOA

UNIVERSIDADE DE LISBOA
INSTITUTO SUPERIOR TÉCNICO

Modeling Radiation Injury and Countermeasure Drug Responses in a Human Intestine Chip

Sasan Jalili Firoozinezhad

Supervisor: Doctor Joaquim Manuel Sampaio Cabral
Supervisor: Doctor Donald E. Ingber

Thesis approved in public session to obtain the PhD Degree in
Bioengineering

Jury final classification: Pass with Distinction

Jury

Chairperson: Doctor Duarte Miguel de França Teixeira dos Prazeres, Instituto Superior Técnico, Universidade de Lisboa

Members of the Committee:

Doctor Pedro Miguel Ribeiro Viana Baptista, Faculdade de Ciência e Tecnologia Universidade Nova de Lisboa
Doctor Joaquim Manuel Sampaio Cabral, Instituto Superior Técnico, Universidade de Lisboa
Doctor Lino da Silva Ferreira, Faculdade de Medicina, Universidade de Coimbra
Doctor Maria Margarida Fonseca Rodrigues Diogo, Instituto Superior Técnico, Universidade de Lisboa
Doctor Tiago Paulo Gonçalves Pinheiro Fernandes, Instituto Superior Técnico, Universidade de Lisboa

Funding Institution - Fundação para a Ciência e a Tecnologia

2019

This PhD thesis has been done in collaboration with the Wyss Institute for Biologically Inspired Engineering at Harvard University

“There are no incurable diseases — only the lack of will.
There are no worthless herbs — only the lack of knowledge”

Avicenna (c. 980—1037)

Resumo

A exposição a radição-γ ionizante, seja terapêutica ou acidental, pode resultar no síndroma de radiação aguda, que está associada a perturbações gastro-intestinais fatais. Ao utilizer o modelo Chip de intestino humano, simulamos uma lesão por radição induzida do intestino e validamos um fármaco potencialmente profilático como contra-medida, a dimetiloxaloilglicina (DMOG). Confirmamos que a DMOG reduz significativamente a apoptose, a permeabilidade intestinal, a rutura de ligamentos e a lesão dos microvilos das células epiteliais intestinais, assim como a geração de ROS e a degradação lipídica em ambos endotélio e epitélio intestinais. Como o microbioma comensal está presente no microambiente intestinal, deverá ter um papel central na toxicidade por radiação intestinal *in vivo*, desenvolvemos métodos de co-cultura de epitélio intestinal humano *vivo* nos Chips intestinais, em contacto directo com as comunidades aeróbica e anaeróbica da microbiota, em condições de gradientes de hipóxia semelhantes aos que se observam *in vivo*. O modelo desenvolvido recapitula com precisão os comportamentos *in vivo*, incluindo a manutenção de bactérias anaeróbicas obrigatórias com rácios entre Firmicutes e Bacteroidetes, semelhantes aos observados nas fezes humanas. O modelo do Chip instestinal humano, compreendido por epitélio, endotélio e microbioma intestinal humano pode servir para descobrir ligações funcionais entre as células epiteliais e bactérias intestinais para compreender os mecanismos da lesão humana por radiação, para descobrir novas contra-medidas terapêuticas e para o avanço da medicina personalizada

Palavras-chave: Radição, Intestino, Organ-on-a-Chip, Microbioma, Descoberta de Farmacos

Abstract

Exposure to ionizing γ-radiation, whether therapeutic or accidental, may result in acute radiation syndrome that is associated with potentially life-threatening gastrointestinal disturbances. Using human Intestine Chip model, we simulated radiation-induced intestinal injury and validated a potential prophylactic radiation countermeasure drug, dimethyloxaloylglycine (DMOG). We confirmed that DMOG significantly reduced apoptosis, intestinal permeability, disruption of tight junctions and microvillus injury of intestinal epithelial cells, as well as ROS generation and lipid degradation in both endothelium and intestinal epithelium. Since commensal microbiome that are present within the intestinal microenvironment are believed to play a pivotal role in intestinal radiation toxicity *in vivo*, we developed methods to co-culture of living human intestinal epithelium in Intestine Chips in direct contact with stable communities of aerobic and anaerobic microbiota derived from human stool specimens under a hypoxia gradient similar to that observed *in vivo*. Our model accurately recapitulates *in vivo* behaviors, including the maintenance of an abundance of obligate anaerobic bacteria with ratios of Firmicutes and Bacteroidetes similar to those observed in human feces. The human Intestine Chip model, comprising human intestinal epithelium, endothelium and complex microbiome, could be served to unravel functional links between intestinal epithelial cells and gut microbes to understand mechanisms of human radiation disease, discover new MCMs, and advance personalized medicine in future.

Keywords: Radiation, Intestine, Organ-on-a-Chip, Microbiome, Drug discovery

Acknowledgements

Undertaking this PhD has been a truly life-changing experience for me and it would not have been possible to do without the support and guidance that I received from many people.

Firstly, I would like to express my sincere gratitude to my advisors Prof. Donald E. Ingber and Prof. Joaquim M. S. Cabral for their continuous support during these past 4 years. Special thanks to Don for giving me the opportunity to work at his lab at the Wyss Institute. I appreciate all his contributions of time, ideas, and funding to make my Ph.D. experience productive and stimulating. Joaquim has been supportive throughout my PhD project, specially for helping me to obtain the Portugal Science Foundation (FCT) fellowship, encouraging and supporting me to pursue my research at the Wyss Institute as well as insightful discussion throughout my PhD project.

My special words of thanks should also go to my research co-guides Dr. Rachelle Prantil-Baun and Dr. Oren Levy for their continuous support, guidance, cooperation and encouragement. Their constant motivation and support have always kept me going ahead. I owe a lot of gratitude to them for always being there for me and I feel privileged to be associated with people like them during my life.

The members of the Ingber group have contributed immensely to my personal and professional time at the Wyss. The group has been a source of friendships as well as good advice and collaboration. A sincere thanks goes to Dr. Amir Bein and Dr. Amy Wen for their continuous encouragement, support, brainstorming and absolute best friendship. I thank my fellow labmates at the Wyss: Amanda Jiang, David Chou, Vik Frismantas, Yuka Milton, Cicely Fadel, Ben Swenor, Vadika Mishra, Pawan Jolly, Diogo

Camacho, Alessio Tovaglieri, Elizabeth Calamari, Olivier Henry, Bret Nestor, Alexandra Sontheimer-Phelps, Ratnakar Potla, Raquel Cunha, Tony Cao, Longlong Si, Mariko Kobayashi, Anna Herland, Zohreh Izadifar, Girija Gayol, Ben Seiler, Jonathan Sabate Del Rio, Tae-Eun Park, Carlos Ng, Youngjae Choe, Nur Mustafaoglu and Bryan Hassel.

I am also grateful to Dr. James Weaver and Dr. Thomas Ferrante for their expert technical advice and assistance with imaging.

I would like to thank Dr. Cláudia Canelas Miranda for helping me with the extended abstract in Portuguese of the thesis.

I would also like to thank my committee members, Dr. Tigao P. G. Fernandes and Dr. Maria Margarida Diogo for serving as my committee members and for their encouragement and insightful comments and questions.

I greatly appreciate the support received through the collaborative work with Dr. David Breault's lab at Boston Children's Hospital.

I would also like to say a heartfelt thank you to my amazing friend, Dr. Mozhdeh Sojoodi, for unconditional support throughout my PhD studies, and to my Mom, Dad, my beloved siblings, Parisa and Payam, and my new family members, Farid and Maryam, for always believing in me and encouraging me to follow my dreams.

Index

Resumo I
Abstract II
Acknowledgements III
Index V
List of Figures VII
List of Abbreviations VIII
List of Publications and Awards IX
Chapter 1. Theoretical Background 1
Introduction 3
Microfluidic intestine chip models 6
Mechanically active intestine chips 7
Human primary intestine models 9
Gastrointestinal human-microbe interface on chip 12
Disease models using human intestine chips 15
Modeling radiation injury using human intestine chip 17
Conclusions 20
References 21
Chapter 2. Modeling radiation injury-induced cell death and countermeasure drug responses in a human Gut-on-a-Chip 27
Introduction 29
Results 31
Establishing a human gut radiation injury model in vitro 31
Recapitulating intestinal organ-level radiation-induced injury 38
Endothelial cells as mediators of radiation damage 41
Radio-protective effects of a potential radiation countermeasure drug 44
Discussion 44
Methods 49
References 57

Supplementary Information 62
Chapter 3. Modeling radiation injury in a primary human Small Intestine-on-a-Chip 67
Introduction 68
Results 71
Establishing a primary human Intestine Chip 71
Incorporation of intestinal endothelial cells 75
Recapitulating intestinal radiation-induced injury on Intestine Chip 81
Discussion 85
Methods 88
References 94
Supplementary Information 100
Chapter 4. A complex human gut microbiome cultured in an anaerobic intestine-on-a-chip 102
Introduction 104
Results 107
Establishing an oxygen gradient across the lumen of the Intestine Chip 108
Co-culture of human intestinal epithelium with an obligate anaerobe on-chip 112
A mucus layer separates the commensal microbes from the epithelium 113
Sustaining a complex human intestinal microbiome in vitro 114
Culture of fresh gut microbiome with primary intestinal epithelium on-chip 125
Discussion 128
Methods 134
References 146
Supplementary Information 154
Chapter 5. Conclusions and Future Directions 170

List of Figures

Figure I-1. The mechanically active human Gut Chip 8
Figure I-2. Evolution of host-microbiome in vitro models 12
Figure I-3. Personalized-medicine approach using human Intestine Chip 16
Figure II-1. Human Gut Chip microfluidic culture device 32
Figure II-2. Radiation-induced apoptosis and cytotoxicity in intestinal epithelium and vascular endothelium, and radio-protective effects of DMOG 34
Figure II-3. Radiation-induced changes in ROS, lipid peroxidation and DNA fragmentation in the presence or absence of DMOG treatment 36
Figure II-4. Morphological analysis of intestinal villus damage induced by radiation exposure 38
Figure II-5. Radiation-induced loss of junctional continuity and mucosal damage and the effects of DMOG pre-treatment 40
Figure II-6. Vascular endothelium mediates the radiation damage 42
Figure III-1. Fabrication of the primary human Intestine Chip 72
Figure III-2. Morphological analysis of Organ Chips lined by primary duodenal organoid-derived epithelial cells in the absence of endothelial cells 74
Figure III-3. Establishment of the primary human intestinal epithelium in the Organ Chip in the presence or absence intestine-specific microvascular endothelium 79
Figure III-5. The primary human Intestine Chip exhibits multi-lineage differentiation 81
Figure III-6. Recapitulating intestinal radiation-induced injury on Intestine Chip 83
Figure IV-1. Oxygen sensitive human Intestine Chip microfluidic culture device 109
Figure IV-2. Co-culture of human intestinal epithelium and obligate anaerobe, Bacteroides fragilis, on-chip 115
Figure IV-3. Analysis of the diversity and relative abundance of microbiota co-cultured in Intestine Chips under aerobic and aerobic conditions 118
Figure IV-4. Anaerobic conditions in the Intestine Chip enhance the growth of multiple genera compared to the aerobic chip and conventional liquid culture 123
Figure IV-5. Anaerobic co-culture of gut microbiome obtained from fresh human patient-derived stool with primary human ileal epithelium in the Intestine Chip 126

List of Abbreviations

2D	two-dimensional
3D	three-dimensional
B. fragilis	*bacteroides fragilis*
DIC	differential interference contrast
DM	differentiation medium
DMEM	dulbecco's modified eagle medium
DMOG	dimethyloxyallylglycine
DSB	double-strand breaks
ECM	extracellular Matrix
EGF	epidermal growth factor
EM	expansion medium
GI	gastrointestinal
Gut Chip	Gut-on-a-Chip
HADA	HCC-amino-D-alanine
HIF	hypoxia-inducible factors
HIMEC	human intestinal microvascular endothelial cells
Hmb	human microbiome
HMI	human-microbiota interaction
HUVEC	human umbilical vein endothelial cell
IBD	inflammatory bowel disease
ICAM	intercellular adhesion molecule
IL	interleukin
Intestine Chip	Intestine-on-a-Chip
iPS	induced pluripotent stem
LDH	lactate dehydrogenase
LGG	*Lactobacillus rhamnosus* GG
LGR5	leucine-rich-repeat-containing G-protein-coupled receptor 5
LPO	lipid peroxidation
LPS	lipopolysaccharide
M-SHIME	mucosal-simulator of the human intestinal microbial ecosystem
MCMs	medical countermeasures
NICU	newborn intensive care unit
OTU	operational taxonomic units
PBMC	peripheral blood mononuclear cell
PDMS	polydimethylsiloxane
PFA	paraformaldehyde
Pk/PD	pharmacokinetic/pharmacodynamic
ROS	reactive oxygen species
SEM	scanning electron microscopic
SIBO	small intestinal bacterial overgrowth
SYP	synaptophysin
TNF	tumor necrosis factor
TUNEL	terminal deoxynucleotidyl transferase-mediated dUTP-biotin nick-end labeling
VE	vascular endothelium
WGA	Wheat Germ Agglutinin
ZO-1	zonula occludens-1

List of publications and Awards

Journal papers:

J1. **S. Jalili-Firoozinezhad**, F. S. Gazzaniga, E. L. Calamari, D. M. Camacho, C. W. Fadel, A. Bein, B. Swenor, B. Nestor, M. J. Cronce, A. Tovaglieri, O. Levy, K. E. Gregory, D. T. Breault, J. M. S. Cabral, D. L. Kasper, R.Novak, and D. E. Ingber. "Complex human gut microbiome cultured in anaerobic human intestine chips". *Nature BME*, (2019).

J2. **S. Jalili-Firoozinezhad**, R. Prantil-Baun, A. Jiang, R. Potla, T. Mammoto, J. C. Weaver, T. C. Ferrante, H. J. Kim, J. M.S. Cabral, O. Levy, D. E. Ingber. "Modeling radiation injury-induced cell death and countermeasure drug responses in a human Gut-on-a-Chip". *Nature-Cell Death & Disease*, 9, 2, 223 (2018).

- **Featured in Harvard Gazette, Nature-BMC, Wyss Newsletter, etc.**

J3. A. Herland , B. Maoz , D. Das , M. Somayaji , R. Prantil-Baun , R. Novak , M. Cronce , T. Huffstater , S. Jeanty , M. Ingram , A. Chalkiadaki , D. Chou , S. Clauson , A. Delahanty , **S. Jalili-Firoozinezhad** , Y. Milton , A. Sontheimer-Phelps , B. Swenor , O. Levy , K. Parker , A. Przekwas and D. E. Ingber, "Quantitative prediction of human drug pharmacokinetic responses enabled by fluidically coupled vascularized organ chips" (2019). [Under review]

J4. A. Tovaglieri, A. Sontheimer-Phelps, A. Geirnaert, R. Prantil-Baun, D. M. Camacho, D. B. Chou, **S. Jalili-Firoozinezhad**, T. de Wouters, M. Kasendra, M. Super, M. Cartwright, C. A. Richmond, D. T. Breault, C. Lacroix, D. E. Ingber. "Species-specific enhancement of enterohemorrhagic E. Coli pathogenesis mediated by microbiome metabolites". *Microbiome* , 7, 43 (2019).

J5. D. B. Chou, V. Frismantas, Y. Milton, R. David, P. Pop-Damkov, D. Ferguson, A. MacDonald, O. V. Bolukbasi, C. E. Joyce, L. S. Moreira Teixeira, A. Rech, A. Jiang, E. Calamari, **S. Jalili-Firoozinezhad** … D. E. Ingber. "Human bone marrow disorders recapitulated in vitro using organ chip technology". *bioRxiv*, 458935 (2018).

- The manuscript is currently under review

J6. R. Novak, Meredyth Didier, E. Calamari, C. F. Ng, Y. Choe, S. L. Clauson, B. A. Nestor, J. Puerta, R. Fleming, **S. Jalili-Firoozinezhad**, D. E. Ingber. "Scalable Fabrication of Stretchable, Dual Channel, Microfluidic Organ Chips". *JoVE (Journal of Visualized Experiments)*, 140, e58151-e58151 (2018).

J7. A. Bein[#], W. Shin[#], **S. Jalili-Firoozinezhad**, M. H. Park, A. Sontheimer-Phelps, A. Tovaglieri, A. Chalkiadaki, H. J. Kim, D. E. Ingber. "Microfluidic Organ-on-a-Chip Models of Human Intestine". *Cellular and molecular gastroenterology and hepatology (CMGH)*, 5, 4, 659-668 (2018).

J8. M. Kasendra[#], A. Tovaglieri[#], A. Sontheimer-Phelps, **S. Jalili-Firoozinezhad**, A. Bein, A. Chalkiadaki, W. Scholl, C. Zhang, H. Rickner, C. A. Richmond, H. Li, D. T. Breault, D. E. Ingber. "Development of a primary human Small Intestine-on-a-Chip using biopsy-derived organoids". *Scientific Reports*, 8, 1, 2871 (2018).

Conference papers:

C1. **S. Jalili-Firoozinezhad**, F. S. Gazzaniga, E. L. Calamari, D. M. Camacho, C. W. Fadel, A. Bein, B. Swenor, B. Nestor, A. Tovaglieri, O. Levy, K. E. Gregory, D. T. Breault, J. M. S. Cabral, D. L. Kasper, R.Novak, and D. E. Ingber. " Modeling the gut-microbiome interface in anaerobic human intestine chips". *New England Science Symposium*, Boston, USA (April 2019). [Podium/Poster]

C2. **S. Jalili-Firoozinezhad**, Y. Milton, V. Frismantas, D. Chou, A. M. Wen, L. M. Teixeira, A. Rech, A. Jiang, O. Levy, R. Prantil-Baun, D. E. Ingber, "Organs-on-Chip as Tools for Evaluating Space Radiation Countermeasures", Space Genetics Symposium, Boston, USA (Nov 2018). [*Podium*]

C3. **S. Jalili-Firoozinezhad**, "Modeling radiation injury and countermeasure drug responses in a human Intestine Chip", Lush Prize Conference, Berlin, Germany (Nov 2018). [*Invited speaker-Podium*]

C4. **S. Jalili-Firoozinezhad**, F S Gazzaniga, E. L. Calamari, D.M. Camacho, C. W. Fadel, B. Nestor, M. J. Cronce, A. Tovaglieri, O. Levy, K. E. Gregory, D. T. Breault, D. L. Kasper, R. Novak, J. M. S. Cabral and D. E. Ingber, "Direct co-culture of complex human gut microbiome with living human intestinal epithelium in anaerobic human intestine chips", Harvard Probiotics Symposium, Boston, USA (Oct 2018) [*Poster*]

C5. **S. Jalili-Firoozinezhad**, R. Prantil-Baun, A. Jiang, T. Mammoto, H. J. Kim, O. Levy, J. M. S. Cabral, D. E. Ingber. "Modeling radiation injury and countermeasure drug responses in a primary human Intestine Chip", American Association for Cancer Research (AACR), Washington D.C., USA (Sep 2018). [*Poster*]

List of Awards:

A1. Lush Prize 2018, Young Researcher Americas (Nov 2018)

A2. First Prize, Ruth and William Silen, M.D. Award for Exceptional Scientific Poster (Apr 2019)

I. Chapter 1

Theoretical Background

This chapter is based on the articles:

1) A. Bein[#], W. Shin[#], **S. Jalili-Firoozinezhad**, M. H. Park, A. Sontheimer-Phelps, A. Tovaglieri, A. Chalkiadaki, H. J. Kim, D. E. Ingber. "Microfluidic Organ-on-a-Chip Models of Human Intestine". *Cellular and molecular gastroenterology and hepatology (CMGH)*, 5, 4, 659-668 (2018).

2) **S. Jalili-Firoozinezhad et al.** " Modeling radiation injuries using human Organs-on-Chips". *In preparation.*

Introduction

The major organ function of the human intestine is to carry out digestion, absorption, secretion, and motility, in addition to establishing a protective epithelial barrier between this digestive environment and our body[1]. In addition, intestines regulate systemic physiology by metabolizing drugs; communicate with other organs, such as the liver [2,3] and pancreas[4], via portal flow; and they contain an enteric nervous system that forms a part of the gut-brain axis[5,6]. The intestine is also the major site at which commensal microbes of the gut microbiome play a crucial role in the regulation of health and disease[7,8]. The gut microbiota is essential for modulating the immune system, controlling drug metabolism, nutrient digestion, and for protection against infections. However, microbial community imbalance can adversely orchestrate host physiology during various disorders such as inflammatory bowel disease, colorectal cancer, diabetes, radiation enteropathy, hepatic steatosis, obesity, and rheumatoid arthritis[9,10]. Thus, the establishment and preservation of balanced host-intestinal microbiota crosstalk are key requirements for maintaining gut homeostasis. Although preclinical animal models have been instrumental in reflecting host-microbe crosstalk and unveiling pathophysiological events underlying some diseases, they often fail to represent complex human host-gut microbiome interactions[11]. Thus, analysis of gut-microbiome interactions with human intestinal cells has been limited to genetic or metagenomics analysis because it has not been possible to co-culture these microbes with living epithelium for more than a day using conventional culture models or even more sophisticated intestinal organoid cultures. Therefore, there have been great efforts to

develop experimental *in vitro* or *ex vivo* models of human intestine that permit analysis of intestinal pathophysiology both in the presence and absence of living microbiome.

The most common *in vitro* intestine models used to study barrier function or model drug absorption involve culturing an established human intestinal epithelial cell line (*e.g.*, Caco-2 or HT-29 cells) on extracellular matrix (ECM)-coated, porous membranes within Transwell insert culture devices[12,13]. While these models are most commonly used by the pharmaceutical industry, this two-dimensional (2D) culture format fails to recapitulate physiological 3D intestinal cell and tissue morphology or reestablish other key intestinal differentiated functions (*e.g.*, mucus production, villi formation, cytochrome P450-based drug metabolism)[14,15]. These conventional static models also cannot support the co-culture of commensal microbiome with human intestinal cells, which we know are critical for gut physiology[14], because the bacteria will rapidly overgrow and contaminate the human cell cultures within a day. Several *ex vivo* models, such as the everted sac or the Ussing chamber have been developed for drug transport assays; however, their expected lifespan (<8 hours) is not sufficient to enable many studies on normal intestinal physiology, develop intestinal disease models, or study clinically relevant host-microbiome crosstalk[16–18].

Emergence of tridimensional organoid models has raised hopes for various applications including human-specific drug testing and regenerative medicine. Through resembling the microenvironmental traits cells experiencing *in vivo*, organoid systems can overcome the conventional *in vitro*/*ex vivo* models' challenges in translating therapies from cellular and animal level to humans. Despite many merits, organoid models share some major challenges, which limits their basic and clinical research applications if they

are not addressed properly. Developing robust, safe and reproducible organoid systems within more defined environments is not easily achievable. While organs are subject to various mechanical forces *in vivo*, which regulate their 3D organization, maturation and function, residing cells in organoids are less likely exposed to organ-relevant mechanical cues[19]. Moreover, lacking immune cells and vasculature along with issues in oxygen and nutrient availability are further roadblocks in recapitulating normal human intestinal functions and long-term growth of the organoids[20,21].

In light of the recent progress in microfluidic organ-on-chip systems, many of the organoid-associated challenges could be addressed in a more physiologically relevant approach. Recent advances with intestinal organoid models confirm the importance of mechanical signals transferred via matrices in modulating the phenotype and directing the differentiation of primary intestine cells.[22] Having fluid shear stresses to exert proper biophysical signals, and medium flow to facilitate nutrient and oxygen adsorption, miniaturized bioreactor technologies have shown great promise in organoids culture.[23] Interestingly, organ-on-chip platforms are not only work as a micro-bioreactor to provide characteristic mechanical cues (*e.g.* cyclic stretch, compression, shear), but also capable of delivering biochemical signals (*e.g.* morphogens, hormonal signals) in a highly controlled, systematic manner.[24] Finally, organ-on-chip microdevices can host different organ-specific cell types, such as endothelial and immune cells, at the vicinity of the primary epithelium/organoids and thus, reconstitute tissue-tissue interfaces and vascular perfusion.[25] Microfluidic organ-on-chips possess number of features at once and has a great potential to be harnessed for culturing primary intestinal cells. Below we describe how microfluidic Intestine Chips offer new capabilities not possible with

conventional culture systems or organoid cultures, including the ability to analyze contributions of individual cellular, chemical, and physical control parameters one-at-a-time; to co-culture human intestinal cells with commensal microbiome for extended times; and to create human-relevant disease models.

Microfluidic intestine chip models

Microfluidic devices containing hollow microchannels less than 1 mm in diameter support laminar fluid flow and control of nano- to micro-liter scale fluid volumes, and thus, they are amenable to use for culture of living cells. By using a syringe or a peristaltic pump, culture medium may be perfused at desired flow rates through each microchannel which can mimic the dynamic ranges of fluid flows and associated shear stresses on the cell surface that are observed in the human intestinal lumen, as well as in the blood capillaries[26,27]. This fluidic control also enables delivery of nutrients, growth factors, drug compounds, or even toxins to the intestinal epithelium grown on the microfluidic channels in a highly regulated spatiotemporal manner.

One simple Intestine Chip model is a single-channel system which is lined with an intestinal cell line on an ECM-coated surface within a channel that is continuously perfused with culture medium[28]. This type of device has been used to study pharmacokinetic/pharmacodynamic (PK/PD) modeling of drug compounds *in vitro*; however, a single-microchannel device does not provide access to the basolateral surface of the epithelium and so it does not permit studies on drug permeability or barrier function. Intestinal epithelial cells cultured in these devices also commonly grow as planar monolayers composed of flattened epithelial cells, and thus, they do not

faithfully mimic either the columnar shape of intestinal epithelial cells or the villus tissue architecture observed in living intestine.

A more complex microfluidic device was created that contains two hollow channels separated by a common porous, ECM-coated polyester or polycarbonate membrane, which had immortalized human intestinal epithelial cells cultured on one of its surfaces[29]. The epithelial monolayer formed in this device could be probed from both the apical and basal sides of the epithelium, and this enabled quantification of tight junction barrier function[30] as well as absorption of nutrients[31] and drugs[29]. However, the cells were seeded at a low density in this study and they were perfused only through the apical channel; as a result, the monolayer of the immortalized intestinal cells could only be cultured for a limited time (<5 days).

To better mimic the 3D form on human intestine using cell monolayers cultured under microfluidic flow, micromolding methods have been used to form polymeric adhesive scaffolds (*e.g.* Ca-alginate or collagen gel)[32,33] into villus-shaped structures[34]. Culturing human Caco-2 intestinal epithelial cells on these crenulated surfaces was shown to promote formation of a similarly crenulated epithelium, and this was accompanied by increased absorption of drug compounds and improved cellular metabolic enzyme cytochrome P450 activity in response to apical fluid shear stress[34]. However, this design did not enable analysis of intestinal barrier function because the solid polymer material blocked the abluminal surface of the epithelium.

Mechanically active intestine chips. A more sophisticated, microfluidic 2-channel Caco-2 Intestine Chip model has been developed that enables human intestinal epithelium, capillary endothelium, immune cells, and even commensal microbial cells to

grow, coexist, and interact while experiencing physiologically relevant fluid flow and peristalsis-like mechanical deformations *in vitro*[35]. The Intestine Chip is made of a flexible, gas-permeable, silicone polymer (polydimethylsiloxane, PDMS) that is crystal clear so that it allows high-resolution imaging by phase contrast, differential interference contrast (DIC), or immunofluorescence confocal microscopy. It contains two parallel microchannels (each less than 1 mm wide) separated by a thin (~20 μm), ECM-coated, flexible, porous PDMS membrane, and it is surrounded on both sides by hollow, full height, side chambers[14,35,36] (**Fig. 1A**). Intestinal epithelial cells are cultured on the top surface of the membrane within the upper 'parenchymal' channel, and microvascular endothelial cells are grown on the lower surface of the same membrane within the lower 'vascular' channel to recreate the intestinal tissue-tissue interface. Importantly, pneumatic application of cyclic suction to the hollow side chambers results in outward deformation of the vertical side walls and attached horizontal ECM-coated membrane with the adherent cell layers, thereby mimicking cyclic mechanical deformations similar to those experienced by the intestinal tissues during peristalsis (**Fig. 1A**). Under these physiological conditions, human Caco-2 intestinal epithelial cells, which characteristically grow as flattened cells within a planar monolayer in conventional 2D cultures, spontaneously undergo villus morphogenesis inside this mechanically dynamic Intestine Chip[15] (**Fig. 1B**). The microengineered villi are lined by all four lineages of differentiated small intestinal cells (absorptive, goblet, enteroendocrine, and Paneth) which exhibit columnar cell morphology similar to that observed in the living intestine[15]. Intestinal villus morphogenesis on-chip is also accompanied by establishment of a crypt-villus axis, including restriction of proliferative cells to the basal crypts and their

upward migration, drug metabolizing activity, mucus production, and glucose reuptake[15].

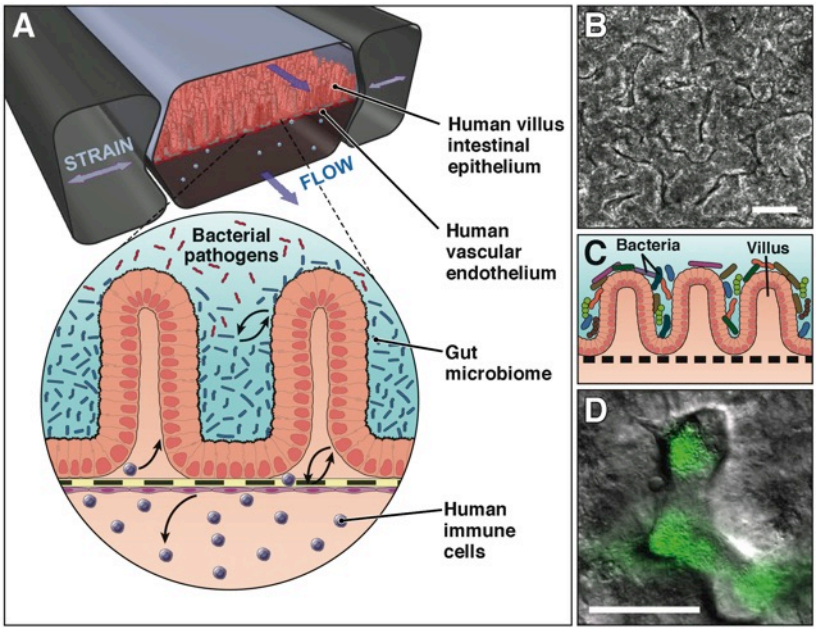

Figure I-1. The mechanically active human Gut Chip. (**A**) Human villus intestinal epithelium and vascular endothelium are lined on opposite sides of a flexible porous membrane under fluid flows and peristalsis-like strains. A zoom-in schematic shows the intestinal microenvironment undergoing complex crosstalk between commensal gut microbiome, bacterial pathogens, and immune cells in parenchymal and vascular channels, respectively. (**B**) Villus morphogenesis of human Caco-2 intestinal epithelium in the Intestine Chip under physiologically controlled motions and flow. (**C**) Schematic showing the gut-microbiome interface on human Intestine Chip. (**D**) An overlaid image of the co-culture of green fluorescent protein–labeled Escherichia coli and microengineered villi in the Intestine Chip. Bars = 50 μm. Figure was adapted from Reference 43.

Human primary intestine models. Although Caco-2 Intestine Chip recreated the villus epithelium of normal intestine and enabled new insights into how flow and cyclic peristalsis affects intestinal differentiation and function, it could not be used to study processes that relied on normal intestinal cells from individual donors, which, for example, is crucial for studying patient-specific responses for personalized medicine. While it had been technically challenging to culture primary human intestinal epithelial cells, intestinal 3D organoid cultures derived from either intestinal crypts containing endogenous intestine cells or from induced pluripotent stem (iPS) cells have

revolutionized the field by maintaining stem cell niches and supporting differentiation of various differentiated intestinal epithelial cell subtypes *in vitro*. When cultured within an 3D ECM gel in medium containing Wnt, R-spondin, noggin, and other growth factors, small intestinal organoids ('enteroids') also spontaneously undergo villus-crypt morphological organization and intestinal histogenesis[37]. Each organoid line derived from an intestinal tissue biopsy of an individual patient can be grown, frozen, and revived for multiple reuses, which can potentially be used to establish biobanks[38,39] as well as develop multiplexed screening platforms for validating new drug candidates and to advance personalized medicine[40]. However, organoids are also limited in that they lack other supporting cell and tissue types found within the living intestine, such as endothelium-lined blood vessels and immune cells, which are important for drug transport, pharmacokinetic (PK) analysis as well as disease modeling. They also do not experience fluid flows and cyclic mechanical deformations similar to those experienced in a peristalsing intestine that contribute significantly to intestinal health and function. Furthermore, because each enteroid forms a closed lumen when cultured within surrounding ECM gel, it is experimentally difficult to sample or manipulate luminal components (*e.g.* microbial cells, nutrients, drugs, or toxins). This structure also significantly limits researchers' ability to study many critical intestinal functions (*e.g.*, absorption, drug PK, or drug metabolism), in addition to critical host-microbiome interactions[41].

These challenges have recently been overcome by the development of human primary Intestine Chip. While organoid approach are leveraged to isolate intestinal stem cells from human biopsies, they could be fragmented and seeded into the "epithelial"

channels of the microfluidic organ chips where they spontaneously form intestinal villi oriented towards the channel lumen, and the epithelium in close apposition to human intestinal microvascular endothelium. The epithelium's maturation into a villus intestinal epithelium with long finger-like extensions was helped along by co-culturing human intestinal microvascular endothelial cells on the opposite side of the shared matrix-coated porous membrane in the "vascular" channel where they assembled a surrogate blood vessel with a hollow lumen through which feeding medium was flowed. Along with intestinal stem cells, this system maintains the native population of differentiated nutrient-digesting and absorbing enterocytes, mucus-producing Goblet cells, hormone-secreting enteroendocrine cells, and microbiome-regulating and sensing Paneth cells[42]. This approach presents a new stepping stone for the investigation of normal and disease-related processes in a highly personalized manner, including the transport of nutrients, digestion, different intestinal disorders, and intestinal interactions with commensal microbes as well as pathogens.

Combining two of the most advanced technologies in the field of tissue engineering, *i.e.* organoid culture and Organ Chips, allows the generation of intestine tissues and organ-level structures lined by human donor-specific cells with morphology, composition, and function strongly resembling that of the duodenal region of normal small intestine. Since the primary Intestine Chip recapitulates the physical microenvironment that cells experience inside the human body, such as fluid flow and cyclic peristalsis-like stretching motions, it exhibits a genome-wide gene expression profile that comes closer to its *in vivo* counterpart than that of the same intestinal cells grown as 3D organoids. As the small intestinal microenvironment can be maintained for weeks in continuously

perfused Organ Chips, they enable both short and longer-term studies whose observations can be related back to the health and physiology of individual donors. Same approach could be applied to different regions of the intestine, such as duodenum, ileum, and colon, whose functions and disease vulnerabilities differ from one another[45].

Gastrointestinal human–microbe interface on chip. The interaction between the gut and its microbiota regulates various physiologic processes that modulate human health and disease states. To unravel the pathophysiological role of gastrointestinal human-microbiome crosstalk, representative models are a prerequisite. Experimental *in vitro* models offer alternative approaches for recreating the GI host-microbiome interface by spatiotemporal tuning of physical cues (*e.g.*, oxygen availability or pH changes), providing flexibility, scalability, controlled delivery of chemokines and therapeutic agents, and facilitating high-resolution/throughput experimentations (**Fig. 2**) [41,44]. Traditional host-microbe *in vitro* models such as centrifuge tubes or Transwell cultures are, however, limited in creating the three-dimensional (3D) architecture and differentiated barrier functions of the intestine[15,45]. More advanced models, such as organoid cultures, have shown great promise for studying host-microbiome interactions. Despite many merits, 3D organoid cultures, are limited in providing an oxygen gradient, peristalsis-like motions and vasculature interface, and also hinder long-term microbiota co-culture[40,46]. Since the Intestine Chip has continuous fluid flow, villi formation and mucus production, it is also possible to co-culture living commensal microbes (*e.g.*, Lactobacillus rhamnosus GG or the VSL#3 clinical probiotic formulation containing 8

different microbial strains) in direct contact with the intestinal epithelial cells within the lumen of the parenchymal channel for weeks *in vitro* without compromising barrier integrity or intestinal cell function[14,35] (**Fig. 1C,D**). In fact, barrier function was shown to increase when the intestinal epithelium was co-cultured with Lactobacillus rhamnosus GG. In addition, transcriptomic analyses targeting approximately 23,000 human genes revealed that the *in vivo* relevant fluid flow and physical deformations dramatically changed the gene expression profiles compared to the static Transwell cultures, and that mechanically active Intestine Chips that also contained a mixture of commensal microbes (VSL#3 probiotic formulation) showed the highest level of genetic similarity to normal human ileum.

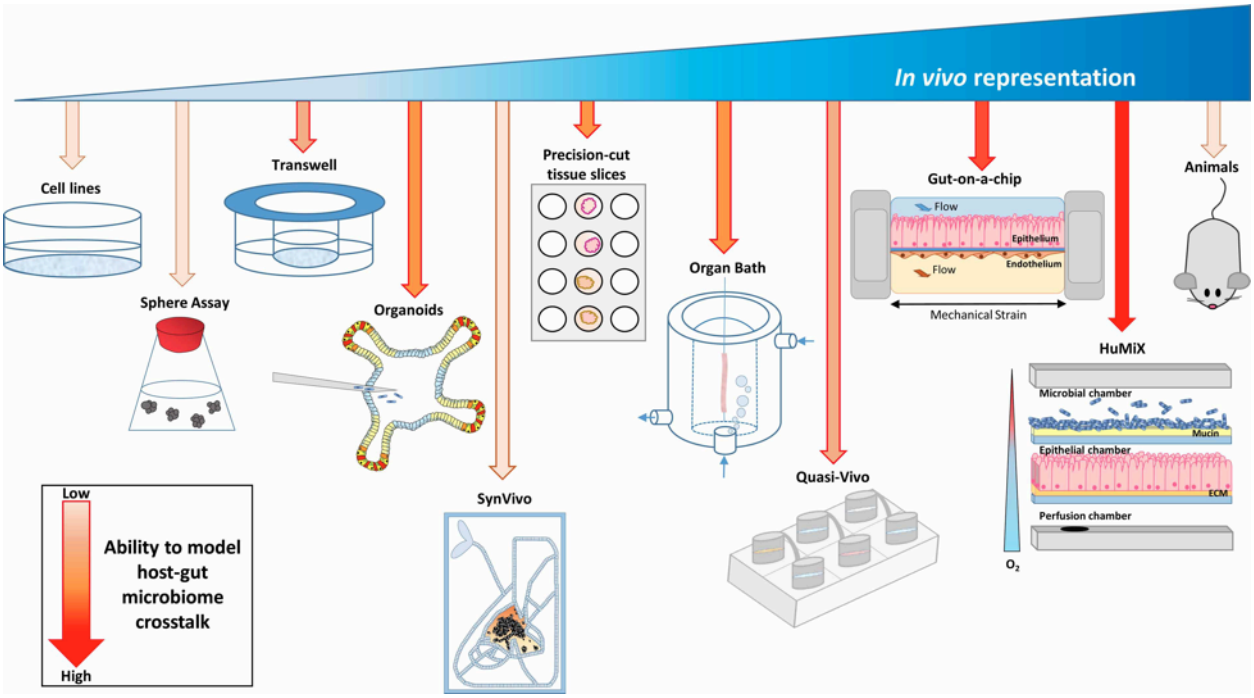

Figure I-2. Evolution of host-microbiome in vitro models. Schematic representation of conventional cell culturing techniques available and their ability to model host–microbiome interactions[44].

Indeed, the Intestine Chip was utilized to demonstrate complex immune-microbiome inflammatory interactions germane to chronic inflammatory diseases, such as inflammatory bowel disease (IBD)[35]. Addition of lipopolysaccharide (LPS) endotoxin to the luminal microchannel also was shown to induce secretion of the proinflammatory cytokines, interleukin (IL)-1β, IL-6, IL-8, and tumor necrosis factor (TNF)-α into the lower vascular channel. Moreover, this was accompanied by increased expression of intercellular adhesion molecule-1 (ICAM-1) on the endothelium, villus blunting, and compromise of intestinal barrier function, but only in the presence of white blood cells (*e.g.* peripheral blood mononuclear cells, PBMCs) that were infused through the capillary microchannel. Moreover, additional experiments confirmed that all four cytokines were required to be present at the concentrations measured within the capillary channel to induce this intestinal injury response. Interestingly, additional studies revealed that cessation of cyclic peristalsis-like mechanical motions caused an increase in bacterial overgrowth in the Intestine Chip, which closely resembled the small intestinal bacterial overgrowth (SIBO) that can result from cessation of peristalsis in patients with ileus. Thus, by being able to control flow independently of mechanical deformations, this study revealed that the past clinical assumption that SIBO results from cessation of fluid flow when peristalsis is inhibited is incorrect; instead, it is the lack of mechanical deformations that drives this bacterial overgrowth response. Thus, the innovative modularity of the microfluidic Intestine Chip (**Fig. 1A**) can be leveraged to gain new insights into intestinal pathophysiology, and to understand disease mechanisms in ways that are not possible using conventional *in vitro* gut models or simpler microfluidic Intestine Chips.

In the absence of anaerobic conditions, the previous attempts to co-culture gut microflora in the Intestine Chip platform remained limited to commensal or mutualistic microorganisms growing under aerobic environments[14]. Absence of systems to regulate and monitor oxygen gradient in past studies challenged the establishment of a stable anaerobic co-culture environment and, thus, hampered the development of a robust *in vitro* system enabling host-microbiome crosstalk. A recent microfluidics-based system, HuMiX[47], supports culturing of aerobic *Lactobacillus rhamnosus* GG (LGG) and a single obligate anaerobe *Bacteroides caccae* under anaerobic conditions on a porcine mucin-coated nanoporous membrane that is physically separated from the intestinal epithelium channel. This human-bacterial co-culture approach, however, lacks the direct contact between microbial and intestinal epithelial cells. This represents a considerable hurdle in studying functional interactions between the gut microbiota and its host, as well as providing a comprehensive picture of molecular mechanisms linking bacterial communities with disease states. Additionally, this system only allows microbial co-culture for 24h, limiting a stable host gut-microbiota crosstalk for an extended culture and, therefore, preventing long-term tissue function studies[41,48,49]. As such, culturing and maintaining a stable multi-species human intestinal microbial community in the vicinity of intestinal epithelium remains a remarkable technical challenge *in vitro*.

Disease models using human intestine chips

Only a small body of work has been published on disease models using microfluidic intestine devices. As described above, the 2-channel human Instestine Chip was used to co-culture multiple commensal microbes in contact with living human intestinal

epithelial cells and to analyze how gut microbiome, inflammatory cells, and peristalsis-associated mechanical deformations independently contribute to intestinal bacterial overgrowth and inflammation, which are associated with IBD[35,50].

A potentially important application of the microfluidic Intestine Chip models would be to study various types of enteropathies for which current *in vitro* models have only a limited ability to recapitulate, such as those associated with environmental enteric dysfunction, colorectal cancer, cystic fibrosis, bacterial infectious diseases, and celiac disease[51–55]. We believe the likelihood that Intestine Chips will be able to meet this challenge to be high given the successful modeling of other complex diseases (*e.g.*, pulmonary edema, asthma, chronic obstructive pulmonary disease, or Barth's syndrome) with other microfluidic Organ Chips[55–59]. In addition to recapitulating disease phenotypes, human Organ Chips offer a unique way to get insight into the molecular, genetic and biophysical basis of disease based on their ability to incorporate different levels of cellular complexity, and to independently control various critical control parameters (*e.g.* chemical gradients, mechanical forces, cell types, and ECM)[25].

In past Intestine Chip disease modeling studies, induction of the pathological phenotype was accomplished by exposure to specific pathogenic organisms, toxins or inflammatory mediators (*e.g.*, cytokines), with combination of two or more of these factors being required to produce disease responses[35]. For example, both LPS endotoxin and immune cells had to be added simultaneously in the Intestine Chip to produce villus blunting and compromise intestinal barrier function, and neither could induce this response on their own[35]. Inclusion of additional components, such as microbiome[14,35], pathogenic bacteria[35], mechanical cues[35,42], ECM, connective tissue

cells, neuronal cells, organ-specific immune cells, and/or hormonal signals might be needed to model other specific phenotypes that result from complex interplay among several signaling pathways. This goal also might be achieved by creating Intestine Chips with cells isolated from intestinal biopsies taken from patients with specific diseases (**Fig. 3**). This approach also could facilitate development of robust personalized disease models for improved drug screening and matching[60,61].

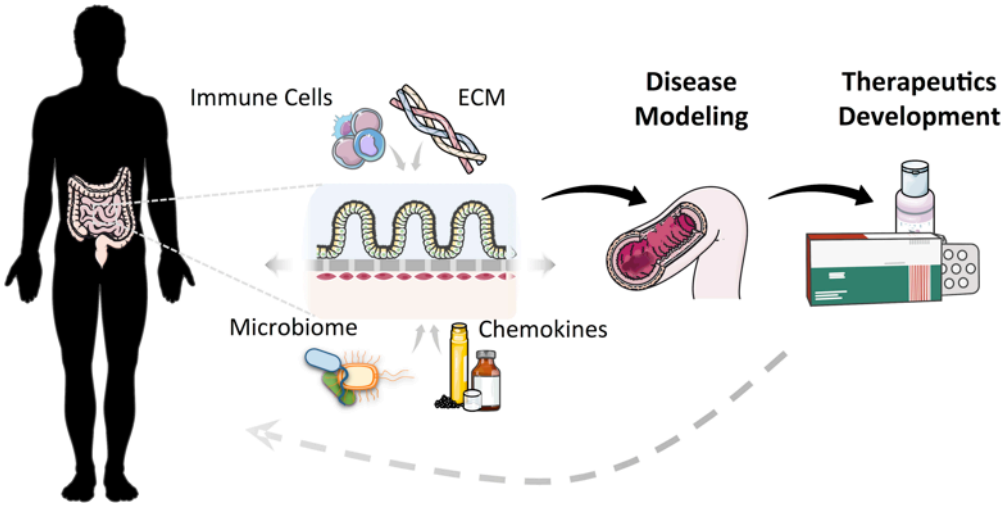

Figure I-3. Personalized-medicine approach using human Intestine Chip. Organ Chip models of intestine have been engineered with increasing complexity that also include neighboring channels lined by human microvascular endothelium, and commensal microbes, immune cells, and pathogenic bacteria, and some permit application of cyclic mechanical forces that mimic peristalsis-like deformations experienced by living intestine in vivo. Intestine Chip platform could be utilized for more complex disease modeling, drug development, and personalized medicine in the future.

Modeling radiation injuries using human Intestine Chip. Radiation syndrome occurs after exposure to γ-radiation during or shortly after cancer radiation therapy or radiological incidences and characterized by the injuries to the healthy organs such as the gastrointestinal (GI) tract. Radiation toxicity in the GI tract is associated with epithelial barrier breakdown, microvascular endothelial apoptosis, morphological

disturbances (*e.g.* villus blunting, shortened microvilli), inflammation, diarrhea, intestinal bleeding and infection, which can consequently lead to death[62,63]. So development of protective therapeutics to alleviate or prevent radiation-induced toxicities is of great importance. Although animal models are currently available for assessing efficacy of medical countermeasure drugs in a number of relevant tissues and organs, these models require expansive and sophisticated radiation equipment that are complicated by serious ethical issues. More importantly, animal models often fail to effectively mimic mechanisms of action or toxicities displayed in humans, additionally, parameters such as age and sex (females are often more radioresistant) of the subject are considered as hurdles on using the animals in the radiation research[64–66]. Hence, despite many scientific efforts in the field of radiation biology, there are great challenges in discovering radio-protective drugs. There is therefore a critical need for predictive models that recapitulate the complex functions of human intestine *in vitro*.

While *in vitro* models can be more conveniently irradiated, they are often not capable of mimicking the complex cellular responses to radiation. Previous attempts to develop intestinal *in vitro* systems such as tumor spheroids, organoids and Transwells cultures were limited in replicating the normal 3D architecture, which is known to greatly contribute in tissue radioresponses[67,68]. Moreover, incorporating vascular tissues, immune cells or bacteria, which immensely contribute in intestinal radiation damage[69,70], is not easily done in these conventional models. Conversely, microfluidic Intestine Chip systems are a promising compromise between the ease of irradiation and the ability to recapitulate the *in vivo*-like radioresponses. Since mechanical forces are directly or indirectly affect the radiation response[71], Intestine Chip devices could be served to

model human radiation syndrome and medical countermeasure drug screening in presence of normal mechanical peristalsis. In a recently study, Caco-2 Intestine Chip was used to model the radiation injury response of human intestine. When Intestine Chip was exposed to a radiation dose of 8 Gray, which is known to cause gastrointestinal effects in humans, significant increases in several markers of cell damage in both the endothelial and epithelial cells were observed: apoptosis (or cell death), generation of reactive oxygen species (ROS, or free radicals), double-stranded DNA breaks, degradation of lipids in the cell membrane, and loss of microvilli structure, as well as disruption of the junctions between neighboring cells and of the mucous membrane that protects the intestinal wall from bacteria and toxins. Interestingly, the endothelial cells in the blood vessel channel was shown to have a stronger response to radiation than the epithelial cells in the intestinal channel in terms of ROS generation, lipid degradation, and DNA fragmentation. Furthermore, the endothelial cells experienced peak apoptosis levels about 24 h after exposure, while epithelial cells were hardest hit at 48 h, suggesting that the endothelium is more sensitive to radiation. Interestingly, in absence of endothelial cells, typical response to radiation such as microvilli blunting, mucosal barrier disruption and ROS generation was observed at much lower extent. This result suggests that endothelial cells play a key role in the gastrointestinal damage observed in radiation injury[72]. Intestine Chip was also served to validate a potential prophylactic radiation countermeasure drug, dimethyloxyallylglycine (DMOG), hat has been shown to prevent radiation injury in rats by increasing the production of the protective proteins hypoxia-inducible factors-1 (HIF-1α) and HIF-2α[73]. DMOG pre-treatment on chip, significantly reduced apoptosis, ROS generation and lipid

degradation in both epithelial and endothelial cells, intestinal permeability, and microvillus injury of intestinal epithelial cells, a result that has never been demonstrated in human tissues before[72]. Thus, the human Intestine Chip could be used to identify new radioprotective drugs by physiologically mimicking radiation damage in the gut.

Conclusion

Microfluidic Organ Chip systems provide unparalleled independent control over multiple key biological, chemical, molecular, cellular and mechanical parameters within the intestinal microenvironment, thereby enabling researchers to apply a synthetic biology approach at the cell, tissue and organ levels which can lead to new insights into intestinal physiology and disease mechanisms. By harnessing these unique capabilities, Intestine Chips can be applied to analyze the molecular processes underlying various enteropathies, and to advance development of new therapies. Creation of personalized Intestine Chips containing stem cells, microbiome and immune cells from the same patient will offer a powerful new approach to define patient-specific drug responses and toxicities, and hence to advance precision medicine. This field is still in its infancy, and there much remains to be done in terms of increasing the robustness of these models and validating their value for drug development and personalized medicine. However, the advantages they provide over conventional culture systems, and even enteroid cultures, are becoming increasingly clear.

References

1. Benet, L. Z., Wu, C.-Y., Hebert, M. F. & Wacher, V. J. Intestinal drug metabolism and antitransport processes: A potential paradigm shift in oral drug delivery. *J. Controlled Release* **39**, 139–143 (1996).

2. Moore, F. A. *et al.* Gut bacterial translocation via the portal vein: a clinical perspective with major torso trauma. *J. Trauma* **31**, 629–636; discussion 636–638 (1991).

3. Bloemen, J. G. *et al.* Short chain fatty acids exchange across the gut and liver in humans measured at surgery. *Clin. Nutr. Edinb. Scotl.* **28**, 657–661 (2009).

4. Ahuja, M. *et al.* Orai1-Mediated Antimicrobial Secretion from Pancreatic Acini Shapes the Gut Microbiome and Regulates Gut Innate Immunity. *Cell Metab.* **25**, 635–646 (2017).

5. Mayer, E. A. Gut feelings: the emerging biology of gut-brain communication. *Nat. Rev. Neurosci.* **12**, 453–466 (2011).

6. Cryan, J. F. & Dinan, T. G. Mind-altering microorganisms: the impact of the gut microbiota on brain and behaviour. *Nat. Rev. Neurosci.* **13**, 701–712 (2012).

7. Round, J. L. & Mazmanian, S. K. The gut microbiota shapes intestinal immune responses during health and disease. *Nat. Rev. Immunol.* **9**, 313–323 (2009).

8. Garrett, W. S., Gordon, J. I. & Glimcher, L. H. Homeostasis and inflammation in the intestine. *Cell* **140**, 859–870 (2010).

9. Sommer, F. & Bäckhed, F. The gut microbiota--masters of host development and physiology. *Nat. Rev. Microbiol.* **11**, 227–238 (2013).

10. Walter, J. & Ley, R. The human gut microbiome: ecology and recent evolutionary changes. *Annu. Rev. Microbiol.* **65**, 411–429 (2011).

11. Arrieta, M.-C., Walter, J. & Finlay, B. B. Human Microbiota-Associated Mice: A Model with Challenges. *Cell Host Microbe* **19**, 575–578 (2016).

12. Hidalgo, I. J., Raub, T. J. & Borchardt, R. T. Characterization of the human colon carcinoma cell line (Caco-2) as a model system for intestinal epithelial permeability. *Gastroenterology* **96**, 736–749 (1989).

13. Eveillard, M. *et al.* Identification and characterization of adhesive factors of Clostridium difficile involved in adhesion to human colonic enterocyte-like Caco-2 and mucus-secreting HT29 cells in culture. *Mol. Microbiol.* **7**, 371–381 (1993).

14. Kim, H. J., Huh, D., Hamilton, G. & Ingber, D. E. Human gut-on-a-chip inhabited by microbial flora that experiences intestinal peristalsis-like motions and flow. *Lab. Chip* **12**, 2165–2174 (2012).

15. Kim, H. J. & Ingber, D. E. Gut-on-a-Chip microenvironment induces human intestinal cells to undergo villus differentiation. *Integr. Biol. Quant. Biosci. Nano Macro* **5**, 1130–1140 (2013).

16. Alam, M. A., Al-Jenoobi, F. I. & Al-Mohizea, A. M. Everted gut sac model as a tool in pharmaceutical research: limitations and applications. *J. Pharm. Pharmacol.* **64**, 326–336 (2012).

17. Rozehnal, V. *et al.* Human small intestinal and colonic tissue mounted in the Ussing chamber as a tool for characterizing the intestinal absorption of drugs. *Eur. J. Pharm. Sci. Off. J. Eur. Fed. Pharm. Sci.* **46**, 367–373 (2012).

18. Smith, P., Mirabelli, C., Fondacaro, J., Ryan, F. & Dent, J. Intestinal 5-fluorouracil absorption: use of Ussing chambers to assess transport and metabolism. *Pharm. Res.* **5**, 598–603 (1988).

19. Dahl-Jensen, S. & Grapin-Botton, A. The physics of organoids: a biophysical approach to understanding organogenesis. *Dev. Camb. Engl.* **144**, 946–951 (2017).

20. Huch, M., Knoblich, J. A., Lutolf, M. P. & Martinez-Arias, A. The hope and the hype of organoid research. *Dev. Camb. Engl.* **144**, 938–941 (2017).

21. Drost, J. & Clevers, H. Translational applications of adult stem cell-derived organoids. *Dev. Camb. Engl.* **144**, 968–975 (2017).

22. Gjorevski, N. *et al.* Designer matrices for intestinal stem cell and organoid culture. *Nature* **539**, 560–564 (2016).

23. Qian, X. *et al.* Brain-Region-Specific Organoids Using Mini-bioreactors for Modeling ZIKV Exposure. *Cell* **165**, 1238–1254 (2016).

24. Gupta, N. *et al.* Microfluidics-based 3D cell culture models: Utility in novel drug discovery and delivery research. *Bioeng. Transl. Med.* **1**, 63–81 (2016).

25. Ingber, D. E. Reverse Engineering Human Pathophysiology with Organs-on-Chips. *Cell* **164**, 1105–1109 (2016).

26. Vickerman, V., Blundo, J., Chung, S. & Kamm, R. Design, fabrication and implementation of a novel multi-parameter control microfluidic platform for three-dimensional cell culture and real-time imaging. *Lab. Chip* **8**, 1468–1477 (2008).

27. Tanaka, Y., Yamato, M., Okano, T., Kitamori, T. & Sato, K. Evaluation of effects of shear stress on hepatocytes by a microchip-based system. *Meas. Sci. Technol.* **17**, 3167–3170 (2006).

28. Sung, J. H., Kam, C. & Shuler, M. L. A microfluidic device for a pharmacokinetic-pharmacodynamic (PK-PD) model on a chip. *Lab. Chip* **10**, 446–455 (2010).

29. Gao, D., Liu, H., Lin, J.-M., Wang, Y. & Jiang, Y. Characterization of drug permeability in Caco-2 monolayers by mass spectrometry on a membrane-based microfluidic device. *Lab. Chip* **13**, 978–985 (2013).

30. Maoz, B. M. *et al.* Organs-on-Chips with combined multi-electrode array and transepithelial electrical resistance measurement capabilities. *Lab. Chip* **17**, 2294–2302 (2017).

31. Imura, Y., Asano, Y., Sato, K. & Yoshimura, E. A microfluidic system to evaluate intestinal absorption. *Anal. Sci. Int. J. Jpn. Soc. Anal. Chem.* **25**, 1403–1407 (2009).

32. Sung, J. H., Yu, J., Luo, D., Shuler, M. L. & March, J. C. Microscale 3-D hydrogel scaffold for biomimetic gastrointestinal (GI) tract model. *Lab. Chip* **11**, 389–392 (2011).

33. Yi, B. *et al.* Three-dimensional in vitro gut model on a villi-shaped collagen scaffold. *BioChip J.* **11**, 219–231 (2017).

34. Shim, K.-Y. *et al.* Microfluidic gut-on-a-chip with three-dimensional villi structure. *Biomed. Microdevices* **19**, 37 (2017).

35. Kim, H. J., Li, H., Collins, J. J. & Ingber, D. E. Contributions of microbiome and mechanical deformation to intestinal bacterial overgrowth and inflammation in a human gut-on-a-chip. *Proc. Natl. Acad. Sci.* **113**, E7–E15 (2016).

36. Huh, D. *et al.* Reconstituting organ-level lung functions on a chip. *Science* **328**, 1662–1668 (2010).

37. Jung, P. *et al.* Isolation and in vitro expansion of human colonic stem cells. *Nat. Med.* **17**, 1225–1227 (2011).

38. Van de Wetering, M. *et al.* Prospective derivation of a living organoid biobank of colorectal cancer patients. *Cell* **161**, 933–945 (2015).

39. Sato, T. & Clevers, H. SnapShot: Growing Organoids from Stem Cells. *Cell* **161**, 1700–1700.e1 (2015).

40. Fatehullah, A., Tan, S. H. & Barker, N. Organoids as an in vitro model of human development and disease. *Nat. Cell Biol.* **18**, 246–254 (2016).

41. Park, G.-S. *et al.* Emulating Host-Microbiome Ecosystem of Human Gastrointestinal Tract in Vitro. *Stem Cell Rev.* **13**, 321–334 (2017).

42. Kasendra, M. *et al.* Development of a primary human Small Intestine-on-a-Chip using biopsy-derived organoids. *Sci. Rep.* **8**, 2871 (2018).

43. Bein, A. *et al.* Microfluidic Organ-on-a-Chip Models of Human Intestine. *Cell. Mol. Gastroenterol. Hepatol.* **5**, 659–668 (2018).

44. May, S., Evans, S. & Parry, L. Organoids, organs-on-chips and other systems, and microbiota. *Emerg. Top. Life Sci.* **1**, 385–400 (2017).

45. Sadabad, M. S. *et al.* A simple coculture system shows mutualism between anaerobic faecalibacteria and epithelial Caco-2 cells. *Sci. Rep.* **5**, 17906 (2015).

46. Dutta, D. & Clevers, H. Organoid culture systems to study host-pathogen interactions. *Curr. Opin. Immunol.* **48**, 15–22 (2017).

47. Shah, P. *et al.* A microfluidics-based in vitro model of the gastrointestinal human-microbe interface. *Nat. Commun.* **7**, 11535 (2016).

48. May, S., Evans, S. & Parry, L. Organoids, organs-on-chips and other systems, and microbiota. *Emerg. Top. Life Sci.* **1**, 385–400 (2017).

49. Eain, M. M. G. *et al.* Engineering Solutions for Representative Models of the Gastrointestinal Human-Microbe Interface. *Engineering* **3**, 60–65 (2017).

50. Lee, J., Choi, J.-H. & Kim, H. J. Human gut-on-a-chip technology: will this revolutionize our understanding of IBD and future treatments? *Expert Rev. Gastroenterol. Hepatol.* **10**, 883–885 (2016).

51. Brown, E. M. *et al.* Diet and specific microbial exposure trigger features of environmental enteropathy in a novel murine model. *Nat. Commun.* **6**, 7806 (2015).

52. Pereira, J. F. S. *et al.* The third dimension: new developments in cell culture models for colorectal research. *Cell. Mol. Life Sci. CMLS* **73**, 3971–3989 (2016).

53. Fisher, J. T., Zhang, Y. & Engelhardt, J. F. Comparative biology of cystic fibrosis animal models. *Methods Mol. Biol. Clifton NJ* **742**, 311–334 (2011).

54. Tarr, P. I., Gordon, C. A. & Chandler, W. L. Shiga-toxin-producing Escherichia coli and haemolytic uraemic syndrome. *Lancet Lond. Engl.* **365**, 1073–1086 (2005).

55. Stoven, S., Murray, J. A. & Marietta, E. V. Latest in vitro and in vivo models of celiac disease. *Expert Opin. Drug Discov.* **8**, 445–457 (2013).

56. Wang, G. *et al.* Modeling the mitochondrial cardiomyopathy of Barth syndrome with induced pluripotent stem cell and heart-on-chip technologies. *Nat. Med.* **20**, 616–623 (2014).

57. Benam, K. H. *et al.* Development of a human COPD model-on-a-chip to mimic disease exacerbation (a small airway-on-a-chip model). *Eur. Respir. J.* **44**, P3340 (2014).

58. Benam, K. H. *et al.* Small airway-on-a-chip enables analysis of human lung inflammation and drug responses in vitro. *Nat. Methods* **13**, 151–157 (2016).

59. Huh, D. *et al.* A human disease model of drug toxicity-induced pulmonary edema in a lung-on-a-chip microdevice. *Sci. Transl. Med.* **4**, 159ra147 (2012).

60. Mack, D. L., Guan, X., Wagoner, A., Walker, S. J. & Childers, M. K. Disease-in-a-dish: the contribution of patient-specific induced pluripotent stem cell technology to regenerative rehabilitation. *Am. J. Phys. Med. Rehabil.* **93**, S155–168 (2014).

61. Astolfi, M. *et al.* Micro-dissected tumor tissues on chip: an ex vivo method for drug testing and personalized therapy. *Lab. Chip* **16**, 312–325 (2016).

62. Hauer-Jensen, M., Denham, J. W. & Andreyev, H. J. N. Radiation Enteropathy – Pathogenesis, Treatment, and Prevention. *Nat. Rev. Gastroenterol. Hepatol.* **11**, 470–479 (2014).

63. Shadad, A. K., Sullivan, F. J., Martin, J. D. & Egan, L. J. Gastrointestinal radiation injury: Symptoms, risk factors and mechanisms. *World J. Gastroenterol. WJG* **19**, 185–198 (2013).

64. Williams, J. P. *et al.* Animal Models for Medical Countermeasures to Radiation Exposure. *Radiat. Res.* **173**, 557–578 (2010).

65. Augustine, A. D. *et al.* Animal models for radiation injury, protection and therapy. *Radiat. Res.* **164**, 100–109 (2005).

66. Kahn, J., Tofilon, P. J. & Camphausen, K. Preclinical models in radiation oncology. *Radiat. Oncol. Lond. Engl.* **7**, 223 (2012).

67. Ley, S. *et al.* Screening of Intestinal Crypt Organoids: A Simple Readout for Complex Biology. *SLAS Discov.* **22**, 571–582 (2017).

68. Morini, J., Babini, G., Barbieri, S., Baiocco, G. & Ottolenghi, A. The Interplay between Radioresistant Caco-2 Cells and the Immune System Increases Epithelial Layer Permeability and Alters Signaling Protein Spectrum. *Front. Immunol.* **8**, 223 (2017).

69. Paris, F. *et al.* Endothelial apoptosis as the primary lesion initiating intestinal radiation damage in mice. *Science* **293**, 293–297 (2001).

70. Crawford, P. A. & Gordon, J. I. Microbial regulation of intestinal radiosensitivity. *Proc. Natl. Acad. Sci. U. S. A.* **102**, 13254–13259 (2005).

71. Jain, R. K., Martin, J. D. & Stylianopoulos, T. The Role of Mechanical Forces in Tumor Growth and Therapy. *Annu. Rev. Biomed. Eng.* **16**, 321–346 (2014).

72. Jalili-Firoozinezhad, S. *et al.* Modeling radiation injury-induced cell death and countermeasure drug responses in a human Gut-on-a-Chip. *Cell Death Dis.* **9**, 223 (2018).

73. Taniguchi, C. M. *et al.* PHD inhibition mitigates and protects against radiation-induced gastrointestinal toxicity via HIF2. *Sci. Transl. Med.* **6**, 236ra64 (2014).

II. Chapter 2

Modeling radiation injury-induced cell death and countermeasure drug responses in a human Gut-on-a-Chip

This chapter is based on the article:

S. Jalili-Firoozinezhad, R. Prantil-Baun, A. Jiang, R. Potla, T. Mammoto, J. C. Weaver, T. C. Ferrante, H. J. Kim, J. M.S. Cabral, O. Levy, D. E. Ingber. “Modeling radiation injury-induced cell death and countermeasure drug responses in a human Gut-on-a-Chip”. *Nature-Cell Death & Disease*, 9, 2, 223 (2018).

Modeling radiation injury-induced cell death and countermeasure drug responses in a human Gut-on-a-Chip

Sasan Jalili-Firoozinezhad[1,2], Rachelle Prantil-Baun[1], Amanda Jiang[3], Ratnakar Potla[3], Tadanori Mammoto[3], James C. Weaver[1], Thomas C. Ferrante[1], Hyun Jung Kim[4], Joaquim M. S. Cabral[2], Oren Levy[1], and Donald E. Ingber[1,3,5]

[1]Wyss Institute for Biologically Inspired Engineering, Harvard University, Boston, Massachusetts

[2]Department of Bioengineering and iBB - Institute for Bioengineering and Biosciences, Instituto Superior Técnico, Universidade de Lisboa, Lisboa, Portugal

[3]Vascular Biology Program and Department of Surgery, Boston Children's Hospital and Harvard Medical School, Boston, MA 02115, USA

[4]Department of Biomedical Engineering, The University of Texas at Austin, Austin, Texas 78712, USA

[5]Harvard John A. Paulson School of Engineering and Applied Sciences, Cambridge, MA 02139, USA

[*]Corresponding Author:

Donald E. Ingber, don.ingber@wyss.harvard.edu

Abstract

Studies on human intestinal injury induced by acute exposure to γ-radiation commonly rely on use of animal models because culture systems do not faithfully mimic human intestinal physiology. Here we used a human Gut-on-a-Chip (Gut Chip) microfluidic device lined by human intestinal epithelial cells and vascular endothelial cells to model radiation injury and assess the efficacy of radiation countermeasure drugs *in vitro*. Exposure of the Gut Chip to γ-radiation resulted in increased generation of reactive oxygen species, cytotoxicity, apoptosis, and DNA fragmentation, as well as villus blunting, disruption of tight junctions and compromise of intestinal barrier integrity. In contrast, pre-treatment with a potential prophylactic radiation countermeasure drug, dimethyloxaloylglycine (DMOG), significantly suppressed all of these injury responses. Thus, the human Gut Chip may serve as an *in vitro* platform for studying radiation-induced cell death and associate gastrointestinal acute syndrome, in addition to screening of novel radio-protective medical countermeasure drugs.

Introduction

Exposure to ionizing γ-radiation, whether therapeutic or accidental, may result in acute radiation syndrome that is associated with gastrointestinal (GI) disturbances leading to massive shortening or 'blunting' of intestinal villi, disruption of tight junctions, increased apoptosis within the microvascular endothelium, mucosal barrier breakdown, inflammation, abdominal pain, diarrhea and vomiting, which can result in intestinal hemorrhage, sepsis and death[1–4]. Development of medical countermeasures (MCMs) to protect against the devastating effects of radiation is therefore of tremendous

importance. Animal models have been primarily used for GI radiation research because they can mimic some of the clinical manifestations of radiation poisoning (*e.g.*, vomiting, diarrhea), however, these *in vivo* models often fail to effectively mimic cellular mechanisms of radiation toxicities or drug mechanisms of action displayed in humans[5,6]. Ethical issues related to animal testing also present a considerable hurdle, particularly when it relates to studies on primates[7]. As a result, the mechanisms underlying the radiation-induced GI syndrome remain unclear, and this represents a major challenge with regards to discovery of new MCMs[8,9].

Understanding of radiation-induced intestinal injury could be greatly facilitated by the availability of experimental *in vitro* models that recapitulate human cell and tissue responses to radiation; unfortunately, this has not been possible using existing culture systems. In particular, the 3D villus architecture and differentiated barrier functions of the intestine are known to contribute greatly to intestinal tissue responses to radiation. It is likely for this reason that past efforts, for example, using Transwell culture systems lined by human Caco-2 intestinal epithelial cells that grow as a flat monolayer failed to model radiation injury[10,8,11]. Furthermore, past *in vitro* models used to study intestinal responses to radiation did not incorporate a human vascular endothelium in the vicinity of the intestinal epithelium to mimic capillary blood vessels, which are situated very close to epithelial cells in the gut mucosa[11]. This is important because while intestinal stem cells have always been assumed to be the major mediator of radiation damage involved in development of the GI syndrome[12,13], recent studies suggest that apoptosis within the microvascular endothelium may be a key mediator of radiation damage that, in turn, leads to stem cell dysfunction[14–16].

To model radiation-induced damage *in vitro,* we adapted a recently described human Gut-on-a-Chip (Gut Chip) microfluidic culture device that is lined by human intestinal epithelium interfaced with a human vascular endothelium, which spontaneously differentiates and forms three-dimensional intestinal villi when cultured in the presence of flow and cyclic peristalsis-like deformations[10,17,18]. Here we show that this microfluidic human Gut Chip can be used to analyze the effects of γ–radiation on villus morphology, barrier function, cell-cell junctions, cellular toxicity, apoptosis, reactive oxygen species (ROS) generation, and DNA fragmentation *in vitro*. We also demonstrate that it can be used as a tool to evaluate the radiation-protecting effects of a potential radiation countermeasure drug, the small-molecule prolylhydroxylase inhibitor dimethyloxalylglycine (DMOG), which has been reported to protect small intestine against radiation damage by stabilizing hypoxia-inducible factor 1α and 2α (HIF-1α and HIF-2α)[19].

Results

Establishing a human gut radiation injury model *in vitro*. The microfluidic human Gut Chip is a microfluidic culture device composed of a clear, flexible, poly-dimethylsiloxane (PDMS) polymer, which contains 2 parallel microchannels separated by a porous, flexible, extracellular matrix (ECM)-coated membrane lined by human Caco-2 intestinal epithelial cells on one side and human umbilical vein microvascular endothelial cells on the other (**Fig. 1a, left**). Medium is perfused through both channels (30 μl hr^{-1}; 0.02 dyne cm^{-2}) and cyclic deformations (0.15 Hz; 10% strain) similar to those experienced by cells within the intestine during peristalsis[20] are induced by

applying cyclic suction through hollow side chambers (**Supplementary Fig. S1a**), as previously described[10,17,18]. When Caco-2 intestinal epithelial cells are cultured under these conditions, they undergo villus differentiation and express multiple features of human small intestine within 5-7 days when analyzed at the molecular, morphological, physiological and transcriptomic levels[10,17,18], even though the same cells in the same medium fail to undergo significant differentiation in Transwell cultures[10]. In contrast to past Gut Chip studies, we cultured endothelial cells on all four sides of the lower channel to engineer a hollow endothelium-lined vascular lumen in these devices (**Fig. 1a, right**). Differential interference contrast (DIC) and immunofluorescence microscopic analysis confirmed that the Caco-2 cells formed a villus intestinal epithelium with polarized epithelial cells lined by ZO-1-containing tight junctions and an apical villin-containing brush border (**Fig. 1b; Supplementary Fig. S1b**). In the lower channel, endothelial cells grew to form a confluent cell monolayer joined by CD31-containing adherens junctions, which covered all four sides of the channel surrounding the hollow vascular lumen (**Fig. 1a right, Fig. 1c**, and **Supplementary Fig. S1b**).

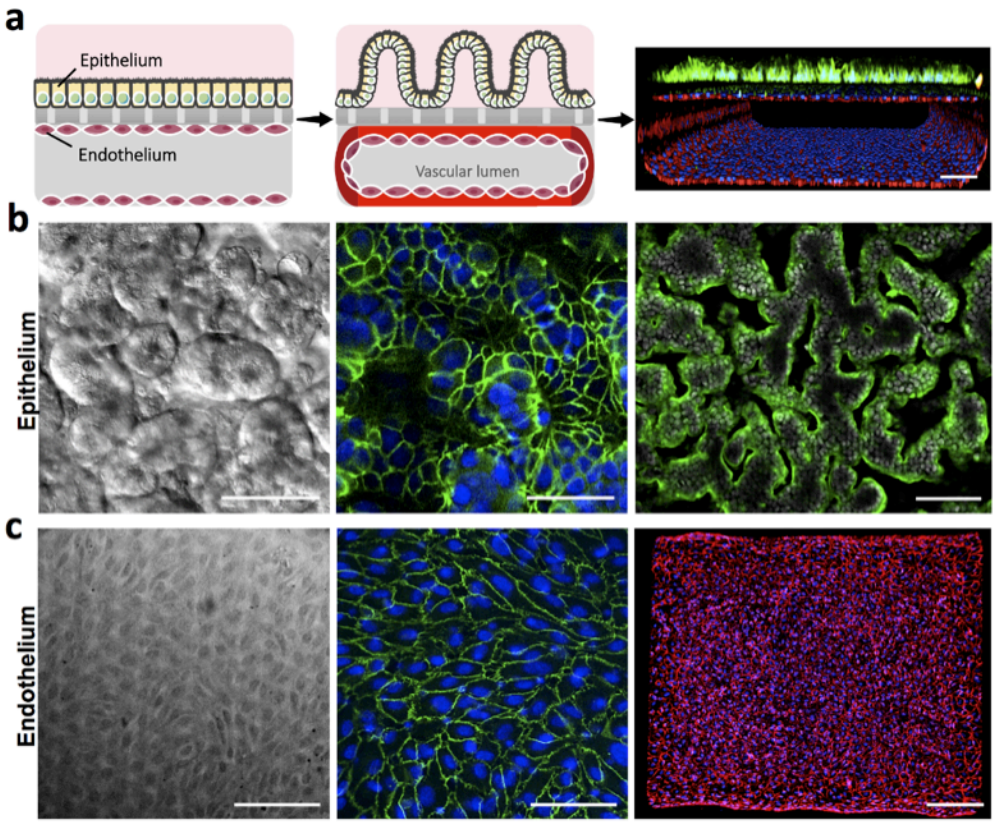

Figure II-1. ***Human Gut Chip microfluidic culture device.*** (**a**) Schematic showing the positions of the human intestinal epithelium and endothelium when initially plated on opposite sides of the matrix-coated porous membrane within the 2-channel microfluidic device (left), and how this progresses to form a villus epithelium in the top channel interfaced with a planar endothelium that forms a lumen in the bottom channel (middle). A representative immunofluorescence confocal micrograph visualizing a cross-section of the Gut Chip device with the villus intestinal epithelium stained for villin (green) to visualize the apical brush border, and the planar endothelium stained for VE-cadherin (red) to visualize adherens junctions, is shown at the right (bar, 100 μm). (**b**) Microscopic views showing the villus morphology of the human Caco-2 intestinal epithelium cultured for about 5 days in the Gut Chip with flow (30 $\mu l.hr^{-1}$) and cyclic strain (10% at 0.15 Hz), when viewed from above by DIC imaging (left; bar, 50 μm) or by immunofluorescence staining for the tight junction protein, ZO-1 (green, middle; bar, 50 μm) and villin (green, right; bar, 100 μm). Blue and gray indicate DAPI-stained nuclei. (**c**) Microscopic views showing the planar morphology of the human endothelium cultured under identical conditions as in **b**, when viewed from above phase contrast imaging (left; bar, 50 μm) or by immunofluorescence staining for the endothelial cell junction-associated proteins PECAM-1 (green, middle; bar, 50 μm) and VE-cadherin (red, right; bar, 200 μm). Blue indicates DAPI-stained nuclei.

We then exposed the human gut chips to γ-radiation. Previous studies have shown that exposure to a level of ~ 4-8 Gray (Gy) of γ-radiation can lead to GI

syndrome and death in the absence of treatment in humans[13,21]. Rodents subjected to total body irradiation at a dose of 8 Gy also show progressive intestinal injury with increased number of apoptotic and mitotic cells, as well as shortening of the villi[22,23]. Exposure of the human gut chips to 8 Gy γ-radiation for 24 hours similarly resulted in significant increases in apoptosis both within the epithelium and endothelium compared to non-irradiated control chips, however, the number of apoptotic endothelial cells was about 5 fold higher in the endothelium at this time (**Fig. 2a,b**). Interestingly, the epithelium appeared to undergo a distinct and slower mechanism of apoptosis induction as the apoptosis labeling index increased significantly 48 hours after radiation exposure, whereas the endothelial apoptosis index was maximal at 1 day (**Fig. 2a,b**). In contrast, both the epithelium and endothelium exhibited similar levels of cell membrane damage at 24 hours, as measured by quantifying extracellular release of the intracellular enzyme, lactate dehydrogenase (LDH), and these levels remained high for at least 72 hours after radiation exposure (**Fig. 2c**). Control studies also confirmed that direct exposure of the chip without cells did not induce cytotoxicity when cells were then cultured on these devices (**Supplementary Fig. S2)**, confirming that cell injury was not caused by radiation-induced release of toxins from the PDMS material.

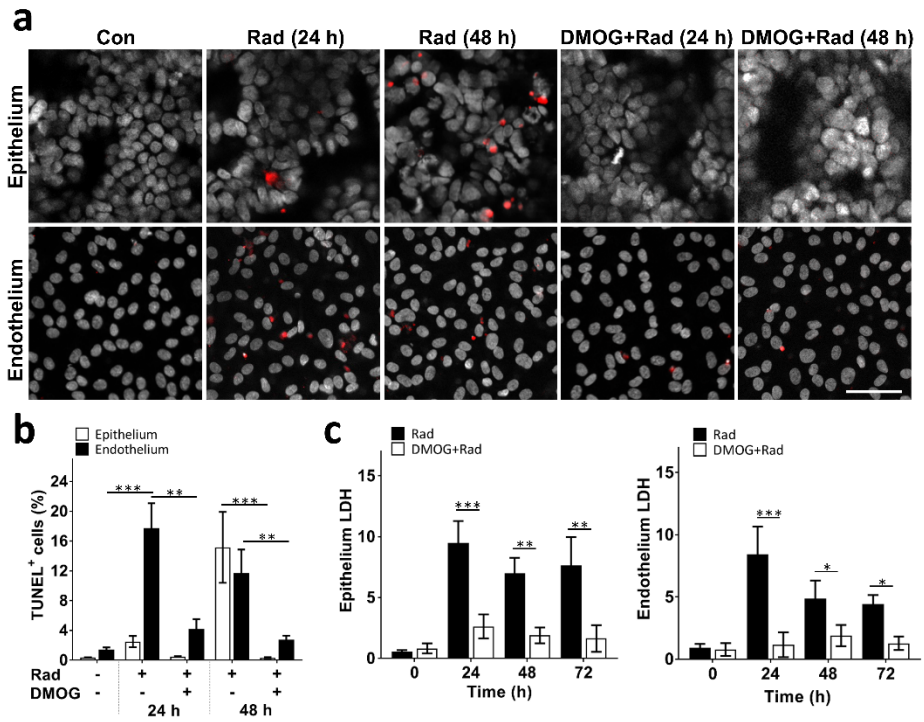

Figure II-2. Radiation-induced apoptosis and cytotoxicity in intestinal epithelium and vascular endothelium, and radio-protective effects of DMOG. (**a**) Representative immunofluorescence micrographs of TUNEL (red) and DAPI (white) staining in epithelial and endothelial cells cultured on-chip in the absence (Con) or presence (+ Rad) of 8Gy of γ-radiation (Rad), with or without DMOG treatment, 24h and 48h after radiation exposure (bar, 50 μm). (**b**) Graph showing the quantification of the percentage of epithelium and endothelium cells that expressed TUNEL staining (TUNEL$^+$ cells) 24h and 48 h after exposure to the conditions shown in **a** (n=3; *P<0.05, **P<0.01, ***P<0.001). (**c**) Graph showing effects on radiation-induced cell death in the epithelium (left) and endothelium (right) exposed to radiation in the absence (Rad) or presence of DMOG (DMOG + Rad), as assessed by quantifying LDH release from cells (data are presented as fold change in LDH levels relative to the non-irradiated control cells; n=3; *P<0.05, **P<0.01, ***P<0.001).

As ROS are critical mediators of radiation-induced damage that have been reported to play a pivotal role in intestinal epithelial injury as well as epithelial and endothelial apoptosis in patients[24–26], we sought to determine if radiation induces ROS formation in the human Gut Chip. Quantification of ROS production using CellROX Green Reagent revealed that endothelial cells generated about twice the level of ROS per cell compared to the intestinal epithelial cells (~8-fold versus 4-fold increases, respectively) (**Fig. 3a,b**). Lipids are one of the main targets attacked by ROS, and this

results in lipid peroxidation and cell membrane damage[27–29]. Consistent with this observation and our ROS results, the level of lipid peroxidation after radiation in endothelium was again almost two times higher in the endothelium compared to the epithelium (**Fig. 3c,d**).

Ionizing radiation is thought to produce many of its damaging effects on cells by producing clustered DNA double-strand breaks (DSB), promoting hyperphosphorylation of DSB-associated proteins, and inducing formation of discrete nuclear foci containing p53 binding protein 1 (53BP1), an important regulator of DSB signaling that is regulated by γ–radiation[30–32]. Similarly, we found that while 53BP1 was diffusely localized in the nuclei of control intestinal epithelial and endothelial cells in the Gut Chip, it relocated to punctate nuclear foci within both cell types when they were irradiated (**Fig. 3e,f**). Again, while more than 95% of endothelial cells exhibited discrete nuclear foci formation, the intestinal epithelial cells only exhibited about half this level of response. These findings appear to be consistent with past studies that suggested radiation-induced epithelial cell injury and DNA damage are mediated by endothelial apoptosis and ROS generation which are upstream from the epithelial cell injury responses[15,33–35].

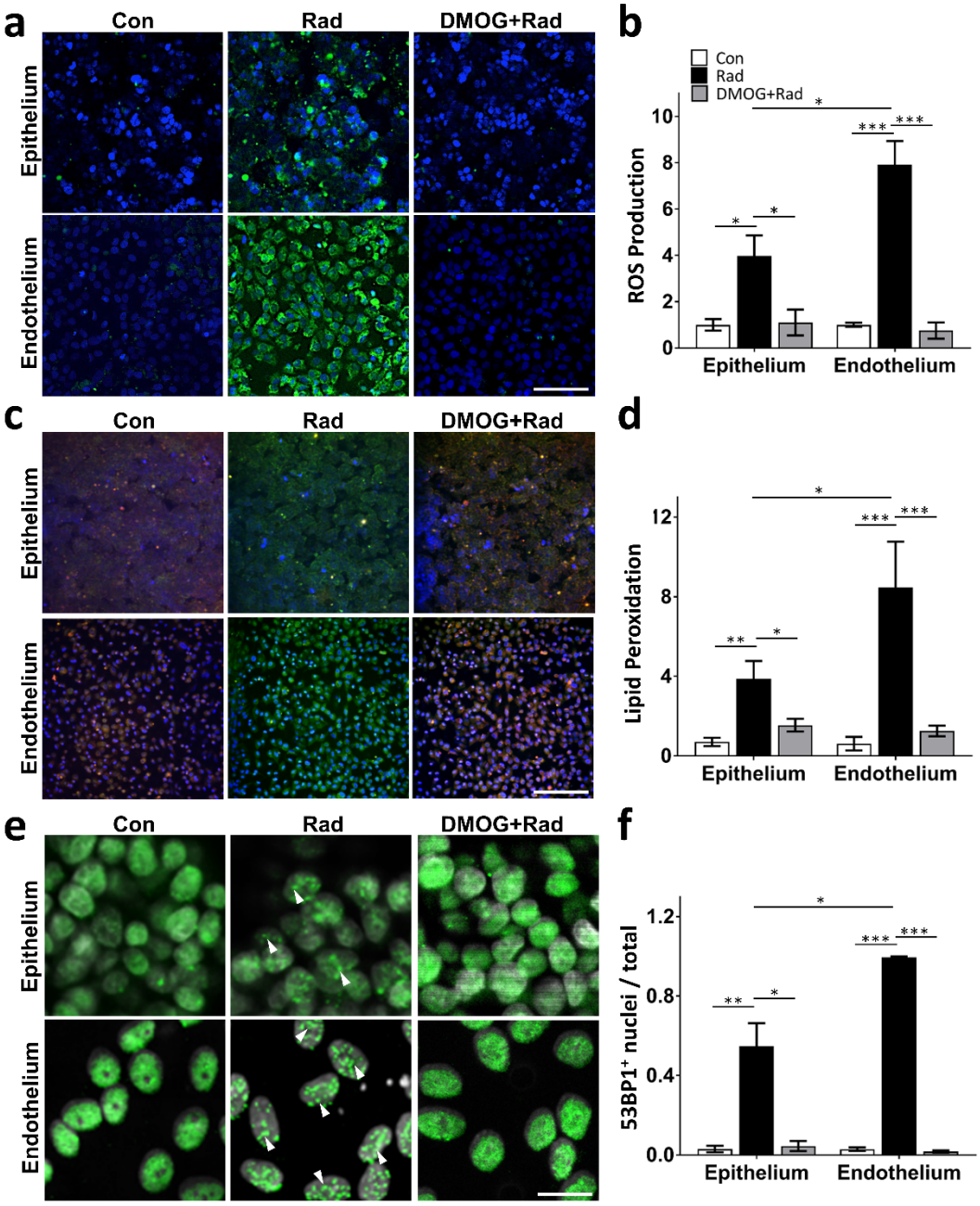

Figure II-3. Radiation-induced changes in ROS, lipid peroxidation and DNA fragmentation in the presence or absence of DMOG treatment. (**a**) Radiation-induced changes in intracellular ROS in the intestinal epithelium (top) and endothelium (bottom) measured 30 min after exposure to γ-radiation (8Gy) in the absence (Rad) or presence of DMOG (DMOG + Rad), or under control non-radiated conditions (Con), as visualized using the CellROX Green Reagent (green) (blue, DAPI-stained nuclei; bar, 50 μm). (**b**) Quantification of ROS production measured under the conditions described in **a**, expressed as fold change relative to non-irradiated control cells (n=3; *P<0.05, ***P<0.001). (**c**) Radiation-induced changes in lipid peroxidation in the intestinal epithelium (top) and endothelium (bottom) measured under the same conditions as shown in **a**, detected using an Image-iT® Lipid Peroxidation Kit in which lipid peroxidation results in a shift of fluorescence emission from 510nm (red) to 590 nm (green) (blue indicated DAPI-stained nuclei; bar, 50 μm). (**d**) Quantification of lipid peroxidation measured under the conditions described in **c**. Data are presented as a shift the ratio of the fluorescence emission peak from 510nm to

590 nm (n=3; *P<0.05, **P<0.01, ***P<0.001). (**e**) Effect of radiation on formation of DNA double strand breaks, as detected by increased punctate staining of 53BP1-positive (53BP1^{+}) nuclei (green); nuclei were counterstained with DAPI (white) (bar, 20 μm). White arrowheads indicate nuclei that display discrete punctate patterns of 53BP1^{+} staining. (**f**) Quantification of the ratio of nuclei that exhibited 53BP1^{+} punctate staining relative to total nuclei measured under the conditions described in **e** (n=5; *P<0.05, **P<0.01, ***P<0.001).

Recapitulating intestinal organ-level radiation-induced injury. The small intestines of patients exposed to high levels of γ-radiation exhibit characteristic morphological changes including decreased villi height and irregular, shortened microvilli ("villus blunting"), as well as cytoplasmic vacuolization and detachment of epithelial and endothelial cells from their basement membrane[36–39]. Similarly, we found that exposure of the Gut Chips to 8 Gy resulted in loss of normal villus architecture and disruption of epithelial and endothelial integrity within 48 h**.** Computerized image analysis of cross-sectional immunofluorescence views of villin-stained epithelium (**Fig. 4a**) revealed a significant reduction in the average height of villi in irradiated versus control chips (68.2 ± 11.3 vs. 160.4 ± 19.6 μm, respectively) (**Fig. 4b**). Moreover, while the heights of the majority of the finger-like villi in control (non-irradiated) chips ranged between 100-200 μm, less than 35% of villus structures in the irradiated chip reached 100 μm or above (**Fig. 4a,c**). In addition, scanning electron microscopic (SEM) analyses showed that the apical surface of the irradiated epithelial cells had very short and irregular microvilli compared to control samples, making it difficult to identify cell boundaries in the irradiated epithelium (**Fig. 4e**). When we analyzed the expression of the cell-cell junction proteins, ZO-1 and VE cadherin, in the irradiated epithelial and endothelial cells, respectively, we observed decreased expression of both molecules and a loss of junctional continuity in the cell layers (**Fig. 5a-c**). Radiation exposure also

resulted in cell detachment and generation of cell-free gaps in the endothelial monolayer.

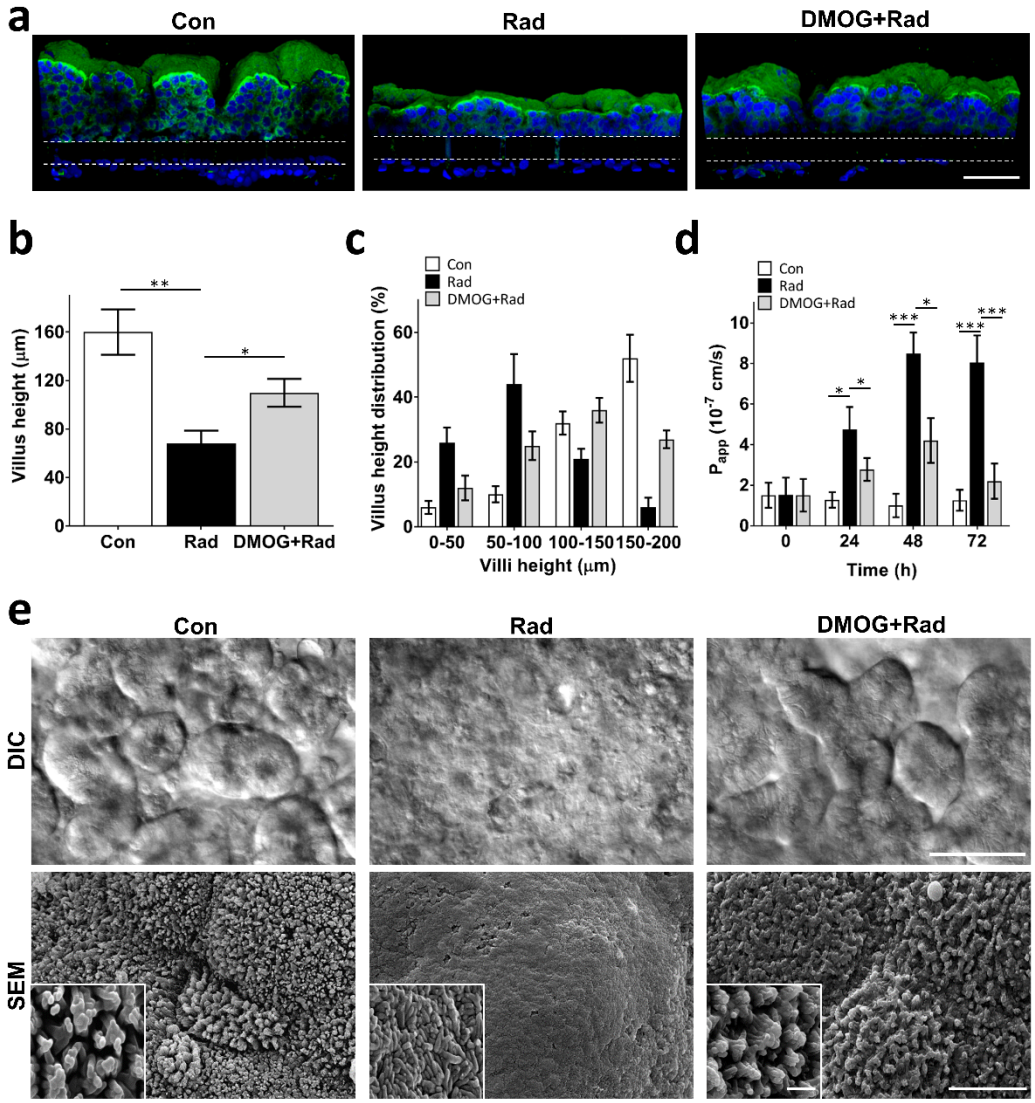

Figure II-4. Morphological analysis of intestinal villus damage induced by radiation exposure. (**a**) Representative vertical cross sectional, confocal, micrographic views through the intestinal epithelium-membrane-endothelium interface of the Gut Chip at 48 h without (Con) or with exposure to γ-radiation (8Gy) in the absence (Rad) or presence of DMOG (DMOG+Rad), when immunostained for villin (green) and nuclei with DAPI (blue) (parallel white dashed lines indicated upper and lower surfaces of the porous matrix-coated membrane; bar, 100 μm). (**b**) Quantification of intestinal injury evaluated by measuring changes in the height of the villi (n = 50) under control conditions (Con) versus after exposure to radiation (8Gy) in the absence (Rad) or presence of DMOG pre-treatment (DMOG+Rad) (*P<0.05, **P<0.01). (**c**) Distribution of villus heights measured under the conditions described in **b**. (**d**) Changes in apparent paracellular permeability (P_{app}) measured by quantitating cascade blue transport across the tissue-tissue interface within the Gut Chip microdevices before (Con) or after radiation in the absence (Rad) or

presence of DMOG pre-treatment (DMOG+Rad) (n=3; *P<0.05, ***P<0.001). (**e**) DIC (top; bar, 50 μm) of the intestinal villi and SEM views (bottom; low magnification bar, 10 μm; High magnification Inset bar, 1 μm) of the intestinal microvilli formed on-chip under control conditions (Con) or after radiation exposure without (Rad) or with pre-treatment with DMOG (DMOG+Rad).

Radiation injury of intestinal villi in humans is also accompanied by breakdown of the intestinal mucosal barrier, which can release bacteria and their toxins through the intestinal wall, leading to further abdominal complications [40–42]. When we evaluated the effect of radiation on intestinal barrier function and mucosal damage by measuring changes in the apparent permeability coefficient (P_{app}), which is a measure of paracellular barrier function in the human Gut Chip, we observed a 4-fold increase in P_{app} (4.9 x 10^{-7} versus 1.2 x 10^{-7} cm s^{-1}) at 24 h after exposure when significant apoptosis was detected in the endothelial cells, and P_{app} almost doubled again (8.7 x 10^{-7} cm s^{-1}) by 48 h (**Fig. 4d**). This was also accompanied by significant loss of expression of the mucin protein, MUC2 (**Fig. 6c,d**), which is the most abundant mucin secreted by goblet cells that plays a pivotal role in organizing the intestinal mucus layers and barrier integrity at the epithelial apical surface[43,44]. Importantly, the suppression of MUC2 levels we detected on-chip is similar to what is observed in radiated intestinal tissue *in vivo*[45]. Thus, the Gut Chip faithfully mimics many facets of the human intestinal injury response to radiation *in vitro*.

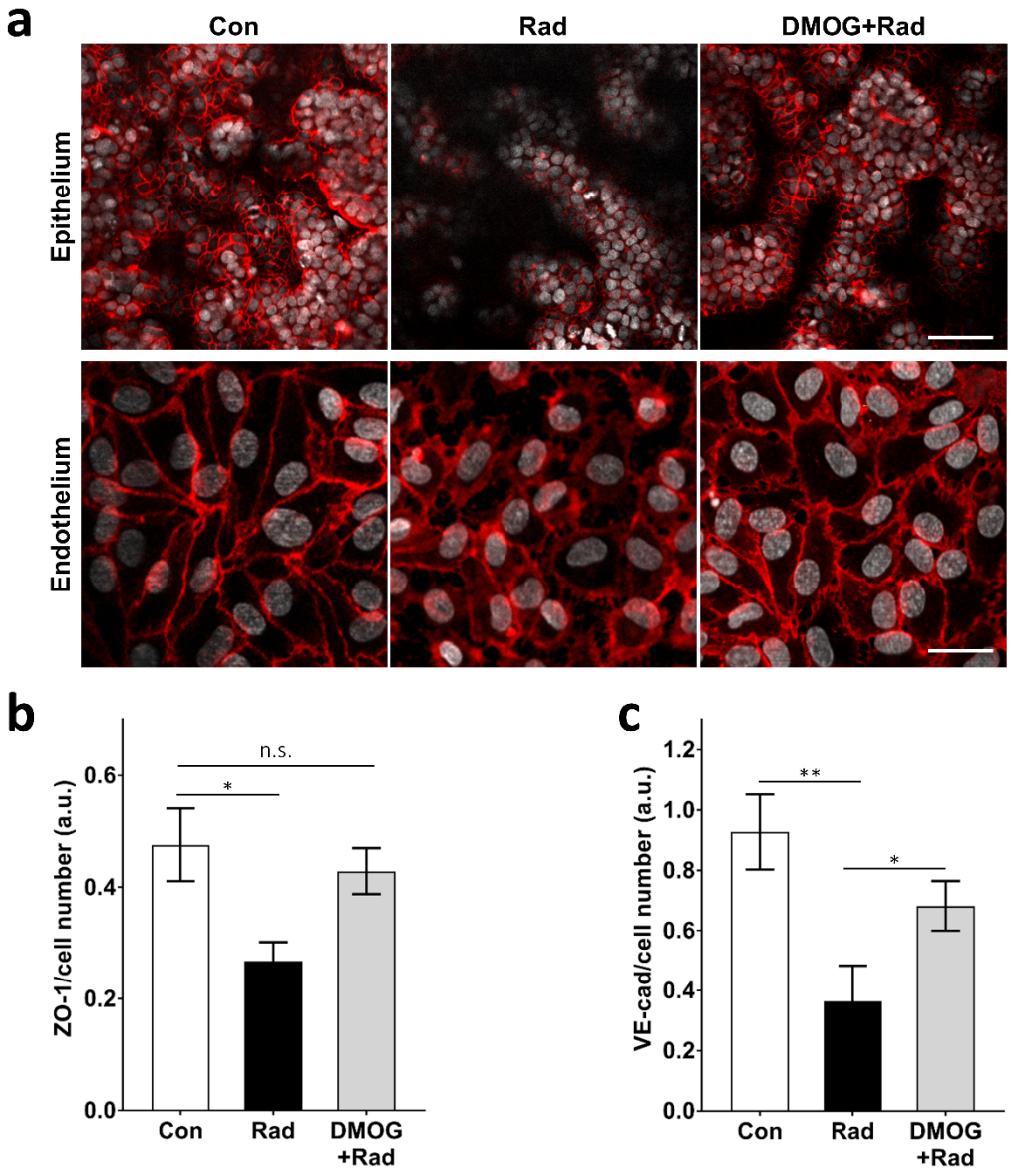

Figure II-5. Radiation-induced loss of junctional continuity and mucosal damage and the effects of DMOG pre-treatment. (**a**) Confocal immunofluorescence micrographs stained showing horizontal views through the mid-section of villi (100 μm above the porous membrane) stained for epithelial tight junctions (ZO-1, red) at the top (bar, 100 μm), and through the middle of the endothelium stained for adherens junctions (VE-cadherin, red) at the bottom (bar, 20 μm), within non-irradiated Gut Chips (Con) versus Gut Chips exposed to 8Gy radiation for 48h without (Rad) or with DMOG pre-treatment (DMOG+Rad). Quantification of fluorescence intensities (a.u.) of (**b**) ZO-1 and (**c**) VE-cadherin normalized per cell number (n=3; $^{*}P<0.05$, $^{**}P<0.01$; n.s., not significant).

Endothelial cells as mediators of radiation damage. To confirm whether vascular endothelium contributes to radiation-induced intestinal epithelium damage, we irradiated the Gut Chips in the absence or presence of endothelial cells and analyzed

effects on radiation-induced epithelium damage at cell and tissue levels. Interestingly, whereas Gut Chips containing both epithelium and endothelium exhibited villus blunting in response to radiation exposure (**Fig. 4**), there was no significant decrease in average height of villi in irradiated chips lined by intestinal epithelium in the absence of endothelium (**Fig. 6a,b**). We also found that the presence of endothelial cells enhanced barrier function (reduced permeability by ~10-fold; **Supplementary Fig. S3c**) and increased mucus secretion (~4-fold; **Fig. 6c,d**) by the epithelium compared to chips lacking endothelium, and this was accompanied by suppressed or delayed responses to radiation damage. For example, ROS generation in irradiated epithelium was significantly lower when endothelium was not present (**Supplementary Fig. S3a,b**). Moreover, in the absence of endothelium, no changes in paracellular barrier function were observed even as late as 24 h and 48 h after radiation (**Supplementary Fig. S3c**). Thus, based on our observations, the endothelium appears to be the principal target of intestinal radiation injury, which is consistent with recent *in vivo* findings[46].

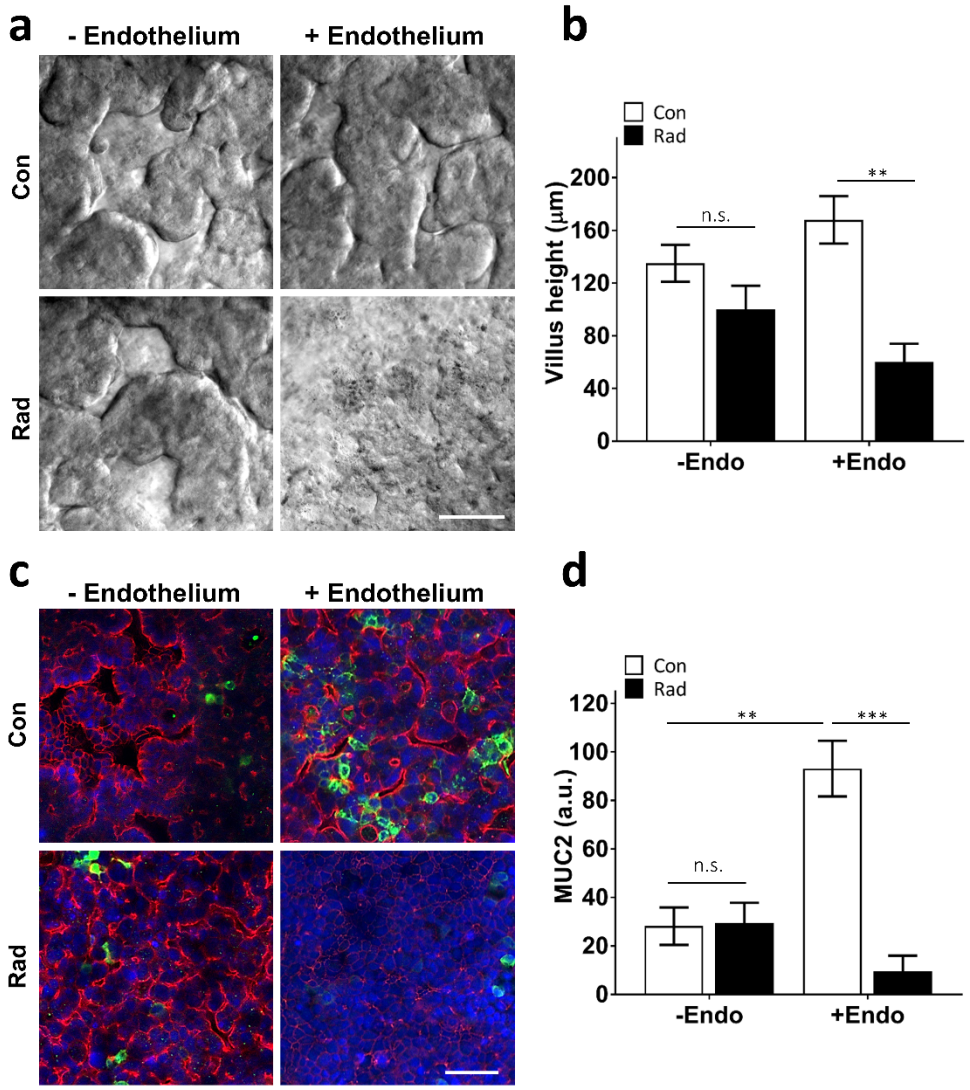

Figure II-6. Vascular endothelium mediates the radiation damage. (**a**) DIC microscopic views showing the villus morphology of the human Caco-2 intestinal epithelium cultured with and without human vascular endothelium under control conditions (Con) or after radiation exposure (Rad) (bar, 50 μm). (**b**) Quantification of villus heights measured under the conditions described in **a** (n=3; **P<0.01; n.s., not significant). (**c**) Representative immunofluorescence confocal micrographs of the Gut Chip device with the villus intestinal epithelium stained for epithelial tight junctions, ZO-1 (red) and intestinal mucin protein, MUC-2 (green) (blue, DAPI-stained nuclei; bar, 50 μm). (**d**) Quantification of fluorescence intensities (a.u.) of MUC-2 normalized per cell number under the conditions shown in **c** (n=3; **P<0.01, ***P<0.001; n.s., not significant).

Radio-protective effects of a potential radiation countermeasure drug. Pharmacologic strategies for preventing or treating radiation-induced intestinal injury are currently very limited; however, a recent study showed that the prolylhydroxylase inhibitor, DMOG, partially prevented murine intestinal wall dysfunction when administered before abdominal irradiation[47]. DMOG elevates levels of Hif-1α and HIF-2α, which are known to promote cell survival under conditions of stress, such as ionizing radiation[19,48]. Similar to the *in vivo* finding, we found that DMOG pre-treatment prevented cell detachment (**Fig. 5a-c**), suppressed the increase in intestinal permeability (**Fig. 4d**), increased MUC2 expression (**Supplementary Fig. 5a,b**) and reduced villus injury (**Fig. 4e**), as evidenced by enhanced expression of ZO-1 (**Fig. 5a**) and increased villus height (**Fig. 4a,b**) in irradiated Gut Chips. In addition, we discovered that pre-treatment of cells with DMOG significantly reduced the number of cells undergoing apoptosis in both the epithelium and endothelium (**Fig. 2b,c**), in addition to inhibiting both ROS generation (**Fig. 3a,b**) and lipid peroxidation (**Fig. 3c,d**) in these cells. As expected this was associated with increased expression of Hif-1α and HIF-2α (**Supplementary Fig. S4a-d**), which is known to prevent ROS generation[49] as well as inhibit apoptosis[50,51]. Interestingly, we also found that DMOG prevents DNA fragmentation (**Fig. 3e,f**), which has never been described previously. Thus, again, the human Gut Chip mimicked the protective effects of this potential radiation countermeasure drug that were previously observed in animal models of intestinal inflammation[51–53].

DISCUSSION

In the present study, we leveraged a mechanically active, microfluidic Gut Chip device to model human intestinal radiation injury *in vitro*. The human Gut Chip recapitulates clinically relevant acute radiation injuries at both cellular and tissue-organ levels. Radiation induces loss of junctional continuity, compromises intestinal barrier function, and inhibits mucus production, in addition to promoting villus blunting and distortion of microvilli. Our data show that the endothelium appears to be more sensitive to radiation injury in terms of ROS generation, lipid peroxidation and DNA fragmentation, which first triggers rapid endothelial apoptosis that then appears to trigger subsequent epithelial cell injury responses, as previously described to *in vivo*[14,33]. Moreover, pre-treatment with a potential MCM drug, DMOG, significantly reduced radiation toxicity in epithelium and endothelium in this *in vitro* model, again mimicking responses that have been previously observed *in vivo*[47].

Because of the urgent need for predictive intestinal radiation models, previous studies have explored the use of other types of *in vitro* cultures, including organoids and Transwell co-culture systems[11,54]. However, they were found to be limited in their ability to replicate normal human intestinal 3D architecture and function, and thus, they could not recapitulate important features of radiation responses, such as villus blunting, which have been observed in human patients. Our results suggest that these past models were ineffective because they failed to recreate the physiologically relevant physical microenvironment of the intestine, including fluid flow and peristalsis-like mechanical deformations, which are present in the human Gut Chip. Moreover, unlike our experimental system, past *in vitro* models did not contain human endothelial cells that are known to serve as key contributors to radiation-induced intestinal dysfunction[15,16].

For example, using the vascularized human Gut Chip, we found that the endothelium responds faster to ionizing radiation compared to the epithelium, with endothelial cells exhibiting an increase in apoptosis within 24 hours after exposure, while epithelial cell death increased over the following day. This is consistent with the past finding that while exposure of mice to γ-radiation results in loss of intestinal villi beginning approximately 24-36 hours after exposure, little apoptotic activity was observed in the intestinal epithelium during the first day[12,55]. Moreover, when Gut Chips were lined by epithelium in the absence of endothelium, we did not detect radiation-induced villus blunting, loss of barrier function, or decreased mucus secretion, confirming that endothelial cells mediate the intestinal radiation injuries as suggested by previous *in vivo* studies[15,16]. In addition, we found out that radiation-induced ROS generation by intestinal epithelium cultured on-chip alone was significantly lower than when it was co-cultured with endothelium. These data suggest that enhanced ROS generation by the endothelium may play a pivotal role in regulating intestinal radiation damage, and hence that it could serve as a target for therapeutics that mitigate radiation toxicity, as suggested by recent *in vivo* reports[25,46]. Although radiation damage is often coordinated by the intracellular actions of ROS[56], further investigation of other potential radiation-mediators, such as inflammatory cytokines, are required to fully understand the crosstalk between epithelial and endothelial cells in response to radiation exposure.

In summary, the results we obtained are fully consistent with past studies which revealed that the microvascular endothelium is the initial target of radiation damage, and that endothelial apoptosis is upstream of damage to the intestinal epithelium[33,35,57]. Other studies have also demonstrated that radiation-induced epithelial cell injury and

DNA damage are mediated via endothelial apoptosis and ROS generation[15,33–35], which trigger cytoskeletal changes and structural alterations within the endothelial cell monolayer[58].

The changes in endothelial cell and tissue architecture that we observed are consistent with the immediate morphological hallmarks of radiation that have been reported to occur in the vascular compartment in patients at clinically relevant doses[59,60]. In addition, the radiation-induced changes in the epithelium we observed in the Gut Chip, ranging from villus blunting to distortion of the tips of the villi to their complete villus, are consistent with clinical findings in patients and animals exposed to ionizing radiation[37,61]. A similar level of damage to apical microvilli at the apical epithelial cell surface also has been reported in both human and mouse irradiated tissues[36,62].

Importantly, we demonstrated that the Gut Chip radiation model can be used to evaluate therapeutic response of potential radiation countermeasure drugs. As a proof-of-concept, we showed that DMOG, which is known to protect murine intestine against radiation damage by stabilizing HIF levels[63], has similar effects in the human Gut Chip. Interestingly, the radioprotective effects of this drug on human cells and tissues have not been previously reported, and thus, our findings provide hope that this potential therapeutic approach could be useful in humans. In addition to replicating effects of DMOG previously observed at tissue and organ level *in vivo* [47], our results also unveiled some novel features of DMOG action at the cell level, including its ability to prevent DNA fragmentation, which also has not been previously described. In the future, our intestinal radiation model could be harnessed to study the safety and efficacy of other

radioprotectants that contain a free radical-scavenging group, such as amifostine, which has been reported to reduce DSB accumulation[46,64].

We used the established human Caco-2 intestinal epithelial cell line in the present study because it reproducibly undergoes intestinal differentiation and exhibits villi formation as well as transcriptional signatures reminiscent of the ileum when cultured within the mechanically active Gut Chip model[10,17,18]. However, two important caveats require consideration when interpreting the results of this study with respect to the effects of radiation on intestinal toxicity. The first is that the Caco-2 cell line was originally isolated from a colon tumor, and thus, while it can recapitulate many features of the human ileum when analyzed at the transcriptional level[18], it does not fully express the phenotype of a normal human intestine. These tumor-derived Caco-2 intestinal epithelial cells also might differ in their sensitivity to radiation as compared to normal epithelial and endothelial cells, so further studies are required to fully elucidate the cross-talk between the two tissue layers in response to radiation. Specifically, this approach could be further strengthened by integrating primary human intestinal epithelial cells which might be more radio-sensitive into the model in the future (*e.g.*, by isolating cells from clinical biopsy samples), and this could enable one to evaluate patient-specific responses to radiation as well. Second, while we were capable of replicating multiple clinical responses of intestinal epithelium and endothelium to radiation, other cells, including immune cells and commensal microbiome that are present within the intestinal microenvironment are believed to play a pivotal role in small intestine radiation toxicity *in vivo*[65,66]. Thus, it will be interesting to explore how the

presence of these other cell types in the model might influence intestinal epithelial and endothelial responses to radiation in the future.

When animals or humans are exposed to total body radiation doses that lead to severe enterocyte depletion, lethality is mainly due to the combined effect of endothelial injury, GI damage and bone marrow failure[7]. Therefore, Past studies focused on preventing GI damage that utilized *in vivo* total body radiation models may therefore have had limited clinical relevance[46]. In contrast, the human Gut Chip radiation model offers the unique capability to analyze the direct effects of radiation toxicity on cells and tissues within a single organ, in the absence of contributions from other organs and systemic factors. However, different vascularized human Organ Chips can be linked by their common endothelium-lined vascular channels to create an effective 'human Body-on-Chips', which could then be used to explore how partial or whole body exposure to radiation modifies the response of intestinal tissues contained within a linked Gut Chip. Using this organ-level synthetic biology approach, it should be possible to identify how individual molecular, cellular and physical factors contribute individually and in combination to radiation toxicity. In addition to enabling study of the underlying mechanisms involved in radiation-induced GI syndrome, the human Gut Chip offers a potentially powerful a tool for discovery and screening of new and more effective countermeasure drugs in the future.

Materials and Methods

Human Gut-on-a-Chip microdevice. The microfluidic Gut-on-a-Chip devices were fabricated from polydimethylsiloxane (PDMS; SYLGARD® 184 silicone elastomer kit) by

soft lithography technique as previously reported[17]. The intestinal epithelium and vascular endothelium channels shared same dimensions (1000 μm wide x 14 mm long x 200 μm high) and separated by a porous (10 μm diameter pores with 25 μm spacing) PDMS membrane (50 μm high). Prior to cell seeding, both microchannels were activated using oxygen plasma (Diener ATTO; pressure, power and plasma time were 0.5 mbar, 30 W and 2 min, respectively), functionalized with (3-Aminopropyl)trimethoxysilane (Sigma, 281778), washed by flowing absolute ethanol (Sigma, E7023) and dried in a 80 C oven. Microchannels were then coated with type I collagen (30 μg ml^{-1}; Gibco, A10483-01) and Matrigel (100 μg ml^{-1}; BD Biosciences, 356237) in the serum-free Dulbecco's Modified Eagle Medium (DMEM; Gibco, 10564011) for 1 h at 37 C. To form vascular lumen, human endothelial cells (Human Umbilical Vein Endothelial Cells (HUVECs); Lonza, C2519A (pooled donor)) cultured in endothelial growth medium (DMEM/F12 (Gibco, 11039-021) plus EGM-2 BulletKit containing 100 U L^{-1} penicillin/100 mg ml^{-1} streptomycin (Pen/Strep; Gibco, 15140-122), hydrocortisone, hFGF-B, VEGF, R^3-IGF-1, ascorbic Acid, hEGF, GA-1000, heparin and 2% FBS; Lonza, CC-4176) were first introduced to the lower microchannel and incubated for 1 h to attach on bottom side of the channel. Afterwards, HUVECs were seeded on the opposite side of the porous membrane in the lower channel by immediate flipping the entire chip upside down and placing it in an incubator for 1 h. The device was flipped over again and human intestinal epithelial cells (Caco2 BBE human colorectal carcinoma cell, Harvard digestive Disease Center) grown in DMEM (Gibco, 10564011) containing Pen/Strep 20% Fetal Bovine Serum (FBS; Gibco, 10082-147) were seeded ($1.5x10^5$ cells cm^{-2}) into the top microchannel of the device and being

allowed to adhere statically for 1 h. Gut chip was then cultured statically in incubator for an overnight to form monolayer. A day after seeding, epithelial medium (DMEM/20%FBS/antibiotics) and endothelial medium with reduced FBS (0.5%) were perfused at 60 μL h^{-1} through top and bottom channels, respectively. To mimic peristalsis-like motions, cyclic stretching (10% strain; 0.15 Hz) was applied through vacuum chambers via a vacuum controller 2 days after seeding. 5 days after seeding, villus intestinal epithelium spontaneously appeared in top channel and endothelial vascular lumen formed in bottom channel. Endothelium-free chips were similarly prepared using the above procedure, except that after coating the chips with ECM, they were seeded with human intestinal epithelial cells (Caco2) in top channel without adding endothelial cells to the bottom channel.

Chip Radiation. Gut-on-a-Chip microdevices containing villus intestinal epithelium (with or without endothelium) were removed from the syringe pump, immediately transferred to irradiation facility and exposed to a single 8 Gy dose of gamma-irradiation (Cs-137; Gammacell 40 Exactor) at 0.98 Gy min^{-1}. Temperature of Irradiation chamber was kept at 37 C thorough the procedure and no temperature fluctuations were observed. To treat the control chips similarly, they were brought to irradiation facility and back without being exposed to irradiation. To validate the prophylactic effect of dimethyloxalylglycine (DMOG) in our Gut-on-a-Chip devices, DMOG (Sigma, D3695) reconstituted in UltraPure DNase/RNase-free distilled water (Gibco, 10977015) and added to epithelium and endothelium channels at 1 mM an overnight before irradiation procedure. Control chips (vehicle) received only distilled water.

Morphological analyses. Morphological analyses were performed using at least 3 independent gut chip samples at each interval, where images of villi were taken at more than 10 different locations. The intestinal villus morphology was evaluated using differential interface contrast (DIC) microscopy (Zeiss Axio Observer Z1 2, AXIO2). The villus microarchitecture was also studied using immunoflorescnece microscopy with a laser scanning confocal microscopes (Leica SP5 X MP DMI-6000 and Zeiss TIRF/LSM 710) inked to a 405-nm diode laser, a white light laser (489-670 nm), or an argon laser (488 nm and 496 nm) and coupled to a photo-multiplier tube or HyD detectors. Acquired images were analyzed using IMARIS (MARIS 7.6 F1 workstation; Bitplane Scientific Software) and ImageJ. High-resolution horizontal or vertical cross-sectional images were obtained using deconvolution (Huygens) followed by a 2D projection process.

For scanning electron microscopy (SEM) analysis, gut chips were designed in a way that top channel was not irreversibly bonded to the membrane, which permitted the device to be dismantled manually without disturbing the cultured cells. Cells were fixed with paraformaldehyde (PFA, 4%; Electron Microscopy Sciences, 157-4) and Glutaraldehyde (2.5%; Sigma, G7776) and incubated in osmium tetroxide (0.5%; Electron Microscopy Sciences, 19152) before serial dehydration in ethanol. Samples were then dried using hexamethyldisilazane (HMDS; Electron Microscopy Sciences, 999-97-3) and imaged with a field emission SEM (Tescan Mira GMU, Czech Republic).

Paracellular permeability measurements. To measure intestinal permeability, 50 μg ml^{-1} of cascade blue (5.9 kDa; ThermoFisher, C687) were introduced to the top channel

of the chips at 60 mL hr^{-1} and fluorescence intensity of top and bottom channel effluents at excitation/emission wavelengths of 390 nm/420 nm were measured using a multi-mode plate reader (BioTekNEO) at different intervals. Apical-to-basolateral flux of the paracellular marker was calculated according to the following equation: Papp=(dQ/dt)/A.dC, where Papp (cm s^{-1}) denotes the apparent permeability coefficient, dQ/dt (g s^{-1}) is molecular flux, A (cm^2) is the total area of diffusion and dC (mg mL^{-1}) is average gradient.

Detection of reactive oxygen species (ROS) and lipid peroxidation (LPO). Immediately after irradiation procedure, cellular ROS and LPO were detected using CellROX Green (Life Technologies, C10444) and Image-iT Lipid Peroxidation Kit (Life Technologies, C10445), respectively, according to the manufacturer's protocol. The signal intensity of intracellular levels of ROS was measured at excitation/emission wavelengths of 485 nm/520 nm (green), and ratios of emission peak from the 590 nm (red) to 510 nm (green) were used to quantify lipid peroxidation in chips.

Cellular toxicity and apoptosis. *LDH activity assay:* CytoTox 96 Non-Radioactive Cytotoxicity Assay (LDH; Promega, G1780) was used according to the manufacturer's instructions to measure epithelium and endothelium death rate at different intervals after irradiation procedure and DMOG treatments. In brief, effluents were collected from top and bottom channels, mixed with LDH substrate reagent and incubated for 30 min. The enzymatic reaction was terminated using stop solution (containing acetic acid) and the absorbance at 492 nm was recorded using a multi-mode plate reader (BioTekNEO).

The LDH activity was assessed using quadruplicate of each group, calculated after subtracting the background absorbance values and reported as a fold change of the total LDH values of control group.

TUNEL assay: Late apoptosis was evaluated by the terminal deoxynucleotidyl transferase-mediated dUTP-biotin nick-end labeling (TUNEL) immunostaining using Click-iT TUNEL Alexa Fluor Assay Kit (Invitrogen, C10247) according to the manufacturer's protocol. Chips were co-stained with DAPI (Invitrogen, D1306) as the nuclear DNA marker and the apoptotic cells were counted from 20 different fields (5 fields each from 4 replicates) to get an average number of TUNEL-positive cells per field.

Immunofluorescence microscopy. For immunofluorescence staining, cells in both channels were first gently washed with PBS, then fixed with paraformaldehyde (PFA, 4%; Electron Microscopy Sciences, 157-4) for 20 min and subsequently washed with additional PBS. Cells were then permeabilized with 0.25% Triton X-100 (0.25%; Sigma, T8787) for 20 min and incubated with blocking buffer containing 1% BSA (Sigma, A4503) and 10% donkey serum (Sigma, D9663) for 30 min at room temperature. Cells were then incubated with antibodies directed against ZO1 (Life Technologies, 33-9100, dilution 1:200), PECAM-1/CD31 (eBioscience, BMS137, dilution 1:100), VE-cadherin/CD144 (BD Biosciences, 555661, dilution 1:200), Villin (Life Technologies, PA5-29078, dilution 1:100), 53BP1 (Abcam, ab36823, dilution 1:100), MUC2 (Santa Cruz Biotechnology, sc-15334, dilution 1:100) or HIF-1α (Abcam, ab16066, dilution 1:100) overnight at 4 C, followed by 6 x 5 min PBS washes. Secondary antibodies (Life

Technologies) were then introduced in the channels for 1 h at room temperature and washed 3 times with PBS. Cells were co-stained with DAPI (Invitrogen, D1306). Microscopy was performed with a laser scanning confocal microscopy (Leica SP5 X MP DMI-6000 or Zeiss TIRF/LSM 710). Quantification of the immunofluorescence images was performed using ImageJ software based on the mean fluorescence intensity on a per cell basis.

Western Blot. To perform Western blot analysis, cell lysates were obtained using RIPA (Alfa Aesar, J63306) buffer supplemented with protease inhibitor cocktail (Roche). Followed by SDS-PAGE fractionation, samples were transferred to a nitrocellulose membrane according to the manufacturer's protocol (BioRad). Westerns were run using precast gradient gels (4−15%, Biorad), with the same amount of protein load in each lane of an individual gel, and the relevant protein ranges were cut out and blotted with the individual antibodies. After blocking the membranes with 5% non-fat milk in TBST (50 mM Tris-HCL, 150 mM NaCl, 0.1% Tween-20), samples were incubated with antibodies against HIF-1α (R&D Systems, MAB1536, dilution 1:500), HIF-2α (Abcam, ab73895, dilution 1:500) and GAPDH (Santa Cruz Biotechnology, sc-32233, dilution 1:500). A horseradish-peroxidase-conjugated goat anti-rabbit or -mouse antibody was then added, and the membranes were developed with the ECL Plus system (GE Healthcare) according to the manufacturer's protocol.

Statistical analysis. All experiments were carried out at n=3-6 (see figure captions), and results and error bars in this article are presented as mean ± standard error of the

mean (s.e.m). Data analysis was performed with a one-way analysis of variance (ANOVA) with Tukey HSD post hoc tests, using Graphpad Prism software. Statistical analysis between two conditions was performed by an unpaired student's t-test. P values of less than 0.05 were considered to be statistically significant (*P<0.05, **P<0.01, ***P<0.001).

Acknowledgements

This research was supported by the U.S. FDA grant HHSF223201310079C, the Wyss Institute for Biologically Inspired Engineering at Harvard University and Fundação para a Ciência e a Tecnologia (FCT) Portugal (project PD/BD/105774/2014 to the Institute for Bioengineering and Biosciences). We are grateful to A. Chalkiadaki, A. Wen, D. Chou and V. Frismantas for their insightful discussions. We also thank M. Cronce, E. Calamari, and Y. Chou for their expert technical assistance.

Author contributions

S.J-F., R.P-B., H.J.K., J.M.S.C., O.L. and D.E.I. designed the research. S.J-F, A.J., T.M., J.W., R.P. and H.J.K. performed experiments. S.J-F., R.P-B., T.F., O.L. and D.E.I. analyzed data. S.J-F., O.L. and D.E.I. wrote the paper with input from all the authors.

Competing financial interests

D.E.I. holds equity in Emulate, Inc., consults to the company, and chairs its scientific advisory board.

References

1 Hauer-Jensen M, Denham JW, Andreyev HJN. Radiation Enteropathy – Pathogenesis, Treatment, and Prevention. *Nat Rev Gastroenterol Hepatol* 2014; **11**: 470–479.

2 Shadad AK, Sullivan FJ, Martin JD, Egan LJ. Gastrointestinal radiation injury: Symptoms, risk factors and mechanisms. *World J Gastroenterol WJG* 2013; **19**: 185–198.

3 Yu J. Intestinal stem cell injury and protection during cancer therapy. *Transl Cancer Res* 2013; **2**: 384–396.

4 Singh VK, Romaine PLP, Newman VL. Biologics as countermeasures for acute radiation syndrome: where are we now? *Expert Opin Biol Ther* 2015; **15**: 465–471.

5 Booth C, Tudor G, Tudor J, Katz BP, MacVittie T. The Acute Gastrointestinal Syndrome in High-Dose Irradiated Mice. *Health Phys* 2012; **103**: 383–399.

6 Williams JP, Brown SL, Georges GE, Hauer-Jensen M, Hill RP, Huser AK *et al.* Animal Models for Medical Countermeasures to Radiation Exposure. *Radiat Res* 2010; **173**: 557–578.

7 Koenig KL, Goans RE, Hatchett RJ, Mettler FA, Schumacher TA, Noji EK *et al.* Medical Treatment of Radiological Casualties: Current Concepts. *Ann Emerg Med* 2005; **45**: 643–652.

8 Augustine AD, Gondré-Lewis T, McBride W, Miller L, Pellmar TC, Rockwell S. Animal models for radiation injury, protection and therapy. *Radiat Res* 2005; **164**: 100–109.

9 Kahn J, Tofilon PJ, Camphausen K. Preclinical models in radiation oncology. *Radiat Oncol Lond Engl* 2012; **7**: 223.

10 Kim HJ, Huh D, Hamilton G, Ingber DE. Human gut-on-a-chip inhabited by microbial flora that experiences intestinal peristalsis-like motions and flow. *Lab Chip* 2012; **12**: 2165–2174.

11 Morini J, Babini G, Barbieri S, Baiocco G, Ottolenghi A. The Interplay between Radioresistant Caco-2 Cells and the Immune System Increases Epithelial Layer Permeability and Alters Signaling Protein Spectrum. *Front Immunol* 2017; **8**: 223.

12 Potten CS, Booth C, Pritchard DM. The intestinal epithelial stem cell: the mucosal governor. *Int J Exp Pathol* 1997; **78**: 219–243.

13 Schuller BW, Binns PJ, Riley KJ, Ma L, Hawthorne MF, Coderre JA. Selective irradiation of the vascular endothelium has no effect on the survival of murine intestinal crypt stem cells. *Proc Natl Acad Sci U S A* 2006; **103**: 3787–3792.

14 Folkman J, Camphausen K. What Does Radiotherapy Do to Endothelial Cells? *Science* 2001; **293**: 227–228.

15 Paris F, Fuks Z, Kang A, Capodieci P, Juan G, Ehleiter D *et al.* Endothelial apoptosis as the primary lesion initiating intestinal radiation damage in mice. *Science* 2001; **293**: 293–297.

16 Garcia-Barros M, Paris F, Cordon-Cardo C, Lyden D, Rafii S, Haimovitz-Friedman A *et al.* Tumor response to radiotherapy regulated by endothelial cell apoptosis. *Science* 2003; **300**: 1155–1159.

17 Kim HJ, Li H, Collins JJ, Ingber DE. Contributions of microbiome and mechanical deformation to intestinal bacterial overgrowth and inflammation in a human gut-on-a-chip. *Proc Natl Acad Sci* 2016; **113**: E7–E15.

18 Kim HJ, Ingber DE. Gut-on-a-Chip microenvironment induces human intestinal cells to undergo villus differentiation. *Integr Biol Quant Biosci Nano Macro* 2013; **5**: 1130–1140.

19 Ayrapetov MK, Xu C, Sun Y, Zhu K, Parmar K, D'Andrea AD *et al.* Activation of Hif1α by the prolylhydroxylase inhibitor dimethyoxalyglycine decreases radiosensitivity. *PloS One* 2011; **6**: e26064.

20 Gayer CP, Basson MD. The effects of mechanical forces on intestinal physiology and pathology. *Cell Signal* 2009; **21**: 1237–1244.

21 López M, Martín M. Medical management of the acute radiation syndrome. *Rep Pract Oncol Radiother* 2011; **16**: 138–146.

22 Thiagarajah JR, Gourmelon P, Griffiths NM, Lebrun F, Naftalin RJ, Pedley KC. Radiation induced cytochrome c release causes loss of rat colonic fluid absorption by damage to crypts and pericryptal myofibroblasts. *Gut* 2000; **47**: 675–684.

23 Kirichenko AV, Mason K, Straume M, Teates CD, Rich TA. Nuclear scintigraphic assessment of intestinal dysfunction after combined treatment with 9-amino-20(S)-camptothecin (9-AC) and irradiation. *Int J Radiat Oncol* 2000; **47**: 1043–1049.

24 Colon J, Hsieh N, Ferguson A, Kupelian P, Seal S, Jenkins DW *et al.* Cerium oxide nanoparticles protect gastrointestinal epithelium from radiation-induced damage by reduction of reactive oxygen species and upregulation of superoxide dismutase 2. *Nanomedicine Nanotechnol Biol Med* 2010; **6**: 698–705.

25 Hatoum OA, Otterson MF, Kopelman D, Miura H, Sukhotnik I, Larsen BT *et al.* Radiation induces endothelial dysfunction in murine intestinal arterioles via enhanced production of reactive oxygen species. *Arterioscler Thromb Vasc Biol* 2006; **26**: 287–294.

26 Hatoum OA, Binion DG, Phillips SA, O'Loughlin C, Komorowski RA, Gutterman DD *et al.* Radiation induced small bowel 'web' formation is associated with acquired microvascular dysfunction. *Gut* 2005; **54**: 1797–1800.

27 Barrera G. Oxidative Stress and Lipid Peroxidation Products in Cancer Progression and Therapy. *Int Sch Res Not* 2012; **2012**: e137289.

28 Kiang JG, Fukumoto R, Gorbunov NV. Lipid Peroxidation After Ionizing Irradiation Leads to Apoptosis and Autophagy. 2012. doi:10.5772/48189.

29 Jagetia GC, Reddy TK. Modulation of radiation-induced alteration in the antioxidant status of mice by naringin. *Life Sci* 2005; **77**: 780–794.

30 Wang M, Saha J, Hada M, Anderson JA, Pluth JM, O'Neill P *et al.* Novel Smad proteins localize to IR-induced double-strand breaks: interplay between TGFβ and ATM pathways. *Nucleic Acids Res* 2013; **41**: 933–942.

31 Rappold I, Iwabuchi K, Date T, Chen J. Tumor Suppressor P53 Binding Protein 1 (53bp1) Is Involved in DNA Damage–Signaling Pathways. *J Cell Biol* 2001; **153**: 613–620.

32 Panier S, Boulton SJ. Double-strand break repair: 53BP1 comes into focus. *Nat Rev Mol Cell Biol* 2014; **15**: 7–18.

33 Maj JG, Paris F, Haimovitz-Friedman A, Venkatraman E, Kolesnick R, Fuks Z. Microvascular function regulates intestinal crypt response to radiation. *Cancer Res* 2003; **63**: 4338–4341.

34 Wang J, Boerma M, Fu Q, Hauer-Jensen M. Significance of endothelial dysfunction in the pathogenesis of early and delayed radiation enteropathy. *World J Gastroenterol* 2007; **13**: 3047–3055.

35 Ch'ang H-J, Maj JG, Paris F, Xing HR, Zhang J, Truman J-P *et al.* ATM regulates target switching to escalating doses of radiation in the intestines. *Nat Med* 2005; **11**: 484–490.

36 Trier JS, Browning TH. Morphologic response of the mucosa of human small intestine to x-ray exposure. *J Clin Invest* 1966; **45**: 194–204.

37 Carr KE. Effects of radiation damage on intestinal morphology. *Int Rev Cytol* 2001; **208**: 1–119.

38 Hauer-Jensen M. Late radiation injury of the small intestine. Clinical, pathophysiologic and radiobiologic aspects. A review. *Acta Oncol Stockh Swed* 1990; **29**: 401–415.

39 Carr ND, Pullen BR, Hasleton PS, Schofield PF. Microvascular studies in human radiation bowel disease. *Gut* 1984; **25**: 448–454.

40 Turner JR. Intestinal mucosal barrier function in health and disease. *Nat Rev Immunol* 2009; **9**: 799–809.

41 Baumgart DC, Dignass AU. Intestinal barrier function. *Curr Opin Clin Nutr Metab Care* 2002; **5**: 685–694.

42 Nejdfors P, Ekelund M, Weström BR, Willén R, Jeppsson B. Intestinal permeability in humans is increased after radiation therapy. *Dis Colon Rectum* 2000; **43**: 1582–1587.

43 Hasnain SZ, Wang H, Ghia J, Haq N, Deng Y, Velcich A *et al.* Mucin Gene Deficiency in Mice Impairs Host Resistance to an Enteric Parasitic Infection. *Gastroenterology* 2010; **138**: 1763–1771.e5.

44 Kim YS, Ho SB. Intestinal Goblet Cells and Mucins in Health and Disease: Recent Insights and Progress. *Curr Gastroenterol Rep* 2010; **12**: 319–330.

45 Jang H, Park S, Lee J, Myung J kyung, Jang W-S, Lee S-J *et al.* Rebamipide alleviates radiation‐induced colitis through improvement of goblet cell differentiation in mice. *J Gastroenterol Hepatol* doi:10.1111/jgh.14021.

46 Korpela E, Liu SK. Endothelial perturbations and therapeutic strategies in normal tissue radiation damage. *Radiat Oncol Lond Engl* 2014; **9**. doi:10.1186/s13014-014-0266-7.

47 Taniguchi CM, Miao YR, Diep AN, Wu C, Rankin EB, Atwood TF *et al.* PHD inhibition mitigates and protects against radiation-induced gastrointestinal toxicity via HIF2. *Sci Transl Med* 2014; **6**: 236ra64.

48 Semenza GL. Hypoxia-Inducible Factors in Physiology and Medicine. *Cell* 2012; **148**: 399–408.

49 Kim J, Tchernyshyov I, Semenza GL, Dang CV. HIF-1-mediated expression of pyruvate dehydrogenase kinase: A metabolic switch required for cellular adaptation to hypoxia. *Cell Metab* 2006; **3**: 177–185.

50 Greijer AE, van der Wall E. The role of hypoxia inducible factor 1 (HIF-1) in hypoxia induced apoptosis. *J Clin Pathol* 2004; **57**: 1009–1014.

51 Hirota SA, Beck PL, MacDonald JA. Targeting hypoxia-inducible factor-1 (HIF-1) signaling in therapeutics: implications for the treatment of inflammatory bowel disease. *Recent Pat Inflamm Allergy Drug Discov* 2009; **3**: 1–16.

52 Robinson A, Keely S, Karhausen J, Gerich ME, Furuta GT, Colgan SP. Mucosal Protection by Hypoxia-Inducible Factor Prolyl Hydroxylase Inhibition. *Gastroenterology* 2008; **134**: 145–155.

53 Cummins EP, Seeballuck F, Keely SJ, Mangan NE, Callanan JJ, Fallon PG *et al.* The Hydroxylase Inhibitor Dimethyloxalylglycine Is Protective in a Murine Model of Colitis. *Gastroenterology* 2008; **134**: 156–165.e1.

54 Ley S, Galuba O, Salathe A, Melin N, Aebi A, Pikiolek M *et al.* Screening of Intestinal Crypt Organoids: A Simple Readout for Complex Biology. *SLAS Discov* 2017; **22**: 571–582.

55 Potten CS. A Comprehensive Study of the Radiobiological Response of the Murine (BDF1) Small Intestine. *Int J Radiat Biol* 1990; **58**: 925–973.

56 Barker HE, Paget JTE, Khan AA, Harrington KJ. The tumour microenvironment after radiotherapy: mechanisms of resistance and recurrence. *Nat Rev Cancer* 2015; **15**: 409–425.

57 Rannou E, François A, Toullec A, Guipaud O, Buard V, Tarlet G *et al.* In vivo evidence for an endothelium-dependent mechanism in radiation-induced normal tissue injury. *Sci Rep* 2015; **5**: srep15738.

58 Gabryś D, Greco O, Patel G, Prise KM, Tozer GM, Kanthou C. Radiation effects on the cytoskeleton of endothelial cells and endothelial monolayer permeability. *Int J Radiat Oncol Biol Phys* 2007; **69**: 1553–1562.

59 Roth NM, Sontag MR, Kiani MF. Early effects of ionizing radiation on the microvascular networks in normal tissue. *Radiat Res* 1999; **151**: 270–277.

60 Baker DG, Krochak RJ. The Response of the Microvascular System to Radiation: A Review. *Cancer Invest* 1989; **7**: 287–294.

61 Carr KE, Hamlet R, Nias AH, Watt C. Damage to the surface of the small intestinal villus: an objective scale of assessment of the effects of single and fractionated radiation doses. *Br J Radiol* 1983; **56**: 467–475.

62 Carr KE, Hamlet R, Nias AHW, Watt C. Multinucleate giant enterocytes in small intestinal villi after irradiation. *J Microsc* 1981; **123**: 169–176.

63 Olcina MM, Giaccia AJ. Reducing radiation-induced gastrointestinal toxicity — the role of the PHD/HIF axis. *J Clin Invest* 2016; **126**: 3708–3715.

64 Liauw SL, Connell PP, Weichselbaum RR. New paradigms and future challenges in radiation oncology: an update of biological targets and technology. *Sci Transl Med* 2013; **5**: 173sr2.

65 Crawford PA, Gordon JI. Microbial regulation of intestinal radiosensitivity. *Proc Natl Acad Sci U S A* 2005; **102**: 13254–13259.

66 François A, Fabien M, Guipaud O, Marc B. Inflammation and Immunity in Radiation Damage to the Gut Mucosa. *BioMed Res Int* 2013; **2013**: e123241.

Supplementary Information

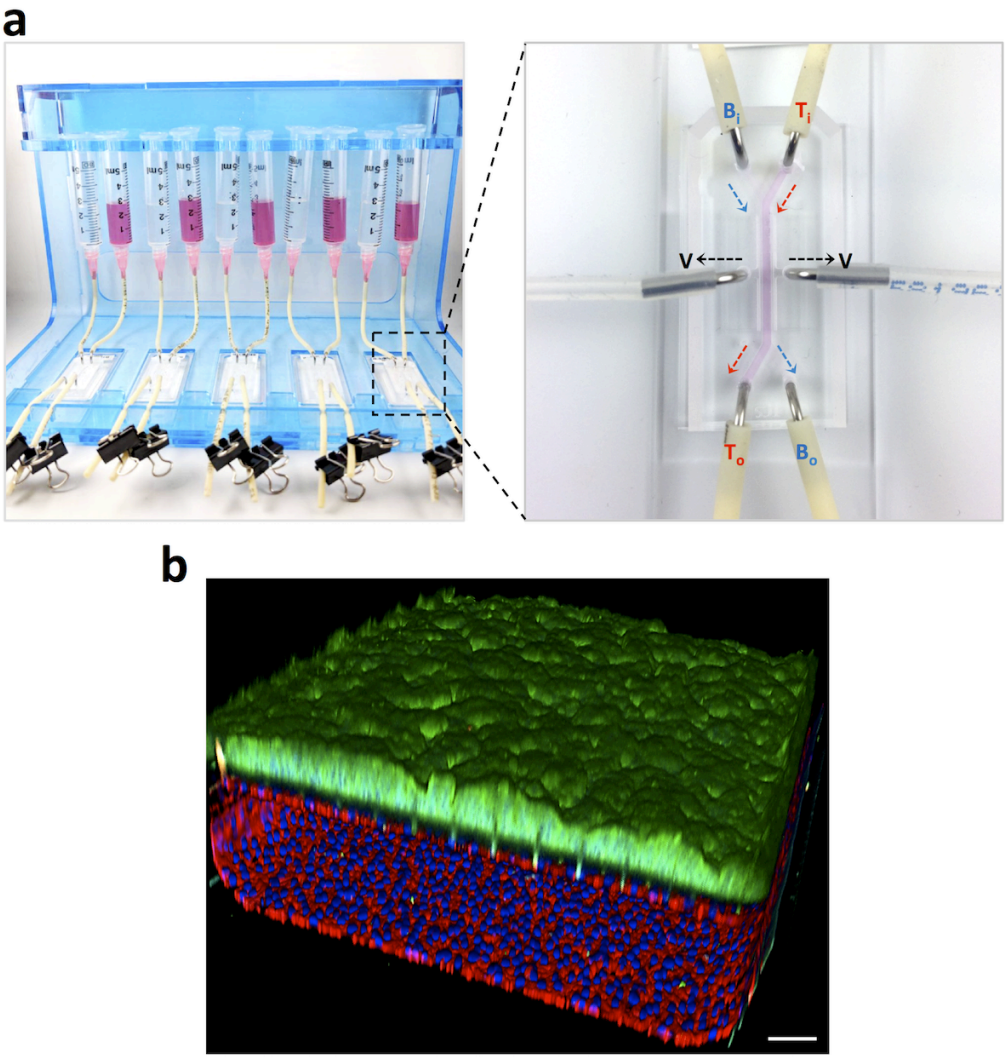

Supplementary Figure S1. (**a**) A photographic image of the Gut Chip operating setup (left) running 5 Gut Chip devices composed of clear PDMS elastomer connected to reservoirs containing epithelium (top, red) and endothelium (bottom, clear) media, and a higher magnification photograph of a single device (right). A syringe pump was used to perfuse medium through tubing from top and bottom channels inlets (T_i and B_i, respectively) towards outlet (T_o and B_o, respectively) while mechanical strain exerted by applying suction to the vacuum (V) chambers. (T, top channel; B, bottom channel; I, inlet; o, outlet). (**b**) Representative 3D confocal immunofluorescence micrographic reconstruction of the human villus intestinal epithelium interfaced with a human vascular endothelium surrounding a central lumen that formed inside the Gut Chip (green, villin; VE-Cadherin, red; DAPI-stained nuclei, blue; bar, 100 μm).

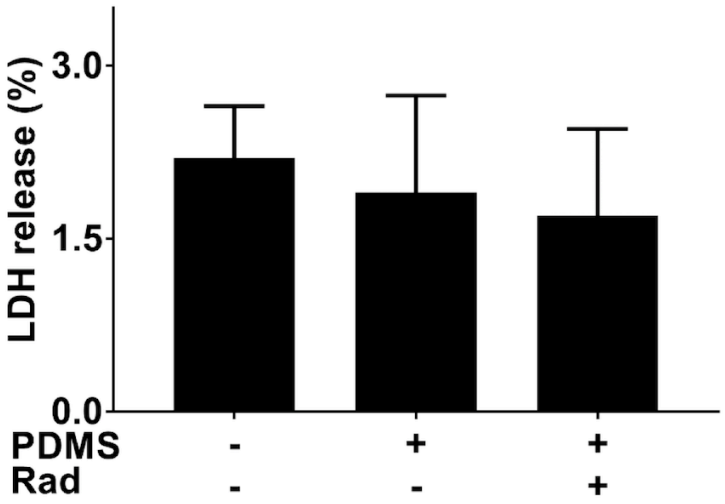

Supplementary Figure S2. Effect of materials leached from PDMS after exposure to γ-irradiation (8Gy) on the viability of intestinal epithelial cells cultured on the irradiated substrates compared to conventional plastic dishes, as assessed by LDH release.

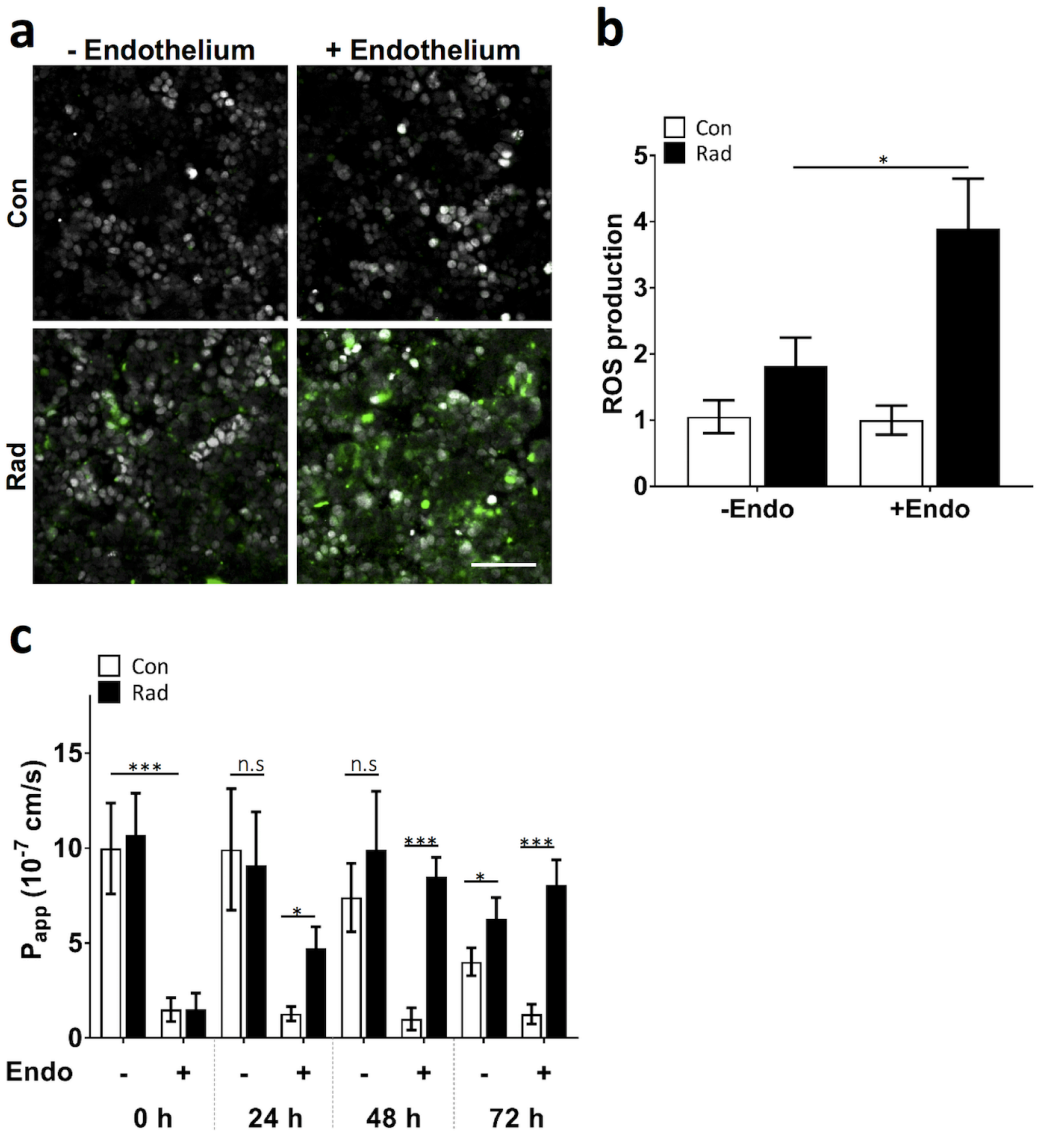

Supplementary Figure S3. (**a**) Radiation-induced changes in intracellular ROS in the intestinal epithelium cultured without (-Endothelium) or with (+Endothelium) endothelium in the lower channel in control (Con) and irradiated (Rad) chips, as visualized using the CellROX Green Reagent (green) (white, DAPI-stained nuclei; bar, 50 μm). (**b**) Quantification of ROS production measured under the conditions described in **a**, expressed as fold change relative to non-irradiated control cells (n=3; *P<0.05). (**c**) Changes in apparent paracellular permeability (P_{app}) measured by quantfying cascade blue transport across the tissue-tissue interface within the Gut Chip microdevices with (+) and without (-) presence of endothelium in control (Con) and irradiated (Rad) chips 24 h, 48 h and 72 h after exposure to γ-radiation (8Gy) (n=3; *P<0.05, ***P<0.001; n.s., not significant).

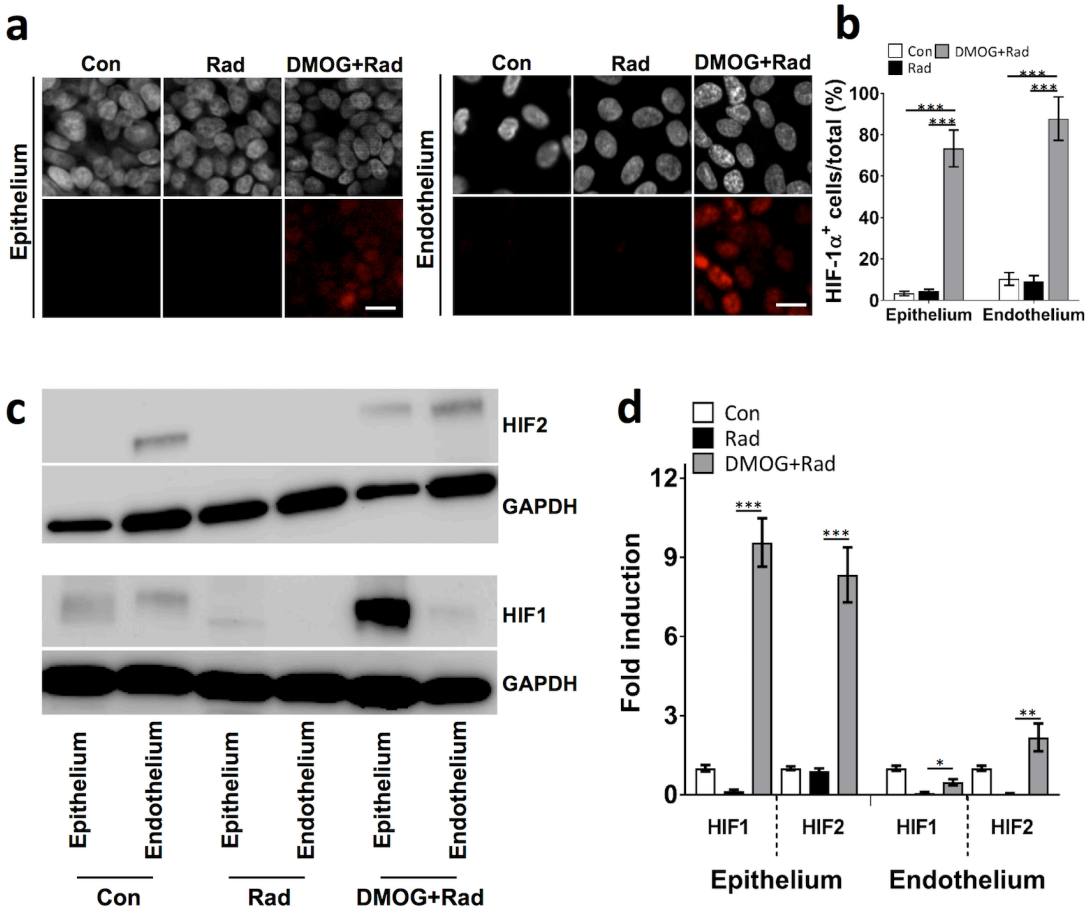

Supplementary Figure S4. Representative images of immunofluorescence staining of nuclei with DAPI (white) at the top and HIF1-α (red) at the bottom in human intestinal epithelial cells and endothelial cells before and after exposure to radiation (8Gy) without (Rad) or with DMOG pre-treatment (DMOG+Rad) (bar, 30 μm). (**b**) Graph showing the quantification of the percentage of epithelial and endothelial cells that expressed HIF1-α (HIF1-α+ cells) after exposure to the conditions shown in **a** (n=3; ***P<0.001). (**c**) Western blot analysis of HIF1-α and HIF2-α protein levels in control (Con), irradiated (Rad) and DMOG-treated (DMOG+Rad) chips. (d) Quantification of HIF1-α and HIF2-α levels from Western blots. GAPDH levels are shown to demonstrate equal loading. (Error bars represent mean ± SEM of relative band intensity values for n=4 chips in each group; *P<0.05, **P<0.01, ***P<0.001).

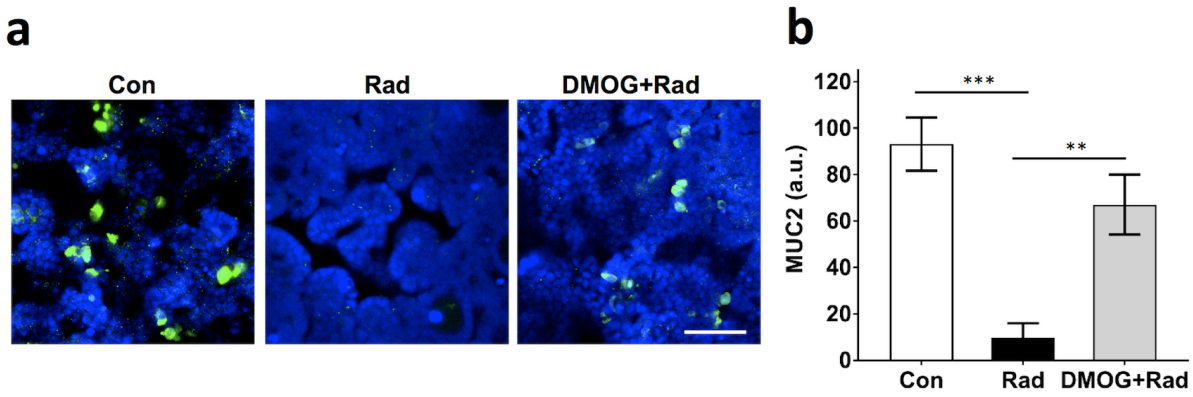

Supplementary Figure S5. (**a**) Immunofluorescence micrographs of intestinal epithelial cells cultured on-chip under control conditions (Con) versus after exposure to 8Gy radiation without (Rad) or with DMOG pre-treatment (DMOG+Rad), and stained for the intestinal mucin protein, MUC-2 (green) and nuclei (blue, stained with DAPI; bar, 30 μm). (**b**) Quantification of fluorescence intensities (a.u.) of MUC-2 normalized for equal cell number.

III. Chapter 3

Modeling radiation injury in a primary human Small Intestine-on-a-Chip

This chapter is based on the articles:

1) M. Kasendra[#], A. Tovaglieri[#], A. Sontheimer-Phelps, **S. Jalili-Firoozinezhad**, A. Bein, A. Chalkiadaki, W. Scholl, C. Zhang, H. Rickner, C. A. Richmond, H. Li, D. T. Breault, D. E. Ingber. "Development of a primary human Small Intestine-on-a-Chip using biopsy-derived organoids". *Scientific Reports*, 8, 1, 2871 (2018).

2) **S. Jalili-Firoozinezhad** et al. " Modeling radiation injury in a primary human Small Intestine-on-a-Chip". *In preparation.*

Abstract

Here we describe a method for fabricating a primary human Small Intestine-on-a-Chip (Intestine Chip) containing epithelial cells isolated from healthy regions of intestinal biopsies from different individuals. The primary epithelial cells are expanded as 3D organoids and subsequently seeded into one microchannel of an Organ Chip microfluidic device where they interface through a porous matrix-coated membrane with human intestinal microvascular endothelium cultured in a parallel microchannel under flow and cyclic deformation. This Intestine Chip recapitulates intestinal villus tissue morphology with multi-lineage differentiation similar to that of intestinal organoids, however, the apical surfaces of the polarized epithelial cells contact an open lumen with continuous fluid flow in the chip as they do *in vivo*. Transcriptomic analysis also indicates that the Intestine Chip more closely mimics whole human duodenum *in vivo* when compared to the duodenal organoids that were used to create the chips. Because fluids flowing through the lumen of the Intestine Chip can be collected continuously, sequential analysis of fluid samples can be used to quantify nutrient digestion, mucus secretion and establishment of intestinal barrier function over a period of multiple days *in vitro*. The Intestine Chip therefore may be useful as a research tool for many applications where normal intestinal function is crucial, including studies of metabolism, nutrition, infection, cancer progression, and drug pharmacokinetics, as well as personalized medicine.

Introduction

The small intestine is the major site for digestion, drug and nutrient absorption,

interaction with commensal microbiome, and development of mucosal immunity, as well as a primary site for many diseases, such as bacterial, viral and parasitic infections and inflammatory bowel disease. Because the lack of human-relevant responses has rendered many animal models unsuitable to study causal factors and treatment strategies for human intestinal infections and disorders[1], three-dimensional (3D) human tissue surrogates, such as intestinal organoids (also known as enteroids) have emerged as promising alternatives. These spheroidal *ex vivo* tissue cultures include $Lgr5^+$ intestinal stem cells[2] and are grown embedded within a complex extracellular matrix (ECM) gel (Matrigel) with Wnt3a, epidermal growth factor (EGF), Noggin and R-spondin 1 (collectively, WENR) to support their indefinite propagation[3,4]. Organoids faithfully recapitulate the cellular diversity of the intestinal epithelium and are ideally suited for *in situ* visualization and continuous monitoring of epithelial development and differentiation[4–8]. However, the presence of an enclosed lumen is non-physiological, as secreted material from goblet, enteroendocrine and Paneth cells, as well as shed apoptotic cells, accumulate within this central space instead of being removed through peristalsis and luminal flow. In addition, the inaccessibility of apical cell surface renders the use of organoids experimentally challenging for transport studies as well as exposure to living commensal microbiome or pathogenic bacteria for more than approximately one day in culture. Finally, organoid cultures lack a tissue-tissue interface, mechanical forces (fluid flow and peristalsis-like motions), immune cells, and a vascular compartment, which are all key contributors to normal intestinal physiology and disease development. Thus, there still remains a compelling need for more complex and physiologically relevant intestinal organ culture systems.

One alternative approach involves the use of 2-channel Organs-on-Chips (Organ Chips), which are microfluidic cell culture devices that contain two parallel hollow culture chambers lined by living human cells and separated by a porous ECM-coated membrane. These chips recapitulate normal tissue-tissue interfaces and mimic the complex physical and biochemical microenvironment of living human organs[9–23]. This technology has been previously applied to develop human Gut Chips that emulate many features of human intestinal structure and function, however, these studies utilized established human intestinal cell lines, such as Caco-2 or HT-29 cells[19–21,24], which were originally isolated from tumor samples and they harbor multiple gene mutations. In these studies, the intestinal cells also were either cultured alone or in the presence of a non-specialized endothelium (e.g., human umbilical vein endothelial cells)[21]. Thus, these human Gut Chips may not fully recapitulate normal human intestinal functions, and they would be inappropriate to use to study many important human conditions where genome fidelity is important (e.g., intestinal cancer, drug development, etc.). Other investigators have engineered *in vitro* intestine models using fetal intestinal tissue explants, but these progressively deteriorate after 24h of culture[25,26]. Thus, in the present study, we set out to develop a primary human Small Intestine Chip (Intestine Chip) using an approach that combines two of the most advanced tissue engineering technologies: intestinal organoids[3,4,27] and Organs-on-Chips (Organ Chips)[9,10].

The Intestine Chip contains normal human intestinal epithelial cells derived from organoids established from endoscopic biopsies or tissue resections of living human intestine, and intestinal tissue-specific microvascular endothelial cells. This microengineered environment recapitulates many key anatomical and functional

features of its *in vivo* small intestine counterpart including 3D intestinal tissue architecture, multi-lineage differentiation, epithelial barrier function, enzymatic activity of brush border enzyme and mucus production. Importantly, the transcriptome of the primary Intestine Chip more closely resembles that of adult human duodenum *in vivo* than the organoids that were used to plate the chips or other currently available intestinal cell culture models, including our previous Caco-2 Gut Chip, especially with regard to expression of genes relating to digestion, response to nutrients, cell proliferation, and host defense response to infection.

RESULTS

Establishing a primary human Intestine Chip. We set out to create an Organ Chip-based surrogate of the human small intestine that incorporates biopsy-derived epithelium, intestinal endothelial cells, physiological fluid flow and peristalsis-like mechanical motions that would allow analysis of human intestinal physiology and pathophysiology in a more *in vivo*-relevant culture microenvironment. Our initial focus was on developing a model that would enable longer term monitoring of host cell-pathogen interactions than is possible with conventional intestinal organoid cultures. To accomplish this, we first established organoid cultures using intestinal crypts derived from macroscopically normal regions of human intestinal endoscopic biopsies. Once the organoids matured (after 5 to 25 passages in culture), we then released organoid fragments through enzymatic treatment and finally seeded these fragments on the upper surface of the ECM-coated porous membrane of a microfluidic Organ Chip (**Fig. 1**). The polydimethylsiloxane (PDMS) chip devices we used contain two parallel, cell

culture microchannels: an upper ‘epithelial’ channel (1 mm high x 1 mm wide) and a lower ‘vascular’ channel (0.2 mm high x 1 mm wide) separated by a thin (50 μm) flexible PDMS membrane containing multiple pores (7 μm diameter, 40 μm spacing) coated with ECM (type I collagen and Matrigel) (**Fig. 1a**). Each microchannel has a dedicated inlet and outlet for the inoculation of human cells, molecules or microbes as well as for the precise control of physicochemical parameters through the perfusion of laminar flow of appropriate culture medium. Dedicated outlets provide means to collect effluents from the individual chambers for downstream characterization. The upper epithelial channel and lower vascular channel are surrounded on either side by two hollow (1 mm high x 300 μm wide) chambers that permit application of cyclic suction to mechanically stretch and relax the sidewalls, as well as the attached flexible PDMS membrane and adherent tissues in the central channel, thereby emulating peristaltic motions of a living human small intestine.

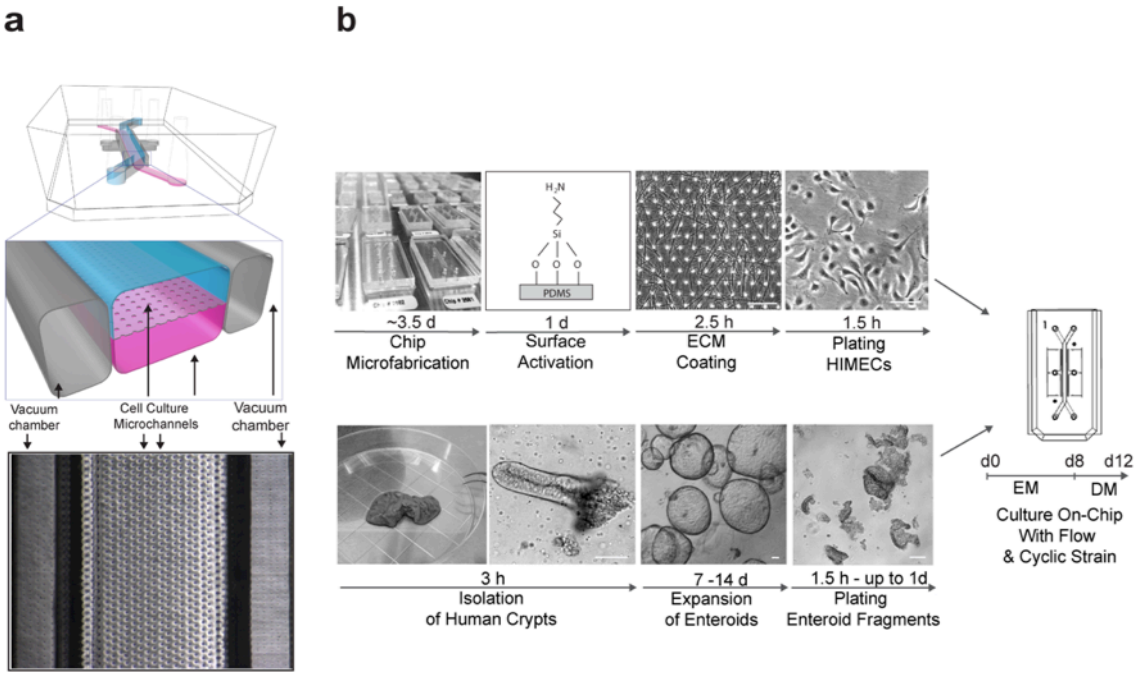

Figure III-1. Fabrication of the primary human Intestine Chip. (a) A schematic cross-sectional view (top) and a phase contrast micrograph of the chip viewed from above (bottom) showing the upper (epithelial; blue) and lower (microvascular; pink) cell culture microchannels separated by a porous, ECM-coated, PDMS membrane sandwiched in-between. The membrane is elastic and can be extended and retracted by the application of cyclic vacuum to the hollow side chambers. This actuation causes outward deflection of the vertical side walls and lateral extension of the attached horizontal, porous elastic membrane, which induces mechanical deformation of the adherent tissue layers cultured in the central channels. **(b)** Schematic representation of the step-by-step procedure involved in the establishment of microfluidic co-cultures of primary human intestinal epithelium and intestinal microvascular endothelium in the Intestine-Chip.

To obtain primary human intestinal epithelial cells, we utilized a previously published cell culture model based on 3D propagation of human intestinal crypts containing functional stem cells to create a bank of organoids derived from normal duodenal endoscopic biopsies or surgical specimens[3,4,28]. Duodenal organoids cultured for 3-5 days after passaging in expansion medium (EM) were than dissociated into fragments and plated in the epithelial channel of the microfluidic devices (**Fig.1b**). Organoids from the duodenal region of the small intestine were used in this study because they display higher culture efficiency than those formed from ileum or jejunum, as previously described[28].

We first cultured the organoid fragment-derived intestinal epithelial cells alone (without endothelium) in the upper channel, while perfusing both channels with epithelial expansion medium (EM). The large majority of cells initially appeared spread individually across the surface of the porous membrane at the start of the experiment and progressively grew to form a continuous epithelium that underwent villus morphogenesis over 8-12 days (**Supplementary Fig. S1a)**. This resulted in formation of a well-developed intestinal epithelium with a high density (~30 villi/cm^2) of characteristic finger-shaped, villus-like protrusions along the entire length of the upper channel by 12 days of culture, as detected by phase contrast (**Supplementary Fig.**

S1b), differential interference contrast (DIC) (**Fig. 2a**), and 3D confocal microscopy (**Fig. 2b**). Immunofluorescence staining of this villus intestinal epithelium for Ki67 and mucin 5AC (MUC5AC) confirmed the presence of proliferative Ki67-positive cells, which were limited to basal regions in close proximity to the PDMS membrane (**Fig. 2c**), much as they are restricted to basal intestinal crypts *in vivo*, whereas mucin producing cells were present primarily along the apical regions of the villi-like structures (**Fig. 2d**), again as is observed in living intestinal villi. Computerized image analysis revealed that these villus-like structures were significantly more elongated than the more spherical organoids from which they were derived, with the villi exhibiting average major and minor axes of 232 ± 17 and 122 ± 7 μm (mean ± SEM) compared to 256 ± 13 and 220 ± 11 μm for the organoids. In the course of these studies, we also found that more effective epithelial cell seeding and efficient monolayer formation can be achieved if organoid fragments are used, as single cell suspensions (produced using longer enzymatic dissociation times) do not expand as efficiently to develop a functional intestinal epithelial barrier (**Fig. 3a**), and whole organoids remain in their cystic spherical form and thus, never form a continuous monolayer (data not shown).

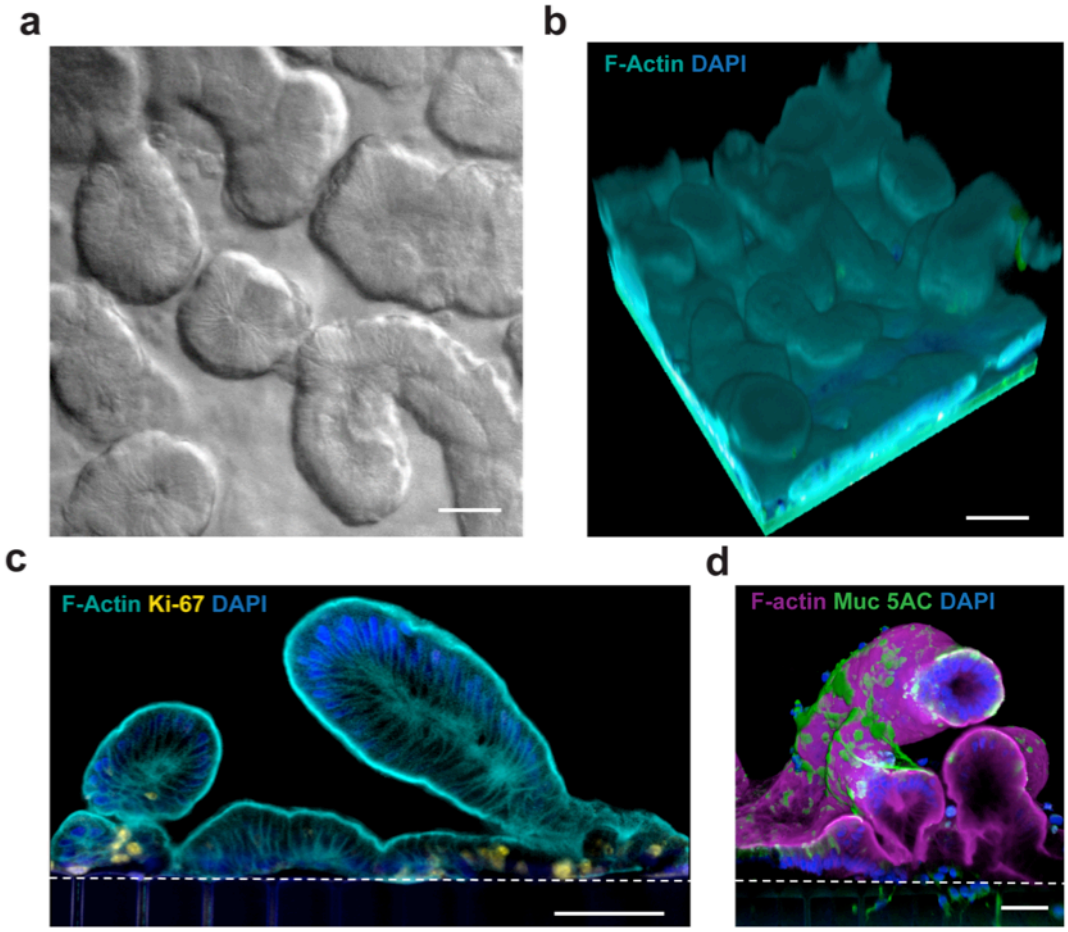

Figure III-2. Morphological analysis of Organ Chips lined by primary duodenal organoid-derived epithelial cells in the absence of endothelial cells. (a) Microscopic views showing the finger-like protrusions of the primary intestinal epithelium cultured on-chip for 12 days under continuous flow (60 µl hr^{-1}), when viewed from above by DIC imaging. **(b)** Representative 3D reconstruction of confocal immunofluorescence micrographs of organoid-derived intestinal epithelium grown on-chip (magenta, F-actin; blue, DAPI-stained nuclei). **(c)** Representative vertical cross sectional view of confocal microscopic images showing intestinal epithelium immunostained for F-actin (magenta) and Ki67 (yellow). **(d)** Representative vertical cross sectional, confocal, micrographic views through the intestinal epithelium-membrane interface of the intestinal epithelium grown on-chip when immunostained for F-actin (magenta) and MUC5AC (green), and nuclei with DAPI (blue) (in **c** and **d**, white dashed lines indicate upper surfaces of the porous matrix-coated membrane).

Incorporation of intestinal endothelial cells. To create an organ-level model of the human intestine containing a tissue-tissue interface, fragments released from intestinal organoids were seeded on the top of the same ECM-coated PDMS membrane, and primary human intestinal microvascular endothelial cells (HIMECs) were plated on the

bottom surface of the same membrane in the lower 'vascular' channel; control studies also were carried out with epithelium alone in the absence of HIMECs. To maintain the viability and growth of the HIMECs, we perfused endothelial cell medium (EGM2-MV) through the lower channel while EM was flowed through the top. These studies revealed that cultures that included HIMECs in the lower channel appeared to require less time to form a confluent epithelium in the upper channel. Organoid fragments achieved confluency within 6 days when seeded alone, while they only required 2 days in chips when they were co-cultured with endothelium (**Fig. 3a**). The presence of HIMECs also did not compromise barrier function and possibly enhanced it to a slight degree: with or without HIMEC, the P_{app} was sustained at 1-2 x 10^{-6} cm s^{-1} for up to 12 days of culture (with 8 days of perfusion of EM, followed by 4 days of DM through the upper channel, while EGM2-MV was flowed through the lower channel) (**Fig. 3b**). After that time, we detected cells that were shed and removed by the fluid flow, as expected from the fast turnover of human intestinal epithelium in which mature enterocytes are shed from the gut lining every 3-5 days[29,30]. The presence of HIMECs in the lower channel also appeared increase the efficiency of monolayer formation when organoids were fully dissociated into single cells prior to culturing them in the microchannel, and formation of putative villi-like structures was also observed in some of these cultures (**Fig. 3a**). However, the reproducibility of seeding protocol was much higher using organoid fragments versus isolated cells (~90% versus 40% success rate), and thus, we used the fragment method in all subsequent experiments.

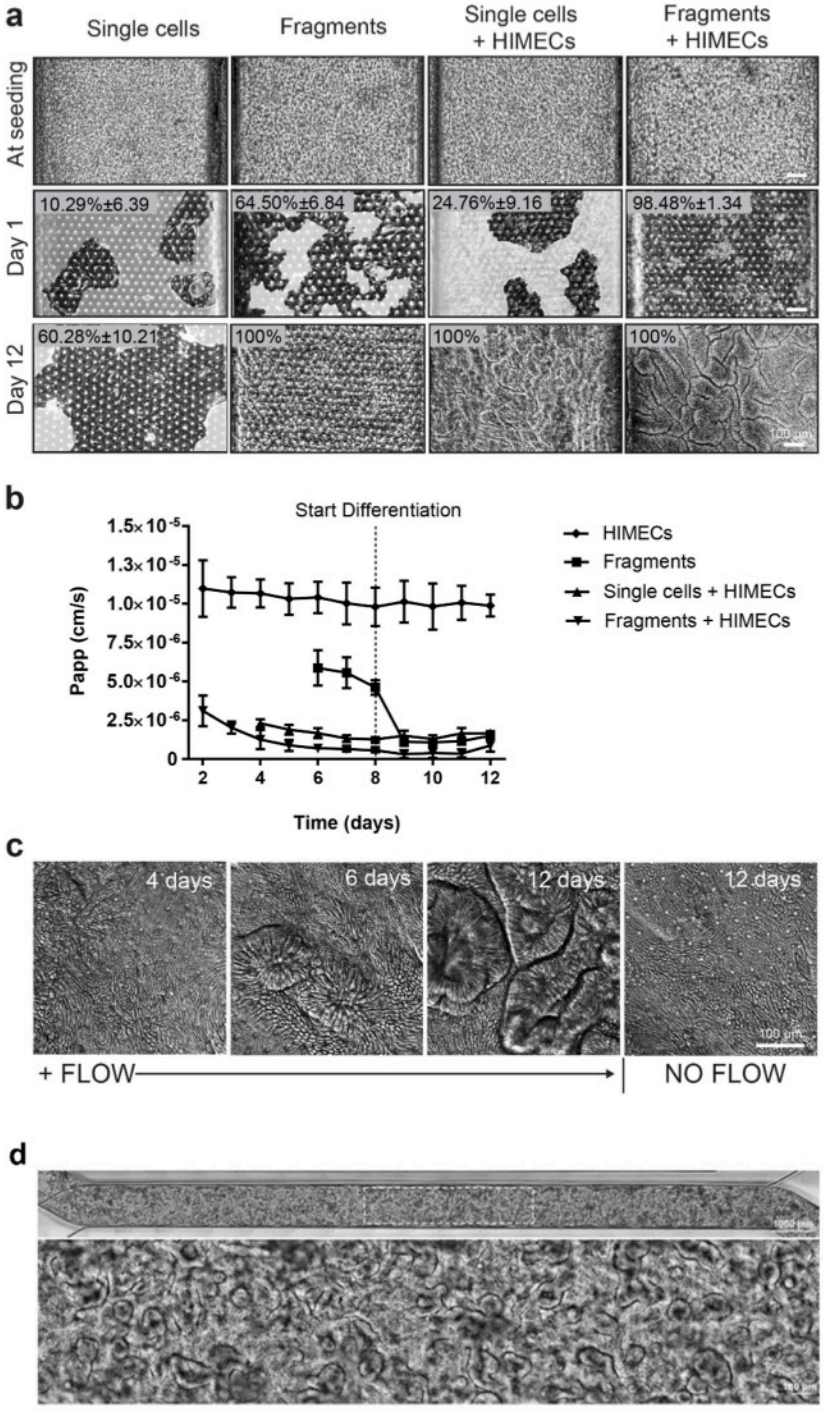

Figure III-3. Establishment of the primary human intestinal epithelium in the Organ Chip in the presence or absence intestine-specific microvascular endothelium. (a) Comparison of the efficiency of intestinal epithelial cell monolayer formation and development of villi-like structures between Organ Chip devices initially seeded with isolated primary epithelial cells or organoid fragments in the presence or absence of human intestinal microvascular endothelial cells (HIMECs), and then were maintained for 1 or 12 days under continuous fluid flow of EM (day 1-8) and DM (day 9-12) apically, while EGM2-MV medium was perfused through the lower channel. White areas delineate empty spaces where initially plated cells detached from the membrane when flow was initiated; dark areas represent patches of

attached cells. Graph shows the percentage of the area covered by epithelium at days 1 and 12 of culture, as assessed across 3 different field of views/chip with at least 3 chip replicates per condition, and expressed as mean ± SEM from 3 independent experiments. Note that when EGM2-MV medium was perfused basally, intestinal villi-like structures only formed in the epithelium when HIMECs were co-cultured on the opposite side of the porous membrane. **(b)** Graph showing maturation of the intestinal barrier function on chips cultured under the same conditions measured by quantifying permeability of fluorescent Lucifer yellow. P_{app} values are presented as mean ± SEM from 3 independent experiments; only P_{app} values for the cultures that reached 100% of confluency are plotted here. Note that the epithelium develops a higher barrier resistance to Lucifer Yellow more quickly when HIMECs are present. **(c)** Representative differential interference contrast images of the primary intestinal epithelium cultured on chip with HIMECs for 4, 6 or 12 days under continuous flow compared to 12 days in the absence of flow (note that formation of intestinal villi-like structures occurred only in the presence of flow). **(d)** Phase contrast microscopy views of the entire length of the epithelial microchannel (top) and a higher magnification of the area highlighted in the white rectangle (bottom) showing the human primary intestinal epithelium co-cultured with intestinal microvascular endothelial cells in the Organ Chip under peristalsis-like motions and flow for 12 days (culture medium was switched from EM to DM on day 8). Note the presence of villi-like structures across the entire length of the channel.

Once confluent epithelial and endothelial monolayers were formed in the presence of physiological fluid flow (60 µl h^{-1}), the Intestine Chip was exposed to peristalsis-like motions (10% strain, 0.2 Hz) generated by applying cyclic suction to the flexible hollow side chambers. Use of these dynamic co-culture conditions, in combination with a shift from use of the EM to a differentiation medium (DM) in the upper channel on day 8**,** led to formation of well-defined intestinal folds throughout the entire length of the epithelial channel (**Fig. 3a,c,d**). Interestingly, culture of these same cells in the absence of flow did not result in changes of epithelial tissue architecture despite continued application of 10% cyclic strain (**Fig. 3c**), which is consistent with previous studies using Caco-2 intestinal cells in a Gut Chip[19]. Importantly, phase contrast and confocal fluorescence microscopic analysis of this dynamic tissue-tissue interface confirmed the presence of a continuous, polarized, epithelial cell monolayer with an apical F-actin-containing brush border and basal nuclei aligned along the boundary of each villus-like extension into the lumen of the epithelial microchannel of the chip (**Fig. 4a**). Scanning electron microscopic (SEM) analysis of the apical surface

of the epithelial cells lining these villus-like luminal extensions revealed the presence of cells with morphology similar to that previously described in SEM micrographs of mucus-producing Goblet cells[31,32] and well-polarized absorptive enterocytes with densely-packed apical microvilli[33] (**Fig. 4b**). Cross-sectional confocal microscopic views of the primary Intestine Chip also confirmed the polarized epithelial cell distribution of basal Integrin β4 receptors and apical F-actin-containing brush border (**Fig. 4c**), as well as the major polarized ion transporters, Na^+/K^+- ATPase and NHE3 in their normal basolateral and apical positions, respectively (**Fig. 4d**). NHE3, which is responsible for electroneutral Na^+ absorption in the small intestine[26], localized along the apical membranes of the epithelium, while Na^+/K^+-ATPase, the major ion transporter responsible for regulating the intracellular Na^+ gradient necessary for absorption of nutrients[34], appeared along the basolateral membranes of these cells (**Fig. 4d**). Reestablishment of normal intestinal epithelial cell polarity was further confirmed by staining for E-cadherin (**Fig. 4e,f**), which appeared along lateral cell borders, and for villin (**Fig. 4e**) and zonula occludens-1 (ZO-1) (**Fig. 4f**) that localized at the cell apex. Thus, in contrast to organoids where the epithelial apex faces an abnormally closed lumen, the villus intestinal epithelium displayed the opposite orientation. Similiarly, immunofluorescence staining of ZO-1 and vascular endothelium (VE)-cadherin demonstrated the presence of well-formed tight and adherens junctions, respectively, in the microvascular endothelium as well (**Fig. 4f**). Taken together, these data confirm that we are able to growth primary human intestinal epithelial cells derived from organoids in co-culture with human organ-specific (intestinal) capillary endothelial cells to form a polarized and dynamic intestinal microenvironment using Organ Chip technology.

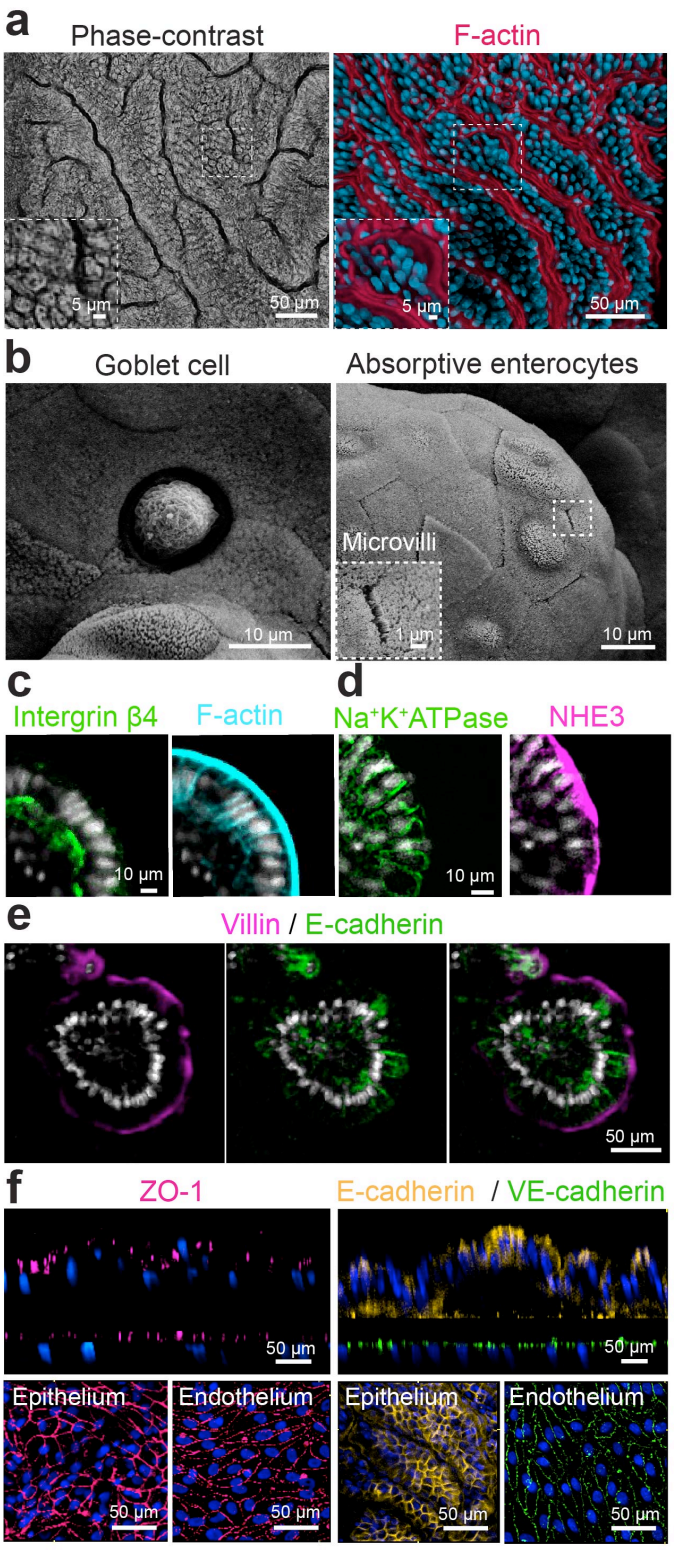

Figure III-4. Morphological analysis of the primary human Intestine Chip. (a) Representative immunofluorescence microscopic views from above of the intestinal epithelium grown on-chip for 12 days in the presence of continuous flow and cyclic strain showing the presence of a continuous brush border along the apical membranes of epithelial villi-like protrusions, which are juxtaposed in close proximity, as

visualized by labeling of the brush border by staining for F-actin (magenta) and for nuclei with DAPI (blue). **(b)** High magnification SEMs of the apical surface of the villus epithelium cultured on-chip showing a goblet cell (left) and absorptive enterocytes (right) with apical microvilli. **(d)** Immunofluorescence micrographs of the Intestine Chip showing polarized distribution of apical NHE3 and villin (magenta) as well as basolateral Na+K+ATPase and lateral E-cadherin (green) in the cross-sectional views of single villus-like structure all counterstained with DAPI (grey). **(e)** Confocal immunofluorescence micrographs showing the presence of apical intact tight junctions in the intestinal epithelium and underlying endothelium labeled with ZO-1 (magenta) as well as adherens junctions labeled for E-cadherin (yellow) and VE-cadherin (green); blue indicates DAPI-stained nuclei.

Recapitulating intestinal differentiation on chip. We next explored whether the primary Intestine Chip faithfully recapitulates normal intestinal differentiation *in vitro*, in which adult intestinal stem cells give the rise to multiple intestinal epithelial cell types, including absorptive enterocytes, enteroendocrine cells, goblet cell and Paneth cells. Removal of Wnt3A and inhibition of Notch signaling, driven by switching the medium in which the epithelial cells are cultured from EM to DM, induced the formation of multiple differentiated intestinal cell lineages. This was demonstrated by detection of increased expression by qRT-PCR of mRNAs encoding alkaline phosphatase and sucrase-isomaltase (absorptive enterocytes); mucin 2 (MUC2) and MUC5AC (Goblet cells); and chromogranin A and synaptophysin (SYP) (enteroendocrine cells) (**Fig. 5a**). Similar results were obtained using primary intestinal epithelial cells isolated from three different donors, and this increase in intestinal cell differentiation also was accompanied by down regulation of expression of the adult intestinal stem cell marker, leucine-rich-repeat-containing G-protein-coupled receptor 5 (LGR5)[35], whereas there was no detectable change in polycomb complex protein BMI1, which is known to be insensitive to Wnt withdrawal[36] (**Fig. 5a**). While expression of the Paneth cell marker, lysozyme, was slightly reduced by Wnt3A removal, we were able to detect the presence of lysozyme-positive cells along with chromogranin A-containing enteroendocrine cells, mucus-producing Goblet cells and enterocytes with positive villin-stained apical brush borders

in the Intestine Chip by the end of the differentiation process using immunofluorescence microscopy (**Fig. 5b**), and similar results were obtained in four different Intestine Chips.

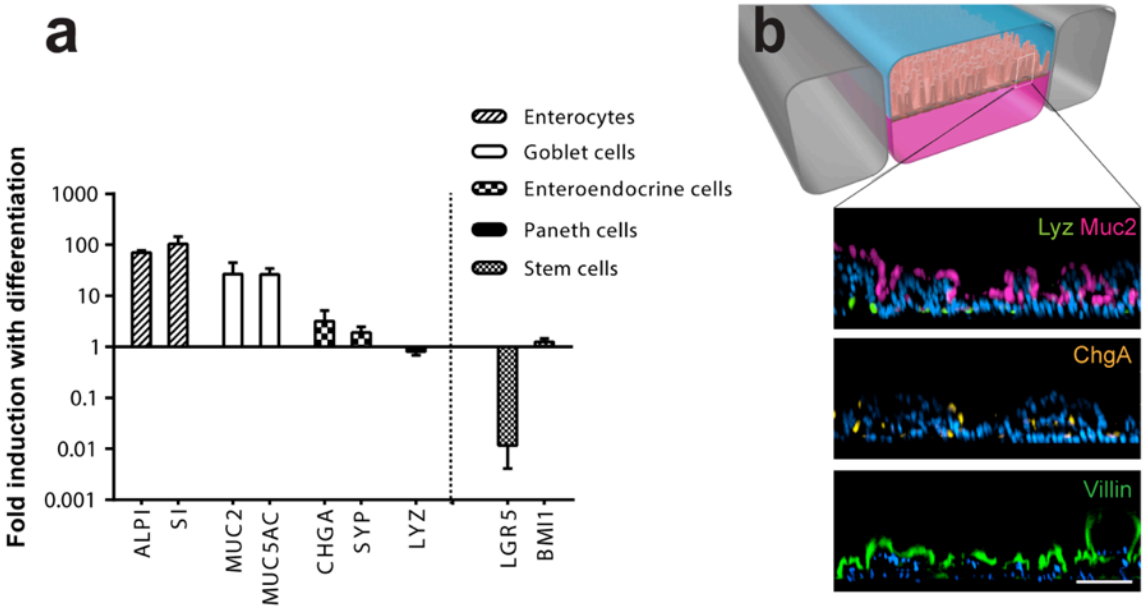

Figure III-5. The primary human Intestine Chip exhibits multi-lineage differentiation. **(a)** Graph showing the fold change in the levels of transcripts from epithelial cells cultured in the Intestine Chip and assessed at day 12 relative to the transcript levels in the undifferentiated state assessed at the day 8 (the medium perfused through the apical channel was switched from EM to DM on day 8). Genes analyzed include sucrose-isomaltase (SI) and alkaline phosphatase (ALPI) that are specific for absorptive enterocytes; mucin 2 (MUC2) and mucin 5AC (MUC5AC) for goblet cells; chromogranin A (CHGA) and synaptophysin (SYP) for enteroendocrine cells; lysozyme (LYZ) for Paneth cells; and leucine-rich-repeat-containing G-protein-coupled receptor 5 (LGR5) and polycomb complex protein *BMI-1* (BMI1) for stem cells. Values are presented as mean ± SEM from 3 independent experiments involving Intestine Chips generated from organoids isolated from 3 different donors (ns, not significant; *, $p \leq 0.05$; ***, $p \leq 0.001$ by Student's t-test). **(b)** A schematic cross-sectional representation of the 3D intestinal epithelial tissue architecture developed on chip (top) and confocal immunofluorescence micrographs (bottom) showing vertical cross-sections of the differentiated epithelium in Intestine Chip stained for lysozyme (Lyz, green), mucin 2 (Muc2, magenta), chromogranin A (ChgA, yellow) and villin (green). Cell nuclei were counterstained with DAPI (blue).

Recapitulating intestinal radiation-induced injury on Intestine Chip.

The small intestines of patients exposed to high levels of γ-radiation exhibit characteristic morphological changes such as decreased villi height, as well as cytoplasmic vacuolization and detachment of epithelial and endothelial cells from their

basement membrane. Similarly, we found that exposure of the primary Intestine Chips to radiation resulted in loss of normal villus architecture and disruption of epithelial and endothelial integrity within 6 days (**Fig. 6a**). When we analyzed the expression of the cell–cell junction proteins, VE-cadherin, in the irradiated endothelial cells, we observed a loss of junctional continuity in the endothelium cell layers (**Fig. 6a**). Radiation exposure also resulted in cell detachment and generation of cell-free gaps in the endothelial monolayer. Computerized image analysis of cross-sectional immunofluorescence views of epithelium (data not shown) revealed a significant reduction in the average height of villi in irradiated versus control chips (**Fig. 6b**).

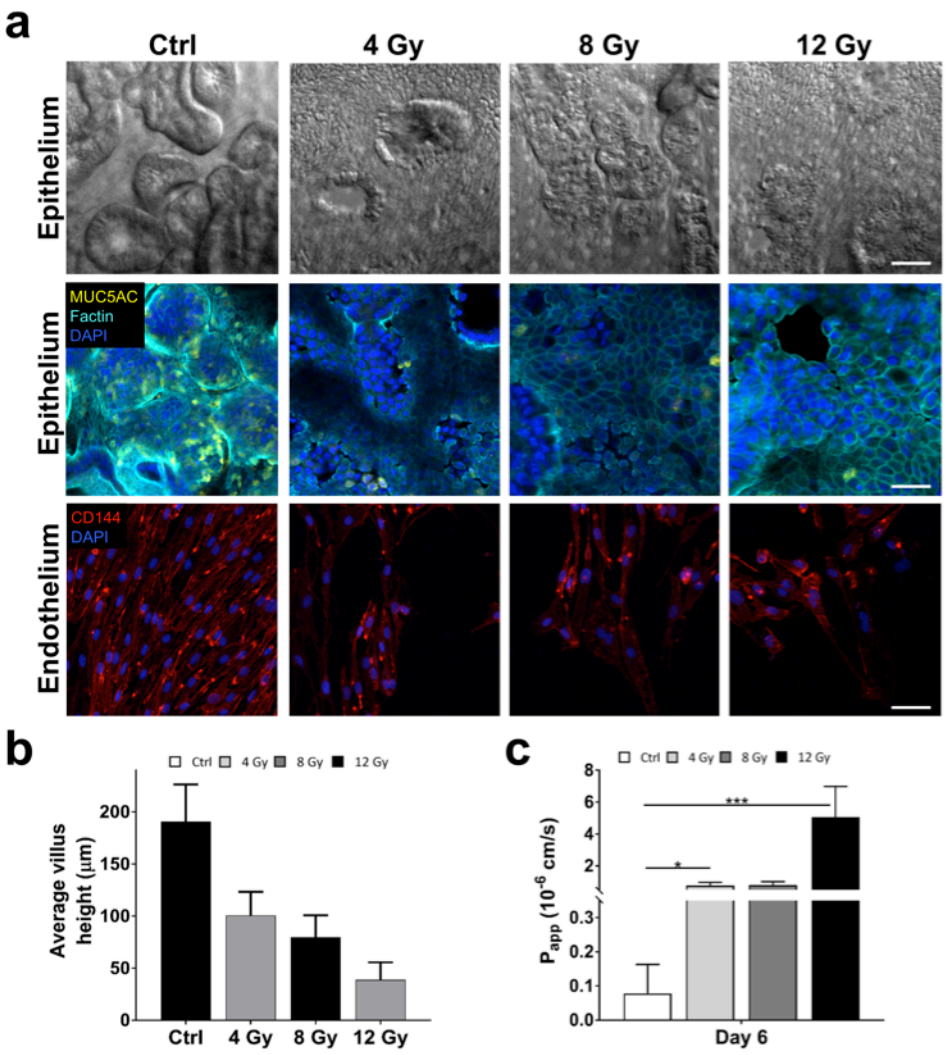

Figure III-6. Recapitulating intestinal radiation-induced injury on Intestine Chip. (**a**) DIC (top) and Confocal immunofluorescence micrographs (middle) showing horizontal views through the mid-section of villi stained for F-actin (cyan) and Muc5AC (yellow) at the top channel, and through the middle of the endothelium (bottom) stained for adherens junctions (VE-cadherin, red) at the bottom channel, within non-irradiated Intestine Chip (Ctrl) versus Intestine Chips exposed to 4 Gy, 8 Gy and 12 Gy γ-radiation for 6 days. Nuclei were counterstained with DAPI (blue). (**b**) Quantification of intestinal injury evaluated by measuring changes in the height of the villi under control conditions (Ctrl) versus after exposure to γ-radiation. (**c**) Changes in the apparent paracellular permeability (P_{app}) measured by quantifying cascade blue transport across the tissue-tissue interface within the Intestine Chip microdevices before (Ctrl) and after radiation.

When we evaluated the effect of radiation on intestinal barrier function and mucosal damage by measuring changes in the apparent permeability coefficient (P_{app}), which is a measure of paracellular barrier function in the human Intestine Chip, we observed

more than tenfold increase in P_{app} (0.8×10^{-7} vs. 1.2×10^{-6} cm s^{-1}) at 6 d after exposure (**Fig. 6c**). This was also accompanied by significant loss in expression of Muc5AC in mucin-producing cells (**Fig. 6a**). While we showed that the primary Intestine Chip faithfully mimics many facets of the human intestinal injury response to radiation *in vitro*, we observed that primary intestinal epithelium is more radio-sensitive compared to Caco-2 epithelium, as we did not detect any damage at 4 Gy in Caco-2 Intestine Chips. However, based on the results obtained at dose response study, 8 Gy is suggested for future radiation experiments on primary Intestine Chips.

DISCUSSION

We report here the development of a bioengineered *in vitro* model of the duodenum portion of the human small intestine by combining microfluidic Organ Chip technology with organoid-based methods for culture of primary epithelial stem cells from duodenal biopsies. The Intestine Chip recapitulates important structural features and functions of the native duodenum, including its three-dimensional villus architecture, barrier function and activity of the brush border digestive enzyme, sucrase. This Organ Chip technology differs substantially from past *in vitro* microfluidic models of human intestine, including a microfluidic human Gut Chip we previously described[20,21,39], as it incorporates the use of primary intestinal epithelium isolated from individual patient biopsy-derived organoids as well as gut-specific microvascular endothelial cells.

The vascularized Organ Chip design we utilized enables application of physiologically relevant mechanical cues, including luminal fluid flow within both the epithelial and vascular channels that is critical for formation of villus-like structures, as

well as peristalsis-like cyclic deformations, in addition to providing precise independent control over the chemical composition of culture medium in each channel. The ability to collect effluents of the two separate channels independently also enables dynamic sampling and analysis of biochemical compounds that are produced or secreted by the intestinal epithelial cells or endothelial cells, such as inflammatory cytokines or metabolic products, which is not possible with conventional organoid cultures. We also could potentially expose the apical surface of intestinal epithelial cells to pathogens, or co-culture them with commensal microbes to model the natural microbiome, as previously demonstrated with the Caco-2 Gut Chip[19]. The presence of the endothelium-lined microchannel (which is absent in organoid cultures) also can enable analysis of absorption of nutrients or oral drug absorption and their bioavailability, as well as characterization of physiologically relevant pharmacokinetic parameters because they are significantly influenced by the passage of drug compounds back and forth across the endothelial-parenchymal tissue-tissue interface. In addition, the presence of the endothelium permits analysis of the contributions of circulating immune cells that may be recruited under physiological flow conditions within microfluidic Organ Chips, as demonstrated in previous studies[11,21,40]. Most importantly, our head-to-head transcriptomic comparison of the Intestine Chip organoids used to supply the cells for the chips revealed that the Intestine Chip more closely mimics living duodenum, and that it better recapitulates many key functions of the living small intestine, including host defense response to infection, cell proliferation, digestion, and response to nutrients, than do the duodenal organoids. Thus, these findings suggest that while organoids may be an outstanding tool to study and probe intestinal stem cell differentiation and

histogenesis, they are limited in comparison to the Organ Chip technology when it comes to studying organ-level functions and pathophysiology, particularly in relation to mechanobiology, immunology, infectious disease and drug development.

This primary human Intestine Chip can be adapted for a wide range of applications, including basic research studies on the intestinal development, stem cell maturation and intestinal epithelial cell differentiation; assessment of nutrient transport, sensing, and absorption; intestinal barrier function and tissue-tissue (e.g., epithelial-endothelial) interactions; evaluation of drug delivery; therapeutic efficacy or toxicity; characterization of host-pathogen responses at the mucosal interface; and regenerative medicine studies. In addition, the ability to create Chips from individual donors as demonstrated in this study opens the possibility of creating Intestine Chips lined by cells from individuals with specific genotypic and disease-related phenotypic characteristics. These chips could be used to investigate patient-specific disease mechanisms as well as response to therapies, and thereby help to advance personalized medicine in the future. A recent report suggests that this approach also may be extended to be used with human induced pluripotent stem cell-derived organoids, which could further enhance personalized medicine approaches[41].

Although future directions include integrating the remaining important components of the living intestine into the Chip, including intestinal fibroblasts, immune cells (e.g., macrophages, intraepithelial lymphocytes and dendritic cells) and the enteric nervous system, previous studies have demonstrated that the power of the Organ Chip technology approach specifically lies in its ability to mimic organ-level complexity by progressively integrating different cell types one-at-a-time and studying the system at

varying levels of system complexity[9,10]. Moreover, this organ-level synthetic biology approach permits one to gain insight into mechanisms of biological regulation by manipulating potential contributing physical factors (e.g., flow, peristalsis) and cellular components separately while simultaneously providing a window on molecular-scale biochemical, genetic and cellular responses in real-time. The microengineered nature of this technology also allows users to reconstitute and control molecular gradients (e.g., Wnt, growth factors, etc.), which play a key role in intestinal development and regeneration. While we have tested the primary human Intestine Chip to model radiation-induced injuries, we believe that the Intestine Chip has extraordinary experimental potential for understanding and modeling development, homeostasis and diseases of the human intestine, including intestinal enteropathies, inflammatory bowel disease, celiac disease and cancer.

Methods

In vitro culture of human intestinal organoids. De-identified endoscopic tissue biopsies were collected from grossly unaffected (macroscopically normal) areas of the duodenum in 10-14 year old patients undergoing endoscopy for gastrointestinal complaints. Informed consent and developmentally-appropriate assent were obtained at Boston Children's Hospital from the donors' guardian and the donor, respectively. All methods were carried out in accordance with the Institutional Review Board of Boston Children's Hospital (Protocol number IRB-P00000529) approval. Tissue was digested in 2 mg ml^{-1} collagenase I for 40 min at 37°C followed by mechanical dissociation, and isolated crypts were resuspended in growth factor-reduced Matrigel (Becton Dickinson)

and polymerized at 37°C. Organoids were grown in expansion medium (EM) consisting of Advanced DMEM F12 supplemented with L-WRN conditioned medium (50% vol/vol, ATCC, cat. no. CRL-3276)[2], glutamax, HEPES, murine epidermal growth factor (50 ng ml^{-1}), N2 supplement, B27 supplement, 10 nM human [Leu15]-gastrin I, 1 mM n-acetyl cysteine, 10 mM nicotinamide, 10 μM SB202190, 500 nM A83-01, as described[4,6]. Differentiation Medium (DM) is EM without L-WRN conditioned medium, nicotinamide and SB202190, but supplemented with 1 μg ml-1 human recombinant R-spondin 1 (Peprotech), 100 ng ml-1 human recombinant Noggin (Peprotech) and 10 μM γ-secretase inhibitor DAPT, as previously described[3,4,27]. Organoids were passaged every 7 days by incubating in Cell Recovery Solution for 40 min at 4°C, followed by mechanical dissociation. Organoids were seeded on chips between passage number 5 and 25 and karyotyping was performed to confirm the absence of chromosomal anomalies.

Intestine Chip culture. Intestine Chips were fabricated from PDMS and assembled as described[19–21], or they were obtained from Emulate Inc. (Boston, MA). Chips were activated by oxygen plasma treatment for 1.5 min followed by incubation with APTMS (2% vol/vol in ethyl alcohol) for 30 min at RT, washing in ethyl alcohol, and incubating the devices at 80°C overnight. Type I collagen (200 μg ml^{-1}) and Matrigel (1% in PBS) were then introduced into the channels, and incubated in a humidified 37°C incubator for 2h before washing with PBS. Epithelial organoids were isolated from Matrigel and the cells dissociated with TrypLE supplemented with 10 μM Y-27632. Epithelial cells were then resuspended in EM (210,000 cells/chip), infused into the top channel, and incubated overnight in static at 37°C; starting the following day EM was perfused at 60

μl h^{-1} through top and bottom channels until day 8 when the medium was switched to DM for additional 4 days (except for the control experiment shown in Fig. 2 where organoid-derived epithelium was perfused with EM apically and basally throughout the entire course of the experiment).

In studies that included an endothelium, Human Intestinal Microvascular Endothelial Cells (HIMECs; ScienCell) were plated (250,000 cells/chip) on the lower side of the ECM-coated porous membrane in EGM2-MV medium, which contains human epidermal growth factor, hydrocortisone, vascular endothelial growth factor, human fibroblastic growth factor-B, R3-Insulin-like Growth Factor-1, Ascorbic Acid and 5% fetal bovine serum (Lonza Cat. no. CC-3202). Chips were inverted and incubated under static conditions for up to 1h at 37°C to promote HIMEC cell adhesion to the membrane before the epithelial cells were plated. The next day, we initiated continuous flow (60 μl h^{-1}) of the EM and EGM2-MV media through the top and bottom channels, respectively. Cyclic, peristalsis-like, membrane deformations (10% strain; 0.2 Hz) were applied after formation of confluent monolayers (3-4 days) using a vacuum pump controlled by an electronic vacuum regulator (ITV009, SMC Corp.) and an Arduino microcontroller.

Intestinal functional assessment. Lucifer Yellow (450 Da) added to the epithelial channel of the Intestine Chip to assess intestinal barrier permeability. The concentration of dye that diffused through the membrane into endothelial channel was measured in the effluent, and apparent paracellular permeability (P_{app}) was calculated using the following formula: $\boldsymbol{P_{app}} = \frac{\boldsymbol{V_{rec} \cdot dC_{rec}}}{\boldsymbol{A \cdot dt \cdot C_{don,t=0}}}$ where $\boldsymbol{V_{rec}}$ is volume receiver (endothelial compartment), $\boldsymbol{C_{rec}}$ concentration receiver, **A** the seeded area and $\boldsymbol{C_{don}}$ concentration

donor (epithelial compartment). To measure sucrase activity, upper and lower chamber of the Intestine Chip device were perfused PBS with Ca^2/Mg^2 for 1h to remove any residual glucose. 30 mM sucrose reaction buffer was prepared in PBS with Ca^2/Mg^2; the NaCl concentration in the PBS was reduced to 120 mM to adjust for osmolarity in the presence of 30 mM sucrose, and the sucrose was replaced with 30 mM mannitol in control samples, as described previously[42]. Sucrose or mannitol reaction buffer was then introduced in the upper microfluidic channel and PBS with Ca^2/Mg^2 into the lower channel. Glucose levels were measured using an Amplex Red Glucose assay kit (Thermo Fisher); total protein content in epithelial cell lysates was determined using a Pierce BCA Protein Assay (Thermo Fisher). Glucose concentrations were determined from a standard curve and sucrase activity expressed as units per gram of protein; 1 unit (1 U) = activity that hydrolyzes 1 μmol substrate min^{-1} at 37°C. To assess MUC2 production, the luminal effluent was collected over night and MUC2 content was measured using a Human Mucin 2 / MUC2 ELISA Kit (LSBio).

Morphological analysis. Intestine Chips and Organ Chips seeded only with intestinal epithelium were formaldehyde-fixed and permeabilized in 5% (wt/vol) BSA/ 0.1% (vol/vol) Triton-X100 before being incubated at 4°C overnight with primary antibodies directed against integrin β4 (mouse monoclonal, Abcam) E-cadherin (mouse monoclonal, Abcam), ZO-1 (mouse monoclonal, Life technology), VE-cadherin (rabbit polyclonal, Abcam), mucin 2 (mouse monoclonal, Santa Cruz Biotechnology), mucin 5AC (mouse monoclonal, Thermo Fisher Scientific), lysozyme (rabbit polyclonal, Dako), chromogranin A (goat polyclonal, Santa Cruz Biotechnology), villin (monoclonal mouse, Abcam), NHE3 (rabbit polyclonal, Novus Biologicals), alpha 1 Sodium/Potassium

ATPase (mouse monoclonal, Abcam) and Ki67 (rabbit polyclonal, Abcam). Appropriate Alexa Fluor secondary antibodies were flowed into the two channels of the chip and incubated in the dark at 4°C overnight. Images were acquired with an inverted laser-scanning confocal microscope (Leica SP5 X MP DMI-6000).

SEM samples were fixed in 2.5% glutaraldehyde, treated with 1% osmium tetroxide in 0.1 M sodium cacodylate buffer, dehydrated in a graded series of ethanols and critical point dried (AutoSamdri-815, Tousimis Research Corp.). Samples were coated with a thin (10 nm) layer of Pt/Pd using a sputter coater (Leica Baltec MED-020, *Leica*, Wetzlar, Germany)[40] prior to imaging using a SEM (Zeiss Supra 55 VP SEM, Carl Zeiss SMT Inc). Villus morphology was evaluated using DIC microscopy (Zeiss Axio Observer Z1 2, AXIO2) or laser scanning confocal immunofluorescence microscopy (Leica SP5 X MP DMI-6000 and Zeiss TIRF/LSM 710). After sectioning the chips using a sharp surgical blade, images of the cross sections were acquired with a confocal immunofluorescence microscope and high-resolution images were obtained applying deconvolution (Huygens) followed by a 2D projection processing. High-resolution top-view images of Intestine Chips and Organoids were used to quantify villi-like structure morphology using the Fiji image processing package of ImageJ[43–45].

RNA isolation, reverse transcription and qRT-PCR. Epithelial RNA recovered from the Intestine Chip was extracted using RNeasy Mini Kit followed by cDNA synthesis with SuperScript VILO cDNA Synthesis Kit (Thermo Fisher Scientific). RT-PCR was performed using TaqMan Fast Advanced Master Mix (Applied Biosystems), TaqMan gene expression assays (Thermo Fisher Scientific; Hs00357579_g1 for intestinal-type alkaline phosphatase (ALPI), Hs00356112_m1 for sucrase isomaltase (SI),

Hs00873651_g1 for mucin 5AC (MUC5AC), Hs00894025_m1 for mucin 2 (MUC2), Hs00900375_m1 for chromogranin A (CHGA), Hs00300531_m1 for synaptophysin (SYP), Hs00426232_m1 for lysozyme (LYZ), Hs00969422_m1 for leucine-rich-repeat-containing G-protein-coupled receptor 5 (LGR5), Hs00409825_g1 for Bmi1 (BMI1), Hs02758991_g1 for glyceraldehyde-3-phosphate dehydrogenase (GAPDH)), and run on a QuantStudio 7 Flex Real-Time PCR System (Thermo Fisher Scientific). Results were normalized relative to GAPDH expression.

Chip Radiation. Intestine Chip microdevices containing villus intestinal epithelium and vascular endothelium were removed from the syringe pump, immediately transferred to irradiation facility and exposed to 4, 8 or 12 Gy dose of gamma-irradiation (Cs-137; Gammacell 40 Exactor) at 0.98 Gy min^{-1}. Temperature of Irradiation chamber was kept at 37 C thorough the procedure and no temperature fluctuations were observed. To treat the control chips similarly, they were brought to irradiation facility and back without being exposed to irradiation.

Statistical analysis. Either a Student's t-test was performed to determine statistical significance, as indicated in the figure legends (error bars indicate standard error of the mean (SEM); *P* values < 0.05 were considered to be significant). Comparison of correlations was performed using R package cocor [PMID25835001].

References

1. Shanks, N., Greek, R. & Greek, J. Are animal models predictive for humans? *Philos. Ethics. Humanit. Med.* **4,** 2 (2009).
2. Sato, T. *et al.* Single Lgr5 stem cells build crypt-villus structures in vitro without a mesenchymal niche. *Nature* **459,** 262–5 (2009).
3. Sato, T. *et al.* Long-term expansion of epithelial organoids from human colon, adenoma, adenocarcinoma, and Barrett's epithelium. *Gastroenterology* **141,** 1762–72 (2011).
4. Vandussen, K. L. *et al.* Development of an enhanced human gastrointestinal epithelial culture system to facilitate patient-based assays. (2014). doi:10.1136/gutjnl-2013-306651
5. Sasai, Y., Eiraku, M. & Suga, H. In vitro organogenesis in three dimensions: self-organising stem cells. *Development* **139,** 4111–21 (2012).
6. Sato, T. & Clevers, H. Growing self-organizing mini-guts from a single intestinal stem cell: mechanism and applications. *Science* **340,** 1190–4 (2013).
7. Wells, J. M. & Spence, J. R. How to make an intestine. *Development* **141,** 752–60 (2014).
8. Fatehullah, A., Tan, S. H. & Barker, N. Organoids as an in vitro model of human development and disease. *Nat. Cell Biol.* **18,** 246–54 (2016).
9. Bhatia, S. N. & Ingber, D. E. Microfluidic organs-on-chips. *Nat. Biotechnol.* **32,** 760–72 (2014).
10. Ingber, D. E. Reverse Engineering Human Pathophysiology with Organs-on-Chips. *Cell* **164,** 1105–9 (2016).

11. Huh, D. *et al.* Reconstituting organ-level lung functions on a chip. *Science* **328,** 1662–8 (2010).

12. Baudoin, R., Griscom, L., Monge, M., Legallais, C. & Leclerc, E. Development of a renal microchip for in vitro distal tubule models. *Biotechnol. Prog.* **23,** 1245–53

13. Jang, K.-J. *et al.* Human kidney proximal tubule-on-a-chip for drug transport and nephrotoxicity assessment. *Integr. Biol. (Camb).* **5,** 1119–29 (2013).

14. Leclerc, E., Sakai, Y. & Fujii, T. Microfluidic PDMS (polydimethylsiloxane) bioreactor for large-scale culture of hepatocytes. *Biotechnol. Prog.* **20,** 750–5

15. Powers, M. J. *et al.* A microfabricated array bioreactor for perfused 3D liver culture. *Biotechnol. Bioeng.* **78,** 257–69 (2002).

16. Tilles, A. W., Baskaran, H., Roy, P., Yarmush, M. L. & Toner, M. Effects of oxygenation and flow on the viability and function of rat hepatocytes cocultured in a microchannel flat-plate bioreactor. *Biotechnol. Bioeng.* **73,** 379–89 (2001).

17. Grosberg, A., Alford, P. W., McCain, M. L. & Parker, K. K. Ensembles of engineered cardiac tissues for physiological and pharmacological study: heart on a chip. *Lab Chip* **11,** 4165–73 (2011).

18. Park, J. *et al.* Three-dimensional brain-on-a-chip with an interstitial level of flow and its application as an in vitro model of Alzheimer's disease. *Lab Chip* **15,** 141–50 (2015).

19. Kim, H. J., Huh, D., Hamilton, G. & Ingber, D. E. Human gut-on-a-chip inhabited by microbial flora that experiences intestinal peristalsis-like motions and flow. *Lab Chip* **12,** 2165–74 (2012).

20. Kim, H. J. & Ingber, D. E. Gut-on-a-Chip microenvironment induces human

intestinal cells to undergo villus differentiation. *Integr. Biol. (Camb).* **5,** 1130–40 (2013).

21. Kim, H. J., Li, H., Collins, J. J. & Ingber, D. E. Contributions of microbiome and mechanical deformation to intestinal bacterial overgrowth and inflammation in a human gut-on-a-chip. *Proc. Natl. Acad. Sci. U. S. A.* **113,** E7-15 (2016).
22. Imura, Y., Asano, Y., Sato, K. & Yoshimura, E. A microfluidic system to evaluate intestinal absorption. *Anal. Sci.* **25,** 1403–7 (2009).
23. Kimura, H., Yamamoto, T., Sakai, H., Sakai, Y. & Fujii, T. An integrated microfluidic system for long-term perfusion culture and on-line monitoring of intestinal tissue models. *Lab Chip* **8,** 741–6 (2008).
24. Shah, P. *et al.* A microfluidics-based in vitro model of the gastrointestinal human-microbe interface. *Nat. Commun.* **7,** 11535 (2016).
25. Yissachar, N. *et al.* An Intestinal Organ Culture System Uncovers a Role for the Nervous System in Microbe-Immune Crosstalk. *Cell* **168,** 1135–1148.e12 (2017).
26. Tsilingiri, K., Sonzogni, A., Caprioli, F. & Rescigno, M. A novel method for the culture and polarized stimulation of human intestinal mucosa explants. *J. Vis. Exp.* e4368 (2013). doi:10.3791/4368
27. Sato, T. *et al.* Single Lgr5 stem cells build crypt – villus structures in vitro without a mesenchymal niche. *Nature* **459,** 262–265 (2009).
28. Zietek, T., Rath, E., Haller, D. & Daniel, H. Intestinal organoids for assessing nutrient transport, sensing and incretin secretion. *Sci. Rep.* **5,** 16831 (2015).
29. Darwich, A. S., Aslam, U., Ashcroft, D. M. & Rostami-Hodjegan, A. Meta-analysis of the turnover of intestinal epithelia in preclinical animal species and humans.

Drug Metab. Dispos. **42,** 2016–2022 (2014).

30. Umar, S. Intestinal Stem Cells. *Curr Gastroenterol Rep* **12,** 340–348 (2011).
31. Elnasharty M. A., Abou-Ghanema I. I., Sayed-Ahmed A., and A. A. E. Mucosal-Submucosal Changes in Rabbit Duodenum during Development. in *International Journal of Biological, Biomolecular, Agricultural, Food and Biotechnological Engineering* **7,** 500–508 (2013).
32. Hassan, S. A. & Moussa, E. A. Light and scanning electron microscopy of the small intestine of goat (Capra hircus). *J. Cell Anim. Biol. Full* **9,** 1–8 (2015).
33. Skrzypek, T. *et al.* Light and scanning electron microscopy evaluation of the postnatal small intestinal mucosa development in pigs. *J. Physiol. Pharmacol.* **56 Suppl 3,** 71–87 (2005).
34. Charney, A. N. & Donowitz, M. Functional significance of intestinal Na+-K+-ATPase: in vivo ouabain inhibition. *Am. J. Physiol.* **234,** E629-36 (1978).
35. Barker, N. *et al.* Identification of stem cells in small intestine and colon by marker gene Lgr5. **449,** (2007).
36. Yan, K. S. *et al.* The intestinal stem cell markers Bmi1 and Lgr5 identify two functionally distinct populations. *Proc. Natl. Acad. Sci. U. S. A.* **109,** 466–71 (2012).
37. Tappenden, K. A. Pathophysiology of short bowel syndrome: considerations of resected and residual anatomy. *JPEN. J. Parenter. Enteral Nutr.* **38,** 14S–22S (2014).
38. Battle, M. A. *et al.* GATA4 is essential for jejunal function in mice. *Gastroenterology* **135,** 1676–1686.e1 (2008).

39. Kim, H. J. Human gut-on-a-chip inhabited by microbial flora that experiences intestinal peristalsis-like motions and flow . Lab Chip Lab on a Chip. (2015). doi:10.1039/c2lc40074j

40. Huh, D. *et al.* A human disease model of drug toxicity-induced pulmonary edema in a lung-on-a-chip microdevice. *Sci. Transl. Med.* **4,** 159ra147 (2012).

41. Workman, M. J. *et al.* Enhanced utilization of induced pluripotent stem cell-derived human intestinal organoids using microengineered Chips. *Cell. Mol. Gastroenterol. Hepatol.* (2017). doi:10.1016/j.jcmgh.2017.12.008

42. Ferruzza, S., Rossi, C., Scarino, M. L. & Sambuy, Y. A protocol for in situ enzyme assays to assess the differentiation of human intestinal Caco-2 cells. *Toxicol. In Vitro* **26,** 1247–51 (2012).

43. Schindelin, J. *et al.* Fiji: an open-source platform for biological-image analysis. *Nat. Methods* **9,** 676–82 (2012).

44. Schneider, C. A., Rasband, W. S. & Eliceiri, K. W. NIH Image to ImageJ: 25 years of image analysis. *Nat. Methods* **9,** 671–5 (2012).

45. Rueden, C. T. *et al.* ImageJ2: ImageJ for the next generation of scientific image data. *BMC Bioinformatics* **18,** 529 (2017).

ACKNOWLEDGMENTS

This work was funded by DARPA (contract N66001-11-1-4180), FDA grant HHSF223201310079C, the Ragon Institute of MGH, MIT and Harvard, the Bill and Melinda Gates Foundation, and the Wyss Institute for Biologically Inspired Engineering at Harvard University (to D.E.I.). The production of human organoids was supported by NIH grants F32DK091995, T32DK007477, 5K12HD5289610, HMS Shore Fellowship, BCH Wolpow/Rubin IBD Fellowship, NASPGHAN Nestlé Nutrition Award, and HDDC Pilot & Feasibility Award (to C.A.R.), R01DK084056, the Timothy Murphy Fund, the IDDRC P30HD18655 and the HDDC P30DK034854 (to D.T.B.). We thank K. Karalis and G. Hamilton for their help initiating this project; A. Monreal, O. Levy, and R. Prantil-Baun for their expert advice; and P. Praveschotinunt for assistance with SEM imaging.

Author Contributions Statement

M.K., A.T., C.A.R., D.T.B. and D.E.I. conceived the study and provided input into experimental design. M.K., A.T., A.S-P., S.J-F., A.B. and A.C. designed and conducted the experiments and analyzed the data; A.S-P., H.R. and W.S. helped prepare human organoid cultures and assisted with the Intestine Chip experiments. C.Z. and H.L performed microarray analysis. M.K. and D.E.I. co-wrote the manuscript with input from all co-authors.

COMPETING FINANCIAL INTERESTS

The authors declare potential competing financial interests as D.E.I is a founder, holds equity and chairs the scientific advisory board of Emulate Inc.

Supplementary Information

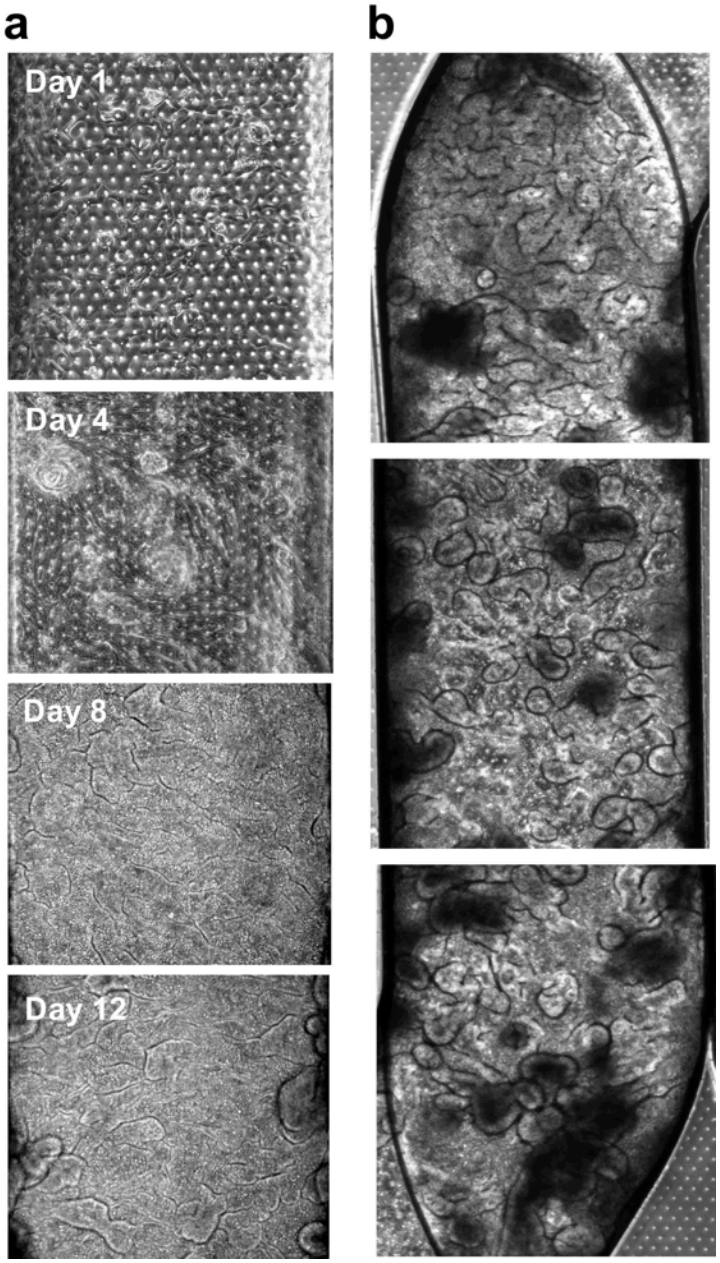

Supplementary Figure S1. Time course and extent of villus differentiation in the Intestine Chip. Representative phase contrast images of duodenal organoid-derived epithelial cells cultured on chip under continuous flow and peristalsis-like motions. **(a)** Comparison of the same field of view (center of the channel) imaged at 1, 4, 8 and 12 days of culture demonstrates that the villi formed *de novo* within these cultures. **(b)** Views of three different regions beginning (top), middle (center) and end (bottom) of the culture channel confirming that villi-like structures form at high density along the entire length of the channel.

IV. Chapter 4

A complex human gut microbiome cultured in an anaerobic intestine-on-a-chip

This chapter is based on the article:

S. Jalili-Firoozinezhad, F. S. Gazzaniga, E. L. Calamari, D. M. Camacho, B. Nestor, M. J. Cronce, O. Levy, J. M. S. Cabral, D. L. Kasper, R.Novak, and D. E. Ingber. "Complex human gut microbiome cultured in anaerobic human intestine chips". Nature BME, (2019)-*In Press*.

A complex human gut microbiome cultured in an anaerobic intestine-on-a-chip

Sasan Jalili-Firoozinezhad[1,2,&], Francesca S. Gazzaniga[1,3,&], Elizabeth L. Calamari[1,&], Diogo M. Camacho[1], Cicely W. Fadel[1], Amir Bein[1], Ben Swenor[1], Bret Nestor[1], Michael J. Cronce[1], Alessio Tovaglieri[1,4], Oren Levy[1], Katherine E. Gregory[5], David T. Breault[6,7,8], Joaquim M. S. Cabral[2], Dennis L. Kasper[3], Richard Novak[1] and Donald E. Ingber[1,9,10*]

[1]Wyss Institute for Biologically Inspired Engineering, Harvard University, Boston, MA 02115, USA
[2]Department of Bioengineering and iBB - Institute for Bioengineering and Biosciences, Instituto Superior Técnico, Universidade de Lisboa, Lisboa, Portugal
[3]Department of Microbiology and Immunobiology, Harvard Medical School, Boston, MA 02115, USA
[4]Graduate Program, Department of Health Sciences and Technology, ETH Zurich, 8092 Zurich, Switzerland
[5]Department of Pediatric Newborn Medicine, Brigham and Women's Hospital, 75 Francis Street, Boston, MA 02115, USA
[6]Division of Endocrinology, Boston Children's Hospital, Boston, MA 02115, USA
[7]Department of Pediatrics, Harvard Medical School, Boston, MA 02115, USA
[8]Harvard Stem Cell Institute, Harvard University, Boston, MA 02139, USA
[9]Vascular Biology Program and Department of Surgery, Boston Children's Hospital and Harvard Medical School, Boston, MA 02115, USA
[10]Harvard John A. Paulson School of Engineering and Applied Sciences, Cambridge, MA 02139, USA

[&]These authors contributed equally

* Corresponding author, don.ingber@wyss.harvard.edu

Abstract

The diverse bacterial populations that comprise the commensal microbiome of the human intestine play a central role in health and disease. A method that sustains complex microbial communities in direct contact with living human intestinal cells and their overlying mucus layer in vitro would thus enable investigations of host–microbiome interactions. Here, we show the extended co-culture of living human intestinal epithelium with stable communities of aerobic and anaerobic human gut microbiota, enabled by a microfluidic intestine-on-a-chip that permits the control and real-time assessment of physiologically relevant oxygen gradients. When compared to aerobic co-culture conditions, the establishment of a transluminal hypoxia gradient in the chip increased intestinal barrier function and sustained a physiologically relevant level of microbial diversity, consisting of over 200 unique operational taxonomic units from 11 different genera, and of an abundance of obligate anaerobic bacteria with ratios of *Firmicutes* and *Bacteroidetes* similar to those observed in human faeces. The intestine-on-a-chip may serve as a discovery tool for the development of microbiome-related therapeutics, probiotics and nutraceuticals.

Introduction

One of the major recent paradigm shifts in medicine relates to recognition of the central role that the microbiome composed of host-specific communities of commensal microbes plays in human health and disease[1]. While human microbiota colonize mucosal surfaces of various tissues, the gastrointestinal tract supports the greatest

mass and diversity of microorganisms[2]. Aerobic and anaerobic commensal gut microbes are essential for maintenance of normal nutrient absorption, drug metabolism, and immune responses, as well as for protection against infectious pathogens[3]. Conversely, changes or imbalances in the microbial community within the intestine can contribute to development of a broad range of pathological disorders within and beyond the gastrointestinal system, including inflammatory bowel disease, colorectal cancer, radiation enteropathy, diabetes, hepatic steatosis, obesity, and rheumatoid arthritis[4,5]. Thus, the establishment and preservation of balanced host-intestinal microbiome interactions are key requirements for maintaining gut homeostasis and human health.

Analysis of gut-microbiome crosstalk has almost exclusively relied on genomic or metagenomic analysis of samples collected *in vivo* because no method exists to establish stable complex communities of gut commensal microbes in direct contact with intestinal epithelium and their overlying mucus layer *in vitro*[6,7]. While animal models have been used to analyse host-microbiome interactions and their contributions to pathophysiology[8–10], there are no *in vitro* systems available to verify these interactions in human cells cultured with complex human microbiome. Thus, there is a great need for experimental models that can sustain complex populations of human aerobic and anaerobic microbiota in contact with living human tissues to analyse dynamic and physiologically relevant human host-microbiome interactions.

Existing *in vitro* models, such as Transwell inserts, have been used to study human host-microbe interactions; however, these studies can only be carried out over a period of hours before bacterial overgrowth leads to cell injury and death[11–13]. Organoid cultures, have shown great promise for studying host-microbiome interactions, but they

also cannot be co-cultured with living microbes for more than ~1 day; they also do not provide a vascular interface nor can they sustain luminal oxygen levels below 0.5%, which is required for co-culture of certain obligate anaerobes[14,15]. Specialized bioreactor models, such as the mucosal-simulator of the human intestinal microbial ecosystem (M-SHIME), have been developed to sustain growth of luminal and mucosal gut microbes *in vitro*, but they do not include living human intestinal epithelium[16]. A human-microbiota interaction (HMI) module was developed that permits analysis of aerobic and anaerobic microbes, including complex living microbiome derived from a SHIME reactor, when co-cultured with human Caco2 intestinal epithelial cells under an oxygen gradient; however, the microbes need to be separated from the human cells by a nanoporous membrane with an artificial mucus layer, and even under these conditions, the co-cultures were only maintained for 48 hours[17]. We previously described a two-channel microfluidic Organ Chip device lined by human Caco2 intestinal epithelial cells cultured under dynamic fluid flow and peristalsis-like mechanical deformations, which enabled establishment of stable co-cultures of a mucus-producing human villus intestinal epithelium with up to 8 different strains of human commensal gut microbes for weeks *in vitro* under aerobic conditions[17–19]. But the human gut microbiome contains hundreds of different types of bacteria, many of which are obligate anaerobes that will not grow in this environment. Thus, no existing *in vitro* model enables analysis of direct interactions among complex communities of anaerobic and aerobic gut bacteria, human intestinal epithelium, and its overlying mucus layer when cultured for multiple days *in vitro*, which is crucial for analysing gut health and disease[20–22].

In this study, we therefore set out to develop an experimental intestine-on-a-chip (Intestine Chip) system that can support dynamic interactions between living, mucus-producing, human intestinal epithelium and a directly apposed complex community of living human aerobic and anaerobic commensal gut microbes with a population diversity similar to that observed in living human intestine. To meet this challenge, we first modified the human Caco2 Intestine Chip by integrating microscale oxygen sensors into the devices for *in situ* oxygen measurements, and placing the chips within an engineered anaerobic chamber to establish a physiologically relevant oxygen gradient across a human intestinal epithelium as well as a microvascular endothelium that are cultured in parallel channels separated by a porous matrix-coated membrane within the device. To ensure a stable source of complex human intestinal gut-microbiota, we used complex microbiota originally derived from healthy human stool specimens, which have been maintained stably in gnotobiotic mice for multiple years, and closely resemble the relative abundance of major bacterial phyla patterns in their respective inocula[23,24]. We also applied the same method to co-culture fresh gut microbiome isolated from human infant stool samples in a primary human Intestine Chip lined by cells isolated from normal human ileum. Here we describe how establishing a hypoxia gradient across the engineered tissue-tissue (endothelium-epithelium) interface of the Intestine Chip allows for stable co-culture of highly complex communities of anaerobic and aerobic human commensal gut bacteria in the same channel as mucus-producing human villus intestinal epithelium while simultaneously monitoring oxygen levels and intestinal barrier function for at least 5 days *in vitro*.

Results

Establishing an oxygen gradient across the lumen of the Intestine Chip. To recapitulate a physiologically relevant intestinal oxygen gradient profile inside Intestine Chips (**Fig. 1a**), we fabricated an oxygen-sensing, dual channel, human Organ Chip composed of optically clear and flexible poly(dimethyl siloxane) (PDMS) polymer (**Fig. 1b; Supplementary Fig. S1a**), as well as an anaerobic chamber (**Supplementary Fig. S2)**. For real-time, non-invasive, monitoring of oxygen tension, six sensor spots containing oxygen-quenched fluorescent particles were embedded in the top and bottom portions of the chip beneath the central microchannels (**Fig. 1b; Supplementary Fig. S1b**). Changes in the fluorescent intensities of these sensors in response to oxygen tension were captured by a VisiSens camera (**Supplementary Fig. S1b**) and translated into oxygen concentrations by comparison with a standard Oxy-4 probe system (**Supplementary Fig. S1c**). As both the chips and sensors are composed of highly gas-permeable PDMS, the sensors respond rapidly (< 30 sec) to changes in oxygen concentrations (**Fig. 1c**).

To simultaneously provide adequate oxygen for maintaining human cells and an anaerobic microenvironment suitable for culturing complex human microbiota while establishing a functional host-microbiome interface, we flushed the custom anaerobic chamber (**Supplementary Fig. S2a,b**) continually with humidified 5% CO_2 in nitrogen gas. This setup enables us to maintain low oxygen levels within the lumen of the upper chamber (**Fig. 1d**), while the epithelium is sustained via diffusion of oxygen through the permeable PDMS membrane from the well-oxygenated medium flowing through the lower endothelium-lined vascular channel from external oxygenated medium reservoirs (**Supplementary Fig. S2a,b**). Using this method, physiologically relevant anaerobic

conditions (<0.5%) can be generated within less than 30 min at 243 ml min^{-1} of nitrogen flow into the anaerobic chamber (**Fig. 1d**). The chamber also can sustain low oxygen levels (<5.0%) for about 15 min after it is disconnected from the nitrogen source (**Fig. 1d**). This allows the chamber to be temporarily moved from the incubator for imaging or into a bacterial glove box (*e.g.* to replenish culture medium or add microbiota) without significantly disturbing the low oxygen environment.

When human Caco-2 intestinal epithelial cells are cultured for 5 to 7 days under aerobic conditions and dynamic flow, they undergo villus differentiation and express multiple features of the ileum portion of the human small intestine, including secretion of a mucus layer overlying the apical surface of the epithelium and establishment of barrier function[25,20,26]. Endothelial cells also can be co-cultured on the bottom of the central porous membrane in the lower channel of the same device, where they form a hollow vascular lumen lined by cells joined by VE cadherin-containing cell-cell junctions under aerobic conditions[26]. The co-culture of endothelium has been shown to enhance barrier function and mucus production (*e.g.*, expression of MUC2 and MUC5AC), as well as influence villi development and cytokine production by intestinal Caco2 epithelium under these conditions[26,27].

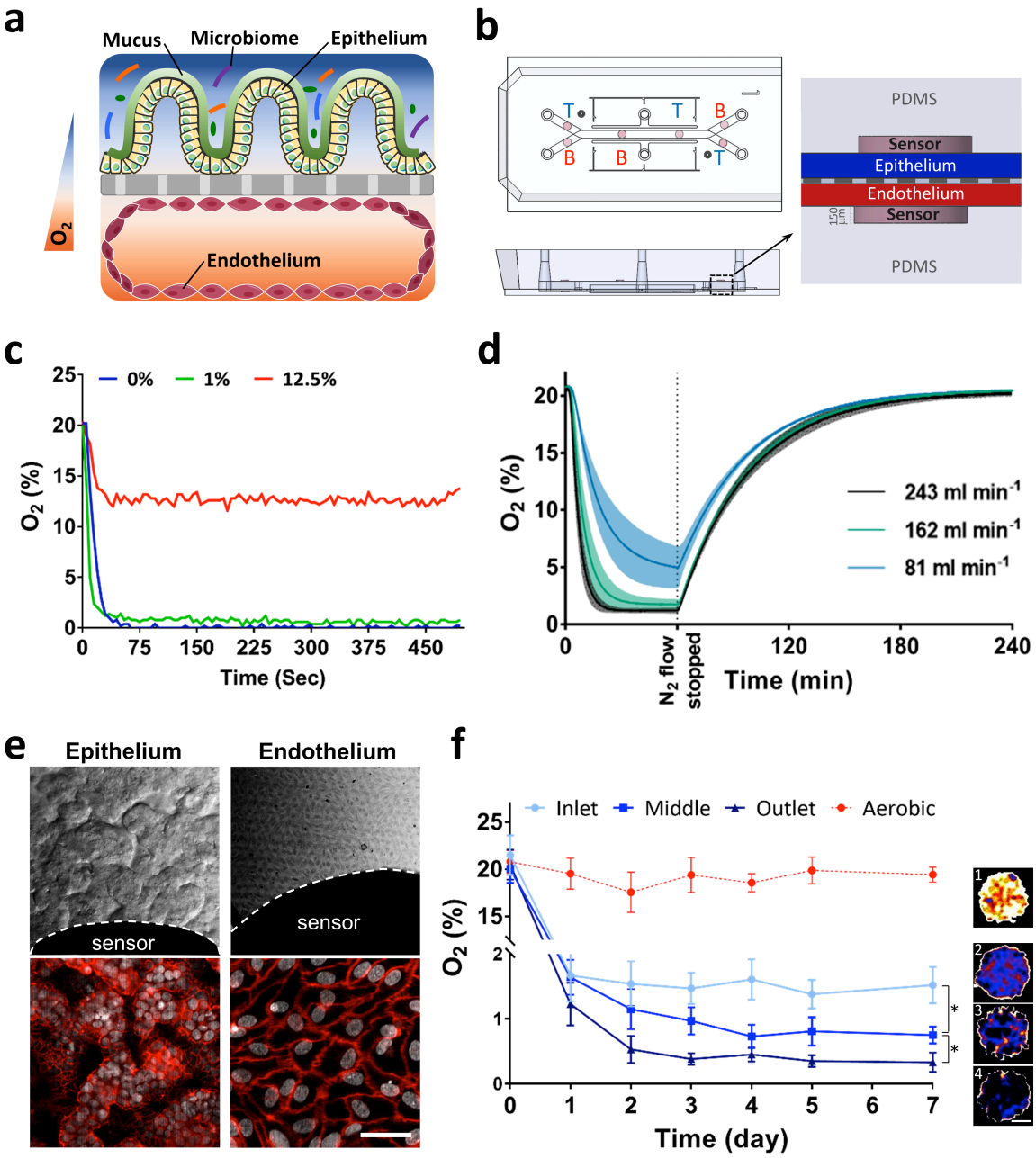

Figure IV-1. Oxygen sensitive human Intestine Chip microfluidic culture device. a, Schematic showing the position of the human intestinal epithelium overlaid with its own mucus layer and complex gut microbiota on top, with vascular endothelium on bottom side of the same ECM-coated porous membrane, within a 2-channel microfluidic Organ Chip device in presence of oxygen gradients. Orange and blue colors indicated high and low levels of oxygen concentration, respectively. **b,** Schematic representation of the Intestine Chip with 6 oxygen quenched fluorescent particles embed in inlet, middle and outlet of top and bottom channels. (T, top channel; B, bottom channel). **c,** Sensitivity analysis of oxygen spots located in the Intestine Chip in response to defined, standard oxygen concentrations. **d**, Anaerobic chamber validation at various N_2 inflow pressures; N_2 was introduced into the chamber at 81 mL min^{-1}, 162 mL min^{-}

^{1}, or 243 mL min^{-1} for 1 h before gas flow was stopped and the chamber was allowed to recover (n=3, shaded regions indicate standard deviation; data are presented as mean ± s.d.). **e,** Microscopic views showing the villus morphology of the human Caco-2 intestinal epithelium (top left; scale bar, 100 μm) and vascular endothelium (top right; scale bar, 100 μm) cultured for 6 days in the Intestine Chip under anaerobic conditions, when viewed from above by DIC and phase contrast imaging, respectively, or by immunofluorescence staining for the tight junction protein, ZO-1 (red, bottom left; scale bar, 100 μm) and endothelial cell junction-associated protein, VE-cadherin (red, bottom right; scale bar, 20 μm). Gray indicates DAPI-stained nuclei; white dashed lines indicate the border of the oxygen sensor spot). **f,** Oxygen concentration profiles within aerobically- and anaerobically-cultured Intestine Chips. Representative pseudocolor insets indicate average oxygen concentration in aerobic chip (1), and inlet (2), middle (3) and outlet (4) of the anaerobically-cultured epithelium channel, at day 7 of culture. Scale bar, 200 μm. (n=3 individual chips; data are presented as mean ± s.d.; significance was calculated by one-way analysis of variance; *P = 0.046).

When we cultured Intestine Chips lined by Caco2 intestinal epithelial cells and human intestinal microvascular endothelial cells (HIMECs) under a hypoxia gradient using our chamber, differential interference contrast (DIC) and immunofluorescence microscopic analysis confirmed that the cells again formed a villus intestinal epithelium containing polarized cells joined by ZO-1-containing tight junctions (**Fig. 1e, top; Supplementary Fig. S3a-d**) that was underlaid by a confluent HIMEC monolayer with cells linked by VE-cadherin-containing tight junctions, even in the presence of this hypoxia gradient (**Fig. 1e, bottom**). Both cell types also remained viable under these conditions, as measured by quantifying release of the intracellular enzyme lactate dehydrogenase (LDH), which remained relatively unchanged compared to the aerobic control during one week of anaerobic culture (**Supplementary Fig. S4a**). Quantification of the apparent permeability (P_{app}) of the intestinal epithelial barrier similarly revealed no changes in the paracellular barrier function, and these human Intestine Chips displayed P_{app} values of about 1 x 10^{-7} cm s^{-1} after 7 days (**Supplementary Fig. S4b**), which are similar to those previously reported[26]. Importantly, we also confirmed that both the human intestinal epithelium and endothelium experienced oxygen gradients by

analysing the expression of hypoxia-inducible factor 1α (HIF-1α). HIF-1α is a key mediator of oxygen hemostasis and intestinal epithelial cell adaptation to oxygen deprivation,[28] which is stabilized in a graded fashion in response to decreasing oxygen concentrations[29]. Expression of nuclear HIF-1α levels were significantly higher (~3-fold; $p < 0.01$) in the lumen of the anaerobically-cultured epithelium than in the adjacent oxygenated endothelium-lined channel (**Supplementary Fig. S5a,b**), which is where our sensors indicated maintenance of a hypoxic environment for up to 7 days in culture (**Fig. 1f** and **Supplementary Fig. S4c**). Similar nuclear HIF1α expression has been previously shown in both mouse and human cells cultured under hypoxic (1% O_2) condition[30].

Co-culture of human intestinal epithelium with an obligate anaerobe on-chip. We next explored whether the hypoxic environment can support co-culture of the intestinal epithelium with the obligate anaerobe, *Bacteroides fragilis* (*B. fragilis*; strain NCTC 9343), which is a human commensal symbiotic bacterium that cannot grow under aerobic (> 0.5% oxygen) conditions[31,32]. During the co-culture procedure which began after the epithelium had been cultured and differentiated on-chip for 7 days under anaerobic condition (**Supplementary Fig. S6a**), *B. fragilis* bacteria (2.5×10^5 CFU; fluorescently labelled with HCC-amino-D-alanine (HADA)[33]; **Supplementary Fig. S6b**) were introduced into the lumen of upper channel where they distributed across the surface of the intestinal epithelium (**Supplementary Fig. S6c**). They were subsequently cultured under either aerobic or anaerobic conditions, while being flushed daily to

remove both luminal and tissue-associated microbes, and CFU counts were carried out by plating.

Continuous monitoring of oxygen concentrations from inoculation to day 3 of co-culture revealed that our anaerobic chip setup maintained a low oxygen environment that decreased from ~ 1% oxygen levels to 0.3% in the presence of *B. fragilis* (**Fig. 2a**). Yet, the intestinal epithelium maintained its ZO-1-containing tight junctions and apical brush border polarity when co-cultured in direct contact with *B. fragilis* under these highly anaerobic conditions (**Fig. 2b**). Interestingly, the presence of this obligate anaerobe enhanced, rather than decreased, barrier function (reduced P_{app} by 1.8-fold compared to aerobic conditions; $*p = 0.033$) after 3 days in anaerobic culture (**Fig. 2c**) and this barrier was maintained for up to at least 8 days in culture (**Supplementary Fig. S6d**). As expected, the *B. fragilis* bacteria continued to grow in the anaerobic chips over 3 days ($p < 0.001$), whereas they started to die off by day 2 and appeared at significantly lower levels at 3 days under aerobic culture conditions (**Fig. 2d**). These data confirm that our chips that experience a hypoxia gradient support the growth of an obligate anaerobic bacterial species in the same channel as living human intestinal epithelial cells, whereas these bacteria would have otherwise died in a conventional aerobic culture system.

A mucus layer separates the commensal microbes from the epithelium. One of the characteristic features of host-microbiome interactions in the living intestine is that they are mediated through an intervening mucus layer that is secreted by the epithelium along its apical surface. Live staining using Wheat Germ Agglutinin (WGA), which has been previously used for mucus visualization *in vitro*[34] and *in vivo*[35], confirmed that *B.*

fragilis resides on top of the mucus layer (**Fig. 2e**), which is secreted by the intestinal Caco2 epithelium, as previously demonstrated[34,36]. This was independently confirmed by scanning electron microscopic (SEM), which clearly revealed a continuous and dense mucus blanket that completely covered the surface of the differentiated villus epithelium separating it from overlying bacteria after 12 days of culture (**Fig. 2f**), much as is and observed *in vivo*[37,38]. This was in contrast to SEM analysis of Caco2 Intestine Chips that were only cultured for 4 days before full differentiation occurred and mucus had accumulated where the microvilli-lined surface of the apical epithelium remained clearly detectable (**Fig. 2f**). Based on these images, the thickness of mucus layer was estimated at ~10 μm, which is similar to that reported with 30-day old mouse ileum[37].

Sustaining a complex human intestinal microbiome in vitro. To optimize growth of a complex microbiome in our culture system, we searched for a source of complex human gut microbes that remains stable over time. Therefore, we inoculated the anaerobic Intestine Chips with a sample of complex gut microbiota originally isolated from human faeces, which has been stably maintained in gnotobiotic mice in isolators for over 30 generations[23,24] and that maintains a composition closely resembling the original human stool inoculum at the genera and species levels[23]. To identify a medium composition that would promote the growth of a complex set of commensal bacteria, we first inoculated the healthy human microbiome (Hmb) stock into 13 different types of culture medium in standard culture tubes, placed the cultures in an anaerobic chamber at 37^{o}C, and then carried out 16S rRNA sequencing after 3 days of culture (**Supplementary Fig. S7a**). Samples of these 13 types of medium were also added to cultured human Caco2 intestinal epithelial cells to test for toxicity (**Supplementary Fig.**

S7b). The medium that promoted the most diverse set of viable microbes without injuring the epithelium contained DMEM, 20% FBS, 1% glutamine, 1 $mg.ml^{-1}$ pectin, 1 $mg.ml^{-1}$ mucin, 5 $\mu g.ml^{-1}$ Hemin and 0.5 $\mu g.ml^{-1}$ Vitamin K1. The microbiota stock was introduced into this medium (0.1 $mg.ml^{-1}$) and perfused through the upper Caco2 epithelium-lined channel of the Intestine Chip while oxygenated endothelial culture medium was flowed through the lower channel. The epithelial channel of the chips was flushed daily with a short (2 min) fluid pulse at higher flow rate (50 $\mu l.min^{-1}$) to remove adherent and luminal bacteria, and 16S rRNA sequencing was carried out using samples from the effluent to assess bacterial diversity in each condition over 3 days of culture (n = 4 for each condition).

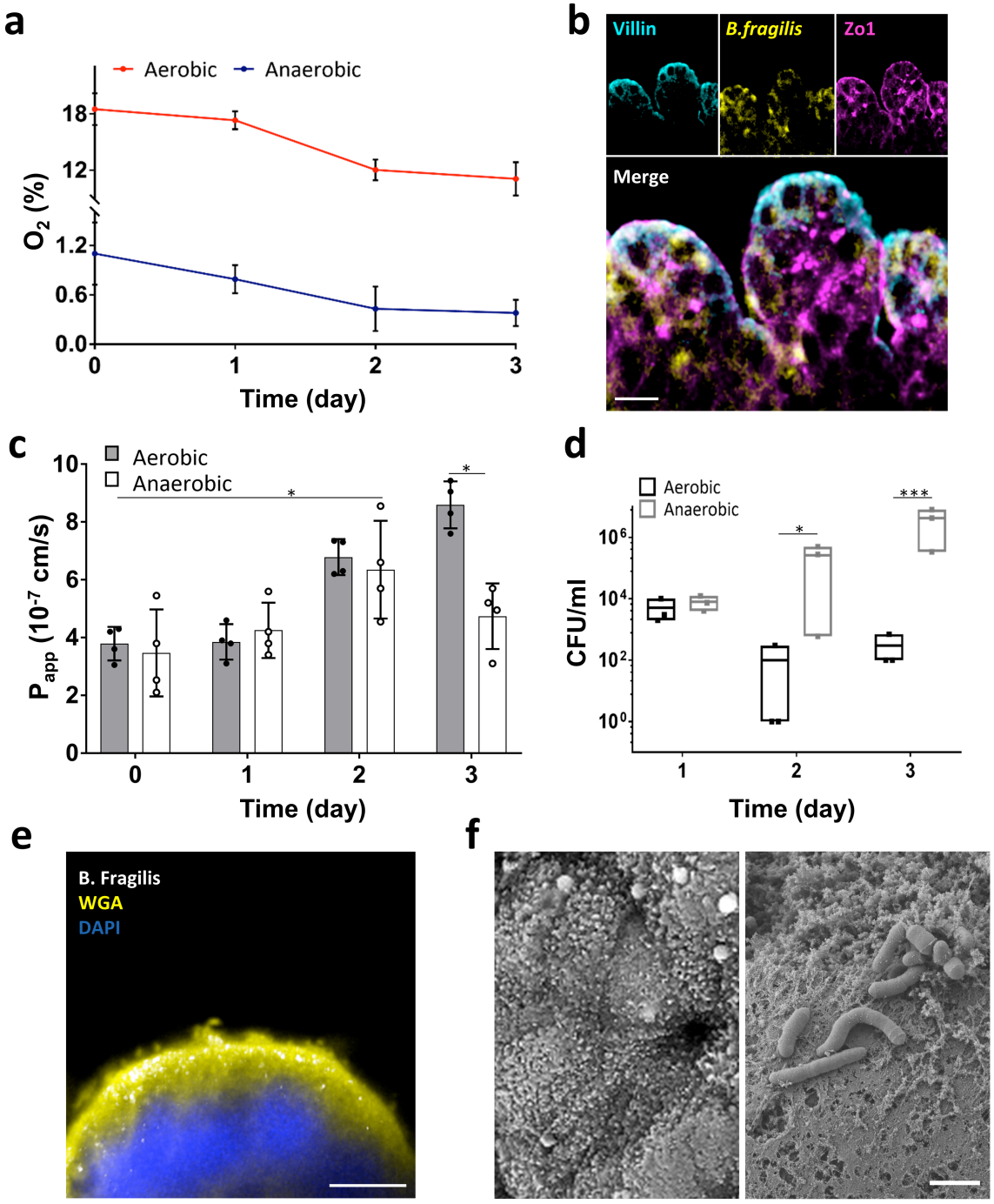

Figure IV-2. Co-culture of human intestinal epithelium and obligate anaerobe, Bacteroides fragilis, on-chip. a, Oxygen concentration profiles in aerobic and anaerobic Intestine Chips co-cultured with Bacteroides fragilis (n=4 individual chips; data are presented as mean ± s.d.). **b,** Representative vertical cross-sectional, confocal micrographic views through the intestinal epithelium-microbiome interface within the Intestine Chip cultured under anaerobic conditions, when immunostained for villin (cyan), ZO-1 (magenta) and nuclei with DAPI (blue). (scale bar, 50 μm; *B. fragilis* was HADA (yellow) labelled; representative images from 4 intestine chips are shown). **c,** Changes in apparent paracellular permeability (P_{app}) measured by quantitating cascade blue transport across the tissue-tissue interface

within the Intestine Chip microdevices co-cultured with *Bacteroides fragilis* under aerobic and anaerobic conditions (n=4 individual chips; data are presented as mean ± s.d.; significance was calculated by one-way analysis of variance; $^{*}P = 0.042$ and 0.033 for anaerobic day 2 vs. day 0 and aerobic vs. anaerobic day 3, respectively). **d,** CFU counts/mL of *Bacteroides fragilis* co-cultured in the Intestine Chip under aerobic and anaerobic conditions (n=3 individual chips; data are presented as mean ± s.d.; significance was calculated by one-way analysis of variance; $^{*}P = 0.031$ for day 2 and $^{***}P<0.001$ for day 3). **e,** Cross-sectional fluorescence microscopic view of the Caco2 epithelium (nuclei stained in blue with DAPI), overlying mucus layer stained with Alexa Fluor 488-conjugated WGA (yellow), and *B. fragilis* bacteria (GalCCP labelled, white) when co-cultured in the Intestine Chip. Scale bar, 10 µm. **f,** SEM views of the apical surface of the Caco2 epithelium in the Intestine Chip comparing the morphology on day 4 of culture before it accumulates a mucus layer and when the surface microvilli are visible (top) versus when *Bacteroides fragilis* have been added on day 12 after the mucus layer has accumulated, which can be seen as a dense mat that separates the bacteria from the epithelial cell surface (bottom). Scale bar, 2 µm.

After data processing, we identified a total of 938 operational taxonomic units (OTUs) among all samples, which corresponded to approximately 200 unique OTUs shared between samples of each chip after filtering and removing singletons, which is similar in scale to the number of OTUs previously observed in human intestinal aspirates (280 OTUs)[39], although, as expected, with a different phylum distribution. Analysis of the alpha diversity between the two conditions showed that the species diversity in anaerobic chips were statistically different (PERMANOVA, $^{***}p < 0.001$) from aerobic chips (**Fig. 3a**). Although the observed diversity and Shannon Index are lower than what is observed in human stool samples (**Supplementary Fig. S8a,b**), we observed an increase in richness compared to our starting inoculum over the course of the 3 days of experiment (**Supplementary Fig. S9a,b**). We identified 11 well characterized genera including *Eubacterium, Oscillospira, Blautia, Sutterella, Biophila, Akkermansia, Ruminococcus, Bacteroides, Parabacteroides, Enterococcus and Citrobacter* (**Fig. 3b**), with an additional 8 OTUs of unknown genera from *Firmicutes* (5 OTUs) and *Proteobacteria* (3 OTUs) phyla, that were present in our chips (phylum level analysis is shown in **Supplementary Fig. S10**). Interestingly, in comparison to aerobic conditions, co-culturing diverse microbiota under anaerobic conditions for 3 days in

direct contact with the human intestinal epithelium did not compromise intestinal barrier integrity, and, instead, it led to an increase in barrier function by almost 2-fold (*i.e.*, decrease in P_{app} from 3.1 x 10^{-7} to 1.6 x 10^{-7} cm s^{-1} in aerobic versus anaerobic chips, respectively; **p* = 0.048) (**Fig. 3c**). In contrast, epithelial barrier function decreased (****p* < 0.001) after day 3 of co-culture under aerobic conditions when co-cultured with the same complex gut microbiome (**Fig. 3c**). Furthermore, to explore the durability of these cultures, we then carried out an additional experiment in which we extended aerobic and anaerobic chips for 5 days with and without the same Hmb stock. Sterile chips maintained barrier function over the five days of culture under both anaerobic and aerobic conditions (**Supplementary Fig. S11a,b**). Again, we observed that while barrier function decreased in aerobic chips with Hmb at day 3 (**Supplementary Fig. S11a**), no compromise of barrier function was seen in anaerobic chips with Hmb even over the 5 days of culture (**Supplementary Fig. S11b**) and these cultures could be extended longer if experimental needs require. Moreover, in the presence of complex microbiota, the intestinal epithelium remained viable, as measured by quantifying release of the intracellular enzyme LDH, which remained unchanged compared to the sterile control chips cultures (**Supplementary Fig. S11c**).

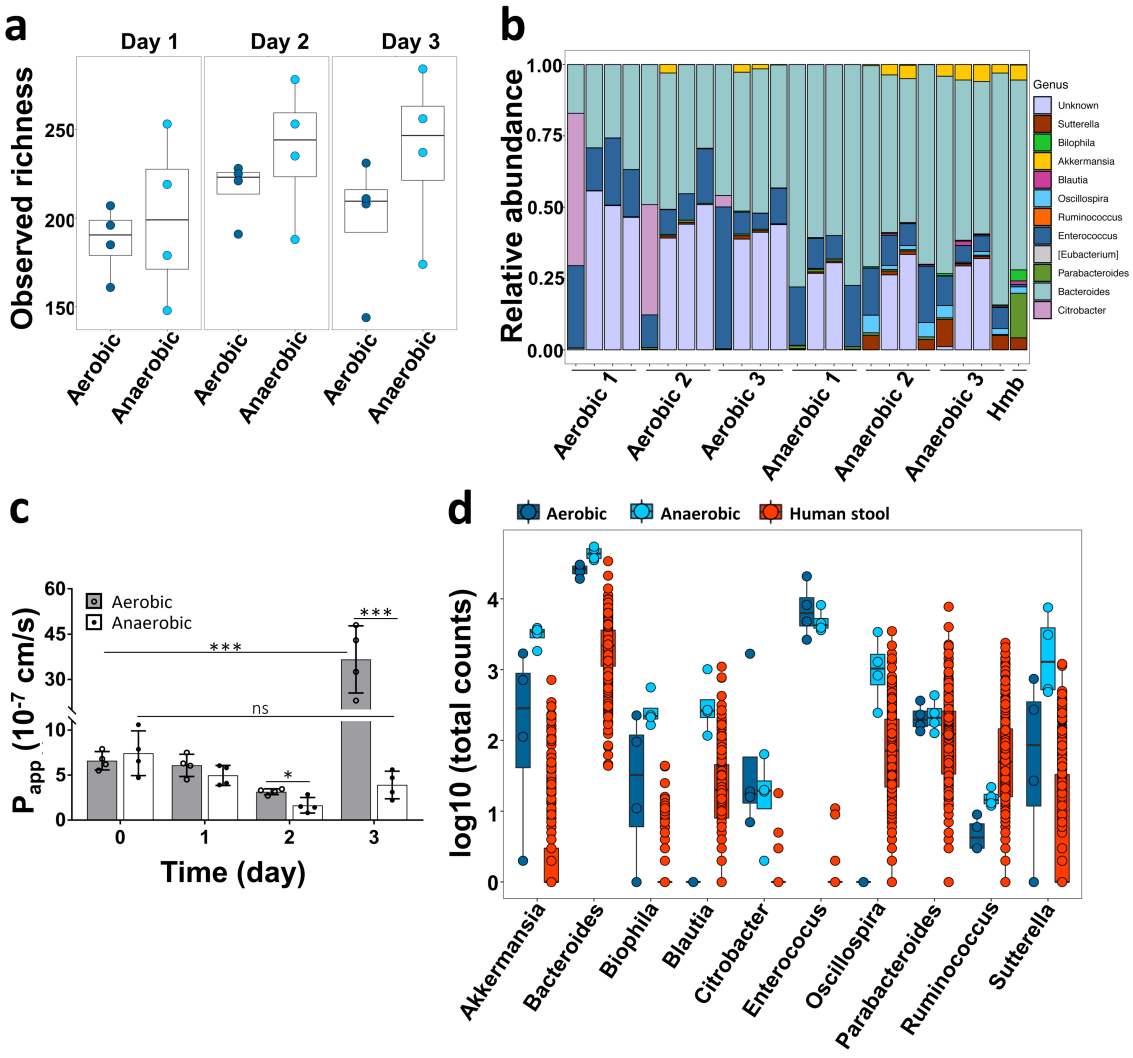

Figure IV-3. Analysis of the diversity and relative abundance of microbiota co-cultured in Intestine Chips under aerobic and aerobic conditions. a, Observed alpha diversity (richness) in our complex gut microbiome samples when cultured for 1 to 3 days in direct contact with human Caco2 intestinal epithelium (each data point represents one Intestine Chip). **b,** Relative abundance of genera measured across all samples highlighting changes in the abundance of the different genera observed over time. Data points represent each of the 3 replicates cultured under aerobic or anaerobic conditions at 0, 1, 2 or 3 days of culture (left to right, respectively); Hmb indicates genera abundance in the complex microbiome stock at time 0. **c,** Changes in apparent paracellular permeability (P_{app}) measured by quantifying cascade blue transport across the tissue-tissue interface within the Intestine Chip after co-culture with complex gut microbiome under aerobic and anaerobic conditions (n=4 individual chips; data are presented as mean ± s.d.; significance was calculated by one-way analysis of variance; $^{*}P = 0.048$, $^{***}P<0.001$, ns = not significant). **d,** Differences in microbial abundance between Intestine Chip samples (dark blue: aerobic; light blue: anaerobic) and human microbiome stool sample from the Human Microbiome Project (red). Data are shown as log10 of the total number of reads; each data point corresponds to a single sample (error bars represent the s.d.; data are presented as box plots with individual data points overlaid, where lower or upper edges of the box represent 25th or 75th percentiles and the middle bar is the median).

To further assess the physiological mimicry obtained using the anaerobic Intestine Chip lined by Caco2 epithelium, we compared the genera identified in this study with publicly available data from studies of human stool generated by the Human Microbiome Project[40] (**Fig. 3d**). We did not expect the composition of the microbiome grown on chip to precisely recapitulate that of stool because the microbiome of the human intestine is known to show regional differences[41,42]. For example previous reports have shown different ratios of the Firmicutes, Bacteroidetes and Actinobacteria phyla in stool samples as compared to small intestine aspirates[41,43]. Nevertheless, our results show that the anaerobic culture system provides an environment for culture of complex gut microbiota in direct contact with living human intestinal epithelium that sustains a diverse bacterial community, which falls into the range of abundances reported in the Human Microbiome Project. Furthermore, the relative abundances of the phyla that dominate the human gut, Bacteroidetes *(Bacteroidetes* and *Parabacteroides* genera*)* and Firmicutes *(Blautia, Enterococcus, Ruminococcus,* and *Oscillospira* genera), were higher in the anaerobic chips than in the aerobic chips with some genera (*Blautia* and *Oscillospira*) missing in the aerobic chips altogether (**Fig. 3d**). Oxygen sensor readouts in aerobic and anaerobic chips cultured with a viable microbiome or under sterile (microbe-free) conditions confirmed that the oxygen concentration was maintained below 1% throughout 5-day co-culture period in the anaerobic co-cultures (**Supplementary Fig. S11d**). Moreover, these results showed a decrease in oxygen concentration in aerobic chips cultured with microbiome over time (**Supplementary Fig. S11d**), which is similar to what we observed in co-cultures with *B. fragilis.* This was likely due to the increased vertical growth of villi we observed in these

chips relative to anaerobic chips, as well as to concomitant oxygen utilization by the bacteria, which increase in numbers by day 1 in both aerobic and anaerobic chips. Although the oxygen concentration in the aerobic chip never reached the low levels obtained in anaerobic chips, this decrease in oxygen could explain the presence of some obligate anaerobes, such as *Akkermansia*, that we observed in the aerobic chips; however, clearly the constant anaerobic conditions are more optimal for maintenance of co-cultures of anaerobic bacteria with viable human cells. Interestingly, the genus *Akkermansia,* which has been recently implicated as an enhancer of gut barrier function[44–46]*,* showed a considerably higher number of total counts in the anaerobic culture system compared to human stool (**Supplementary Fig. S12, S13**). Additionally, the genus *Enterococcus* was found to be present at higher levels in both chip culture systems compared to the stool samples, suggesting that some gut microbial species may grow better under conditions that more closely mimic regions of the living intestine than in stool. Taken together, these data confirm that this anaerobic human Intestine Chip system enables living human intestinal epithelium to be co-cultured in the same channel as a complex human gut microbiome containing a range of bacterial genera that come much closer to what is observed in healthy human donors than has ever been possible before.

To determine the stability of the microbial communities in the anaerobic Intestine Chip system, we analysed their change in abundance over 3 days of co-culture with human Caco2 intestinal epithelium and underlying endothelium. Our results show that genera composed of obligate anaerobes, such as *Akkermansia, Blautia, Bilophila,* and *Suterella,* increased in abundance over time, presumably due to maintenance of low

oxygen concentrations (**Fig. 4a, top**). *Bacteroides*, the highest abundance genus in the anaerobic Intestine Chips, remained relatively stable over time. Additionally, in a subsequent experiment, we cultured anaerobic Intestine Chips with the same Hmb microbiome stock for 5 days and plated serial dilutions of the flush on anaerobic Brucella culture plates in the presence or absence of vancomycin. Our results show that the bacterial load increased at day 1 compared to the seeding inoculum, and then remained constant throughout the experiment (**Supplementary Fig. S11e**). Vancomycin kills Gram positive bacteria, and thus the difference in counts between Brucella plates in the presence versus absence of vancomycin suggests both Gram positive bacteria and Gram negative bacteria (*i.e.*, that survived in the vancomycin plates) remained viable over 5 days of co-culture with the intestinal epithelium on-chip. Thus, although serial dilutions of a mixed population of bacteria do not provide accurate total counts, these data show that both Gram positive and Gram negative bacteria remained viable and proliferated (increased in number) over time in the human Intestine Chips.

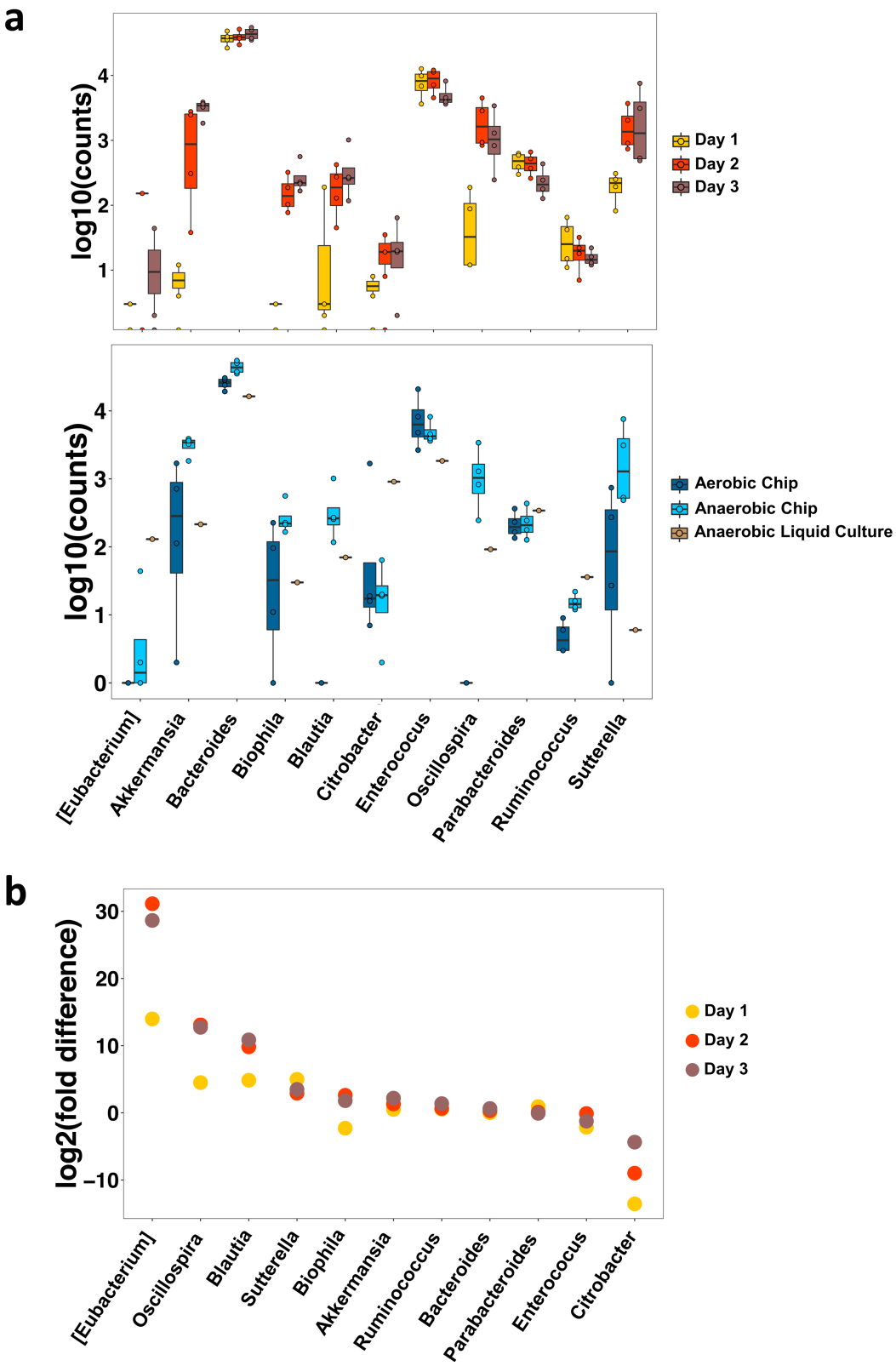
a
log10(counts)
Day 1
Day 2
Day 3
log10(counts)
Aerobic Chip
Anaerobic Chip
Anaerobic Liquid Culture
[Eubacterium]
Akkermansia
Bacteroides
Biophila
Blautia
Citrobacter
Enterococcus
Oscillospira
Parabacteroides
Ruminococcus
Sutterella
b
log2(fold difference)
Day 1
Day 2
Day 3
[Eubacterium]
Oscillospira
Blautia
Sutterella
Biophila
Akkermansia
Ruminococcus
Bacteroides
Parabacteroides
Enterococcus
Citrobacter

Figure IV-4. Anaerobic conditions in the Intestine Chip enhance the growth of multiple genera compared to the aerobic chip and conventional liquid culture. a, Differential abundance bacterial genera in the Caco2 Intestine Chip measured under anaerobic conditions over 3 days of culture (top), or at day 3 in the anaerobic chip compared to the aerobic chip or anaerobic liquid culture (bottom). Data are presented as log10 of the total read counts for each genus; each data point represents one chip.The total read counts for all genera at the bottom are normalized to their counts in liquid culture (data are presented as box plots with individual data points overlaid, where lower or upper edges of the box represent 25^{th} or 75^{th} percentiles and the middle bar is the median). **b,** Differential abundance in bacterial genera measured over 1 to 3 days of co-culture in the anaerobic versus aerobic Intestine Chip (data are represented as log2 fold change; each data point corresponds to the differential abundance for a given genus at a given day, comparing anaerobic to aerobic cultures; n=4 chips for each group on each day; error bars represent the s.d.).

Importantly, when we compared the growth of microbiota cultured for 3 days in the anaerobic Intestine Chip with that produced by culturing the same microbiome samples in conventional liquid medium culture in an anaerobic chamber, we observed significantly different growth responses for multiple genera (**Fig. 4a, bottom**). Notably, the genus *Akkermansia* shows preferential growth in the anaerobic Intestine Chip, presumably due to the presence of high levels of mucus that is produced by the Caco2 intestinal epithelium on-chip[46] (**Fig. 2e,f**), which complements the mucins already present in the medium. Bacteria in the *Blautia*, *Bilophila*, *Oscillospira*, and *Suterella* genera also showed enhanced growth in the anaerobic chips containing living human intestinal epithelium compared to anaerobic liquid culture, whereas the Gram-negative obligate aerobe*, Citrobacter*, was less abundant on-chip. Thus, the presence of human intestinal epithelium that secretes a natural mucus layer above its apical surface[25] (**Fig. 2e,f**) is crucial for culturing and sustaining the complex features of human microbiome *in vitro*.

To complement these analyses, we calculated the differential abundance of the different genera over time in the anaerobic versus aerobic Intestine Chips. Our results show that the obligate anaerobes, *Eubacterium*, *Oscillospira*, *Blautia*, and *Suterella*

were significantly more abundant in the anaerobic chips compared to aerobic chips over our time course (FDR q < 0.05), whereas the obligate aerobe, *Citrobacter,* consistently showed a lower abundance in the anaerobic chip (**Fig. 4b**). Whether taking into account the abundance of the various genera in anaerobic liquid culture (**Supplementary Fig. S12**) or in the Hmb microbiome stock (**Supplementary Fig. S13**), quantification of the total read counts confirmed that the total numbers of obligate anaerobes, including *Sutterella*, *Blautia*, *Oscillospira*, *Bilophila*, and *Akkermansia*, were significantly higher in the anaerobic chips. Taken together, these results confirm that the hypoxia gradient system combined with the presence of a living human intestinal epithelium provides a unique and preferential environment for sustained culture of anaerobic as well as aerobic gut bacteria from diverse genera.

Culture of fresh gut microbiome with primary intestinal epithelium on-chip. Finally, we explored whether this experimental approach can be used to co-culture complex gut microbiome obtained from *fresh* human stool specimens in direct contact with *primary* human intestinal epithelium (*i.e.*, rather than using the established Caco2 intestinal cell line). To do this, we engineered human Intestine Chips lined with intestinal epithelial cells isolated from organoids derived from normal regions of surgical biopsies of human ileum, which exhibit multi-lineage differentiation, villi formation, and mucus production when grown on-chip[27]. We then inoculated the epithelial channels of 4 different chips with complex microbiome isolated from fresh human stool samples collected from four different infants (one with a corrected gestational age of 30 week and three with an age of 36 week). DIC (**Fig. 5a**) and confocal fluorescence microscopic (**Fig. 5b and Supplementary Fig. S14a**) imaging of the primary human

Ileum Chips confirmed the presence of a villus intestinal epithelium lined by a continuous polarized epithelium with F-actin- and villin-containing brush borders along its apical membrane, MUC2-producing cells, and basal nuclei. Importantly, when we measured production of secreted mucus using alcian blue staining (**Supplementary Fig. S14b**), we observed blue stained mucus over the apical surface of the epithelium, and we detected up to 600 $ug.ml^{-1}$ of mucin in the chip outflow (**Supplementary Fig. S14c**). As expected, the bacterial richness was reduced in the infant stool stock (586 OTUs) compared to adult human-derived stool (938 OTUs) at the same dilution per gram of materials, and these differences in richness were accurately recapitulated on-chip. We again found that the primary human intestinal epithelium could be co-cultured in direct contact with this complex gut microbiome without compromising epithelial barrier function, and this co-culture was stably maintained for up to at least 5 days on-chip (**Fig. 5c**), much as we had observed with the Caco2 epithelium. Importantly, the microbiome cultured in these primary Intestine Chips also maintained a high bacterial richness, ranging from 118 to 135 OTUs (**Fig. 5d**) corresponding to 6 phyla (Actinobacteria*,* Bacteroidetes*,* Cyanobacteria*,* Firmicutes*,* Proteobacteria *and* Tenericutes) and 32 unique genera. Thus, the hypoxic Intestine Chip method can be used to sustain a complex community of human microbes in direct contact with normal, patient-derived, human intestinal epithelial cells for many days in culture, which could be valuable for personalized medicine in the future.

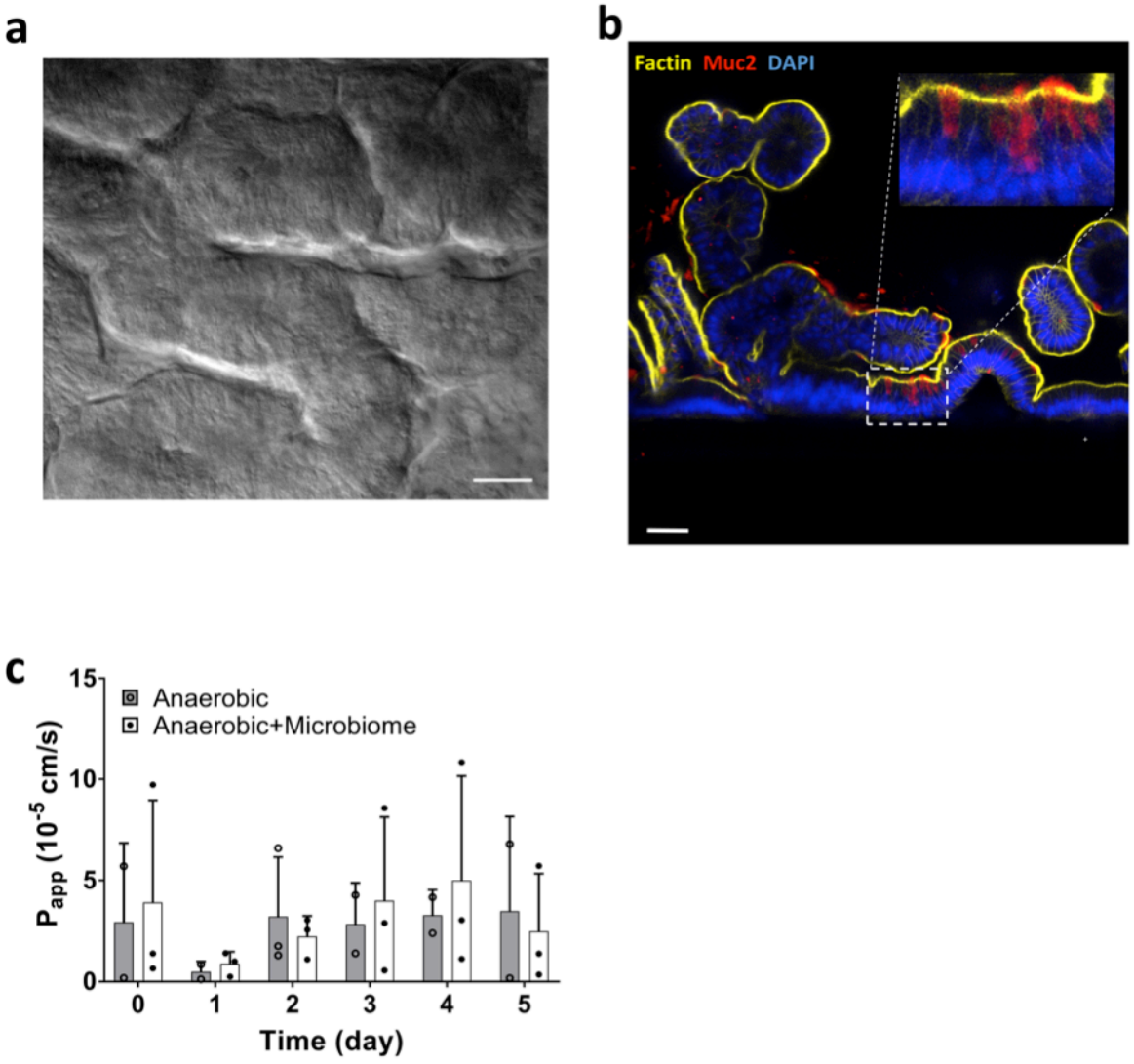

Figure IV-5. Anaerobic co-culture of gut microbiome obtained from fresh human patient-derived stool with primary human ileal epithelium in the Intestine Chip. a, Microscopic views showing the villus morphology of the primary ileal epithelium cultured for 5 days in the Intestine Chip under anaerobic conditions when viewed from above by DIC (scale bar, 50μm) or **b,** shown in cross-section by confocal immunofluorescence imaging for MUC2 (red), F-actin (yellow) and DAPI (blue) (scale bar, 50μm; inset shows area highlighted in white dashed line at higher magnification; representative images from 4 intestine chips are shown). **c,** Changes in apparent paracellular permeability (P_{app}) measured by quantifying cascade blue transport across the tissue interface within the primary Intestine Chip during co-culture with or without complex human gut microbiome under anaerobic conditions (bacteria contained with patient-derived stool samples were added on day 0; n=3 individual chips; data are presented as mean ± s.d.). For richness and Shannon diversity of bacteria in effluent samples of primary Intestine Chips refer to Supplementary Table S2.

Discussion

Given the importance of commensal gut microbiome for human health and the lack of any *in vitro* model that can faithfully mimic the complex epithelial-microbe interactions that occur across the host-microbiome interface, we leveraged human Organ Chip technology to develop a device that enables human intestinal epithelium to be co-cultured with the highly diverse community of commensal microbes that comprises the human gut microbiome under aerobic and anaerobic conditions. Our results show that the anaerobic human Intestine Chip offers a robust modular platform for recapitulating the human intestinal-microbiome interface *in vitro*. Using this device, for the first time, it is possible to stably co-culture a complex living microbiome in direct contact with living mammalian cells and their naturally produced overlying mucus layer for 5 days or more *in vitro*. This is significantly longer than past studies using the HMI model that only sustained co-cultures of intestinal epithelium with complex microbiome for 48 hours, and in which the bacteria had to be physically restricted from contacting the epithelium by a semi-permeable membrane to ensure epithelial viability[17,47]. Importantly, providing a physiologically-relevant low oxygen microenvironment on-chip also sustained a higher level of microbial diversity (~200 unique OTUs) and increased abundance of obligate anaerobic microbiota compared to aerobically-cultured chips, in addition to maintaining a diverse community of commensal microbes that closely resembled that of the human gut microbiome *in vivo*. For example, when the complex gut microbiome was cultured in the anaerobic Intestine Chip, it maintained abundant amounts of obligate anaerobic bacteria, with ratios of Firmicutes and Bacteroidetes similar to those observed in human faeces[44]. Additionally, we found that co-culturing intestinal epithelium with either single

commensal gut microbes (*e.g.*, *B. fragilis*) or over 200 different bacterial OTUs under physiologically relevant anaerobic conditions actually enhanced epithelial barrier function compared to aerobic chips, which again is consistent with *in vivo* findings[39]. This is in direct contrast to past studies in which co-culture of pathogenic bacteria (*e.g.*, enteroinvasive *E. Coli*) was shown to rapidly compromise barrier function in the same Caco2 cells-lined Intestine Chips[21]. This ability to discriminate between healthy versus injury responses of human intestinal epithelium in the presence of commensal versus pathogenic bacteria, and study these direct intercellular interactions under controlled conditions *in vitro*, is a significant advantage of this model versus approaches that separate the microbes from the epithelium by nanoporous membranes.

Oxygen tension is one of the main regulators of intestinal function and pathogenesis of GI diseases[49,50]. By integrating non-toxic oxygen sensors into our devices, we were able to control and measure oxygen levels throughout the microfluidic Intestine Chips without interference with microscopic imaging, device fabrication or cell culture. Use of these sensors, rather than incorporating multiple external oxygen-detecting probes, enables this approach to be more easily scaled so that many miniaturized Organ Chip platforms can be created. The anaerobic chamber we engineered also generates radial oxygen gradients across the endothelium-epithelium-microbiome interface that allows oxygenation of the human tissues while providing an anaerobic environment for growth of the obligate anaerobes. Anaerobic incubators or glove boxes can be used to maintain hypoxic conditions for bacterial cultures, but they commonly provide a single uniform low oxygen concentration, rather than physiologically-relevant oxygen gradients directed across tissue-tissue interfaces. In

contrast, our anaerobic chamber is portable, highly customizable, compatible with imaging, and most importantly, capable of engineering oxygen gradients across the endothelial-epithelial interface of any Organ Chip on demand.

Oxygen concentrations in the lumen of the human intestine are known to affect the spatial distribution and metabolism of gut flora[51], and most intestinal bacteria are obligate anaerobes, many of which fail to grow at oxygen concentrations greater than ~0.5%[52]. Any culture system that is designed to recapitulate the host gut-microbiome interface must therefore be able to achieve and sustain oxygen concentrations at these low levels. A microfluidic-based anaerobic culture system has been described previously that maintains oxygen levels as low as 0.8% in the presence of a facultative anaerobe[47], but this level is still too high to support obligate anaerobes. Moreover, this past model used both a synthetic mucus layer and a nanoporous membrane to physically separate bacteria from the intestinal epithelium[47]. Using our custom anaerobic chamber, we were able to attain an oxygen concentration of less than 0.3% in the epithelial channel where we cultured the commensal microbes, which is much closer to that found in the gut lumen *in vivo*[53]. Additionally, we validated the relevance of these hypoxic culture conditions by showing that they support the growth of an obligate anaerobe *B. fragilis* that cannot grow in the presence of greater than ~0.5% dissolved oxygen[32,54]. Furthermore, the finding that co-culture of the human intestinal epithelium with *B. fragilis* under anaerobic conditions also increased (rather than decreased) intestinal barrier function on-chip is consistent with the finding that oral delivery of *B. fragilis* corrects intestinal permeability defects in a mouse autism model[55].

More importantly, we found that the hypoxic human Intestine Chip supports co-culture of complex human microbiota composed of over 200 unique OTUs and at least 11 different genera of bacteria for multiple days in co-culture. Bacterial members of the *Bacteroidetes* and *Firmicutes* phyla, and to a lesser degree *Verrucomicrobia* and *Proteobacteria*, which comprise the human intestinal microbiome *in vivo*[56], also colonized our Caco2 Intestine Chips at similar ratios. Anaerobic chips had increased levels of anaerobic *Clostridia*, *Bacteroides*, and *Akkermansia*, whereas *Proteobacteria,* which accumulate mainly at more oxygenated regions of the proximal gastrointestinal tract,[53,57] dominated the aerobic chips. One limitation of our approach is the need to dilute the complex microbiome inoculum to avoid rapid unrestrained bacterial overgrowth. This may result in exclusion of some rare bacteria; however, this could be ameliorated by using larger Intestine Chips, optimizing the lumen perfusion rate, applying cyclic (peristalsis-like) mechanical deformations that can suppress growth of some commensals[21], or altering medium conditions to limit bacterial overgrowth in the future. Nevertheless, these data show that the Intestine Chip with the hypoxia gradient and anaerobic conditions in the lumen of the epithelial channel promoted more bacterial diversity than the aerobic system. Moreover, the anaerobic human Intestine Chip supported a wide range of bacterial genera similar to those found in human stool, which is much more complex than any microbiome community that has been previously cultured in direct contact with mammalian cells, and we could sustain these co-cultures for at least 5 days *in vitro*.

Others have previously maintained complex microbiota in test tube cultures[58], however, our results indicate that the presence of a more *in vivo*-like intestinal tissue

microenvironment significantly influences the composition of the microbial community. For example, the mucus degrading, obligate anaerobe genus *Akkermansia* was found in higher abundance in the anaerobic Intestine Chips which contain human intestinal epithelial cells that secrete mucus than in liquid cultures maintained under similar anaerobic conditions that were artificially supplemented with mucin. In contrast to liquid cultures, the anaerobic Intestine Chip also allows inferences to be made regarding the effects of commensal microbes on the host epithelium and *vice versa*. It is interesting that the enhanced growth of *Akkermansia* in the anaerobic Intestine Chip was accompanied by increased intestinal barrier function since the high abundance of this organism has been previously suggested to enhance gut barrier function *in vivo*[44–46].

HIF-1α is believed to control barrier integrity by regulating multiple barrier-protective genes, and its dysregulation may be involved in GI disorders[59,60]. Interestingly, although we observed elevated levels of nuclear HIF-1α in anaerobic Intestine Chips, we did not detect any changes in barrier function unless we also co-cultured complex microbiota. Thus, this experimental system allows us to parse out which physiological effects are due to changes in oxygen levels alone and which are due to the presence of commensal microbes under low oxygen conditions. Defining the causative relationship between the abundance of each individual genus of bacteria and distinct functions of the co-cultured human intestinal epithelium is beyond the scope of this study. However, this system could be harnessed to address these types of questions, as well as how different commensal microbes contribute to the pathophysiology of various gastrointestinal diseases[61] in the future. This model also could be used to analyse fluctuations in microbiome abundance, function, and location

within the chip (e.g., under conditions of antibiotic exposure, hormonal stimulation, etc.) and their effects on intestinal epithelial physiology. Moreover, the clinical relevance of these studies could be further enhanced by developing patient-specific Intestine Chips with both host cells and gut microbiome isolated from the same patients, as well as by obtaining microbiome isolates from different regions of the intestine (*e.g.*, duodenum, jejunum, ileum, colon) and culturing them on chips lined by cells from each of these regions.

The purpose of this study was to develop a method for co-culturing a complex living human gut microbiome, including obligate anaerobes which require strict anaerobic conditions (*i.e.*, < 0.5-1% O_2) to survive, in direct contact with human intestinal epithelial cells and their overlying mucus layer for extended times *in vitro*. While we did not intend to model any specific region of gastrointestinal system using our chips, it should be noted it is possible to create Organ Chips lined by cells from different regions of the intestine (*e.g.*, duodenum, jejunum, ileum, colon) and to use oxygen tensions appropriate for each region (*e.g.*, from 5% to 0.5% moving from duodenum to colon), and potentially introduce the microbiome aspirates from each of these regions. We have previously shown that primary Intestine Chip better recapitulates the morphology, multicellular composition, and gene expression patterns of the intestinal segment from which it was derived than other *in vitro* intestinal culture systems, such as the Caco2 chip and 3D intestinal organoids[27]. Furthermore, by integrating primary epithelial cells from intestinal biopsies as we did here, or patient-derived induced pluripotent stem (iPS) cells[62], in combination with microbiomes obtained from the same patients, it should be possible to develop patient-, disease-, and location-specific, host-

microbiome co-culture models, and thus, pursue a personalized-medicine approach in the future. That said, the Caco2 Intestine Chips also recapitulate many features of human intestinal physiology and pathophysiology, and these cells can be obtained commercially (rather than requiring a patient biopsy), which would enable their widespread use by academic and industrial laboratories, as well as regulatory agencies (*e.g.*, FDA). In addition, the modular nature of the Organ Chip technology allows for the incorporation of additional cell types. In this study, we incorporated intestinal endothelium in our Intestine Chips because it enhances intestinal barrier function, villi development and mucus production[26,27,63], but other cell types, such as immune cells and pathogens that play crucial roles in host gut-microbiome interactions[64,65]could be incorporated as well. Our oxygen sensing chips also have the potential to be combined with on-chip TEER technology[66] for real-time monitoring of intestinal barrier function in the presence of different cell types and individual strains of bacteria. Thus, this methodology could be used in the future to unravel complex functional links between intestinal epithelial cells, immune cells, and gut microbes to understand mechanisms of human disease, discover new therapeutics, and advance personalized medicine. It may be possible to modify this Organ Chip platform to model and study host-microbiome interactions in other organs (*e.g.*, vagina, skin, lung, etc.) as well.

Methods

Fabrication of the oxygen-sensing Organ Chip. Oxygen sensor spots were prepared by mixing oxygen sensitive and optical isolating particles (PreSens GmbH, Germany) at weight ratio of 1:1 in methanol (sigma, 50 mg ml^{-1}) for 2 h under constant stirring. PDMS prepolymer (Sylgard 184, Dow Corning) was then added to the mixture at 1 g ml^{-1} and

solvent was subsequently removed by applying -70 kPa vacuum at 55 ^{o}C for 2 h. PDMS prepolymer was then mixed with curing agent (Sylgard 184, Dow Corning) at weight ratio of 10:1 for 4 min under vacuum, spin-coated (150 μm thick) onto a 5 cm silanized silicon wafer at 800 rpm for 2 min and cured at 60 ^{o}C for at least 30 min. The wafer was removed and the 150 μm thick film was punched into 1 mm diameter sensor discs using a biopsy punch. The sensor discs were dip coated in an uncured PDMS (PDMS prepolymer:curing agent 10:1) and embedded into the PDMS channels of a 2-channel Organ Chip by placing them in moulds at the inlet, middle and outlet of both upper (epithelium) and lower (endothelium) channels, and cured in place at 60 ^{o}C for 30 min. Organ Chip fabrication was then followed as described previously[67]. Using this two-step moulding process, these sensors were placed directly on the surface of both the vascular and epithelial channels of the Organ Chips at their inlet, middle and outlet regions. The chip fabrication and sensor integration steps involving plasma treatment did not interfere with sensor function or the functionality of the microfluidic chips, and the thickness of the sensors did not affect the oxygen readouts when maintained between 150 to 300 μm in height.

Anaerobic chamber fabrication and validation. To fabricate the anaerobic chamber, acrylic parts were cut using a laser cutter (Epilog) and assembled together with an acrylic solvent (SciGrip Acrylic Cement). Gaskets were lasercut from adhesive-backed silicone rubber sheets (20 Shore A hardness, McMaster-Carr) and magnetic clasps were attached using adhesive backed magnets. The anaerobic chamber was tested using a calibrated Oxy-4 optical probe system (PreSens GmbH, Germany) to verify the hypoxic conditions. To do so, the chamber was purged with 5% CO_2 in N_2 bubbled

through deionized water at 81 ml min^{-1}, 162 ml min^{-1}, or 243 ml min^{-1} for 1 h at which point N_2 flow was stopped and the chamber allowed (3 h) to recover to atmospheric oxygen.

Oxygen sensing in the Intestine Chip. To visualize and quantify the concentration of oxygen throughout the chip, oxygen measurements were performed through non-invasive fluorescence read-out using VisiSens-system (PreSens GmbH, Germany). Using a CCD-camera and the VisiSens software (V1.1.2.10), oxygen amount was detected at sensor spots, and displayed using a computer code in pseudo colours. The software has been designed to calculate oxygen levels on the sensor spots via calibration of fluorescence reading with defined oxygen levels at 0 and 100% air saturation (*i.e.* 20.9% O_2 of all dissolved gas by volume). In all experiments, oxygen levels were quantified after comparing the readings with the calibration values. Air-saturated water and oxygen-free solution (Oakton, WD-00653-00) were used to calibrate the sensor spots. Since the field-of-view of the VisiSens camera is inherently small, we designed a linear positioning system that can position the camera directly beneath the Intestine Chips in the hypoxia chamber. This allows indexed motions of the camera to any sensor spot along the chip or between the chips and thus, facilitates reproducibly imaging multiple chips in one run. The sensors do not obscure regular imaging of the chips as they only cover a small portion of the culture area (~3 mm^2), allowing for regular monitoring of cultures throughout the experiment. We also designed a black opaque box that covers entire chip culture chamber and VisiSens camera to block extraneous light. To analyse the accuracy of sensor spots inside the chips Oxygen concentrations were measured in gas phase using calibrated gas tanks with

known oxygen concentration, *i.e.* 0, 1, and 12.5% O_2. The VisiSens imaging system was validated using an Oxy-4 optical probe system (PreSens) with optical fibers (POF-L2.5, PreSens, Germany).

Oxygen sensor analysis. Images of oxygen sensors were processed in MATLAB (Mathworks) and binarized using Otsu's method [68]. Morphological erosion and dilation were preformed to eliminate any spurious artefacts created during binarization. Simulated annealing was applied to find the correct assignment of sensors in each image regardless of the chip alignment. The sum of the distance of each of the sensor's centroids in the current image between the nearest sensor's centroid in the original image was minimized. After aligning the images, the sensors in the current image were registered consistently with the sensors in the former image, and colorimetric analyses were computed. The average intensities were calculated for each of the red, blue, and green channels, in each sensor. The uncalibrated signal from each sensor was taken to be the average green intensity divided by the average red intensity. The uncalibrated signal was then fit to a calibration curve. We used a modified Michaelis-Menten two-point calibration as the most generalizable model, $C_{oxy=}\ k_{min}+\ (k_{max}-k_{min})\ x\ [x_{g:r}\ /\ (k_{rate}+x_{g:r})];\ k_{max}=a\ x\ k_{atm}$, where $x_{g:r}$ denotes the ratio of average green intensity to average red intensity, C_{oxy} is the fraction of atmospheric oxygen, k_{min} is the sensor signal at anaerobic conditions, k_{max} is the sensor signal when saturated with oxygen, and the concentration of oxygen is given as C_{oxy}. k_{rate} explains the effect that the observed signal, $x_{g:r}$, has on the concentration of oxygen. The atmospheric oxygen concentration does not fully saturate the sensor with oxygen. To overcome this, actual maximum possible signal from a sensor, k_{max}, is estimated by multiplying the

uncalibrated signal at atmospheric concentration, k_{atm}, by a scale factor α. The Michaelis-Menton curve was approximately linear between $x_{g:r}=k_{atm}$ and $x_{g:r}=k_{max}$, scaling by a linear coefficient did not hamper the equation's ability to generalize between sensors. The curve was fit using images acquired at known oxygen concentrations. The known concentrations were measured by Oxy-4 optical probe system (PreSens GmbH, Germany). The oxygen concentrations were also validated by flowing oxygen at known concentrations over the probe and sensor. Both k_{rate} and α were fit using the data. The model produced a suitable fit for the data (R^2=0.990 training, R^2=0.997 and 0.998 for testing). The fitted model generalized well for trials repeated in different chips and on different days.

Cell culture procedures. Prior to cell seeding, microfluidic sensor chips were activated using oxygen plasma (Diener ATTO) and functionalized with (3-Aminopropyl) trimethoxysilane (Sigma, 281778), as reported previously[26]. Chips were then washed with ethanol, oven-dried at 80^{o}C and coated with 30 μg ml^{-1} Collagen (Gibco, A10483-01) and 100 μg ml^{-1} Matrigel (BD Biosciences, 356237) in the serum-free Dulbecco's Modified Eagle Medium (DMEM; Gibco, 10564011) for 1 h at 37 ^{o}C. To fabricate the Caco2 Intestine Chip, human intestinal microvascular endothelial cells (HIMECs; ScienCell) were first seeded (1.5x10^{5} cells cm^{-2}) in the bottom channel of the chips, on opposite side of the porous membrane. Chips were then placed in 37^{o}C incubator for 1.5 h. For HIMECs culture, endothelial growth medium (EGM2-MV) containing human epidermal growth factor, hydrocortisone, vascular endothelial growth factor, human fibroblastic growth factor-B, R3-Insulin-like Growth Factor-1, Ascorbic Acid and 5% fetal bovine serum (Lonza Cat. no. CC-3202) was used. Human intestinal epithelial cells

(Caco2 BBE human colorectal carcinoma cell, Harvard Digestive Disease Center) were then seeded into the top microchannel of the chip ($1.5x10^5$ cells cm^{-2}) and incubated for 1.5 h. Epithelial cells were fed with DMEM (Gibco, 10564011) containing Pen/Strep and 20% Fetal Bovine Serum (FBS; Gibco, 10082-147). After washing with 200 μl of medium, chips were cultured statically overnight to allow cells to form monolayers on both sides of the membrane. A day after seeding, top and bottom channels were perfused (60 μl h^{-1}) with epithelial medium and reduced-FBS endothelial medium, respectively. Chips were kept in this condition until villus-like intestinal epithelium spontaneously appeared. For anaerobic culture, the same procedure was followed except that after 1 day of perfusion in aerobic conditions, chips were placed in an anaerobic chamber and continuously perfused with 5% CO_2 in N_2 flowed at 243 mL min^{-1}.

To create primary Intestine Chips, we used cells isolated from human intestinal organoids that were derived from resected tissue of a 15 year-old patient diagnosed with ulcerative colitis and collected from grossly unaffected (macroscopically normal) areas of the terminal ileum during endoscopy procedure, as described previously[27]. Informed consent and developmentally-appropriate assent were obtained at Boston Children's Hospital from the donors' guardian and the donor, respectively. All methods were carried out in accordance with the Institutional Review Board of Boston Children's Hospital (Protocol number IRB-P00000529) approval.

Organ Chips with the same 2-channel design, but obtained from Emulate Inc. (Boston, MA), were used to create the primary human Intestine Chip. The chips were chemically activated using ER1 and ER2 solutions (Emulate Inc.) before introducing type I collagen

(200 μg.ml^{-1}) and Matrigel (1% in PBS) into the channels, and incubating in a humidified 37 °C incubator for 2 h to coat the porous membrane with ECM before washing with PBS. Primary human intestinal epithelial cells that were isolated from the ileal organoids using collagenase and mechanical dissociation as described previously[27] were then resuspended in expansion medium (EM) consisting of Advanced DMEM/F12 supplemented with L-WRN conditioned medium (50% v/v, ATCC), glutamax, HEPES, murine epidermal growth factor (50 ng.ml^{-1}), N2 supplement, B27 supplement, human [Leu15]-gastrin I (10 nM), n-acetyl cysteine (1 mM), nicotinamide (10 mM), SB202190 (10 μM) and A83-01 (500 nM). A small volume (30μl) of the EM solution containing the primary intestinal cells (6 × 10^6 cells.ml^{-1}) was used to infuse and fill the apical chamber of each chip resulting in ~180,000 cells.chip^{-1}; these chips were then incubated overnight under static conditions at 37°C to promote cell adhesion. The following day EM without cells was perfused (60 μl.h^{-1}) through the top and bottom channels and cyclic suction was applied to hollow side chambers using a vacuum pump controlled by an electronic vacuum regulator (ITV009, SMC Corp.) and an Arduino microcontroller to exert peristalsis-like stretching motions (10% cell strain, 0.15Hz frequency) on the porous membrane and attached epithelium. Chips were maintained under these conditions until villus like structures were detected visually under phase contrast imaging (~14 days). Before adding microbiota, peristalsis-like cyclic stretching was stopped and the apical medium was then replaced with antibiotic-free DM containing microbial supplements (1 mg.ml^{-1} pectin, 1 mg.ml^{-1} mucin, 5 μg.ml^{-1} Hemin and 0.5 μg.ml^{-1} Vitamin K1) and the basal medium was replaced with antibiotic free EM.

Bacterial and Microbiota culture. *B. fragilis* (9343 strain) was grown overnight at 37 ^{o}C under anaerobic conditions (80% N_2, 10% H_2, 10% CO_2) in rich media containing yeast extract (5 g L^{-1}), proteose peptone (20 g L^{-1}), NaCl (5 g L^{-1}), hemin (5 mg L^{-1}), vitamin K1 (0.5 mg L^{-1}), K_2HPO_4 (5 g L^{-1}) and HADA (HCC-amino-D-alanine, λ_{em} ~ 450 nm; 0.8 mM) or GalCCP (*N*- cyclopropenyl galactosaminyl carbamate; 250 μm). Hemin, vitamin K1, K_2HPO_4, and HADA[33] were added through a 0.22 μm filter after autoclaving the other ingredients. For HADA labelling, *B. fragilis* was pelleted at 5000 g, washed once in DMEM, and re-suspended in Caco2 media (DMEM 20% FBS, 1% glutamine, 1 mg ml^{-1} pectin, 1 mg ml^{-1} mucin, 5 μg ml^{-1} Hemin, 0.5 μg ml^{-1} Vitamin K1) at 1 x 10^7 CFU ml^{-1}. For GalCCP labelling, *B.* fragilis was pelleted at 5000 g washed twice with PBS, once with 1% BSA in PBS, then incubated with 5 μM Tetrazine-Cy3 for one hour at 37 ^{o}C. Bacteria were pelleted and washed twice with 1% BSA in PBS, one with PBS[33], and re-suspended in Caco2 media. For microbiota co-culture, colon and cecum content from five mice colonized with healthy human microbiota (Hmb) [23] were collected and re-suspended in sterile PBS inside an anaerobic chamber (100 mg of content ml^{-1}). The slurry was then filtered (40 μm) and aliquoted and stored at -80 °C as the human microbiome stock, which was diluted 1:100 in epithelial medium when added to Intestine Chips. For microbiota co-culture with patient-derived specimens, fecal samples were collected from infants born at Brigham and Women's Hospital in Boston, MA and cared for in a single-centre Newborn Intensive Care Unit (NICU). Parental consent was obtained and all study procedures followed a protocol that was approved by the Partner's Human Research Committee for Brigham and Women's Hospital and Massachusetts General Hospital (Protocol number 2012-P-002453). Fecal samples

were collected from preterm infants born prior to 32 weeks of gestation from birth until discharge. Briefly, diapers with fecal samples were collected daily by the bedside nurse, placed in a specimen bag, and stored at 4 °C for no more than 24 hours. Fecal material was extracted from diapers using sterile procedures and immediately frozen at -80 °C. Selected samples were suspended in Brain Heart Infusion media (100 $mg.ml^{-1}$) to create a stock solution.

Co-culture with gut microbes and complex microbiome in the Intestine Chips. One day before adding bacteria, media reservoirs were washed with PBS and antibiotic-free media was then added to Intestine Chips in a tissue culture hood (aerobic conditions) or in an anaerobic chamber (anaerobic conditions). The next day, 25 μl of *B. fragilis* (1×10^7 CFU ml^{-1}) or diluted microbiota stock was added to the apical side of differentiated Intestine Chips in a tissue culture hood (aerobic conditions) or in an anaerobic chamber (anaerobic conditions). Chips were left static for 30 min and then perfused at 1 μl min^{-1}. Every 24 h, a 2 min flush at 50 μl min^{-1} was performed and the flush outflow was collected and serial dilutions were plated on Brucella plates incubated at 37°C in an anaerobic chamber (*B. fragilis* cultures), Brucella plates +/- 6 μg ml^{-1} vancomycin (Hmb cultures) or sent for 16S rRNA sequencing (Diversigen).

Morphological analyses. For each experiment, regions of 3 different Intestine Chips were analyzed morphologically at each interval. The villus structures formed by the intestinal epithelium were evaluated using DIC microscopy (Zeiss Axio Observer Z1 2, AXIO2) or immunoflorescence microscopy with a laser scanning confocal microscope (Leica SP5 X MP DMI-6000 and Zeiss TIRF/LSM 710). High-resolution horizontal or vertical cross-sectional images were obtained using deconvolution (Huygens) followed

by a 2D projection process. IMARIS (MARIS 7.6 F1 workstation; Bitplane Scientific Software) and ImageJ were used for analysing the obtained images.

For SEM analysis, Intestine Chips were designed in a way that top channel was not irreversibly bonded to the membrane, which permitted the device to be dismantled manually without disturbing the cultured cells. Chips were first treated with Carnoy's solution for mucus fixation, and then fixed with paraformaldehyde (PFA, 4%; Electron Microscopy Sciences, 157–4) and glutaraldehyde (2.5%; Sigma, G7776) and incubated in osmium tetroxide (0.5%; Electron Microscopy Sciences, 19152) before serial dehydration in ethanol. Samples were then dried using a critical point dryer and imaged with a field emission SEM (Hitachi S-4700).

Immunofluorescence microscopy. Epithelial and endothelial cells were washed with PBS, fixed with 4% paraformaldehyde (PFA; Electron Microscopy Sciences, 157-4) and subsequently washed with additional PBS. Permeabilization of cells was accomplished with 0.25% Triton X-100 (Sigma, T8787), followed by incubation in blocking buffer containing 1% BSA (Sigma, A4503) and 10% donkey serum (Sigma, D9663) at room temperature. Primary antibodies against ZO1 (Life Technologies, 33-9100, dilution 1:200), VE-cadherin/CD144 (BD Biosciences, 555661, dilution 1:200), Villin (Life Technologies, PA5-29078, dilution 1:100), Muc2 (Santa Cruz Biotechnology, sc-15334, dilution 1:100) or HIF-1α (Abcam, ab16066, dilution 1:100) were added and incubated overnight at 4^{o}C, followed by multiple PBS washes. Cells were then incubated with secondary fluorescent antibodies (Life Technologies) at room temperature and washed with PBS; nuclei were co-stained with DAPI (Invitrogen, D1306). Microscopy was

performed with a laser scanning confocal microscope (Leica SP5 X MP DMI-6000 or Zeiss TIRF/LSM 710).

Mucus Detection. For the mucus visualization, Wheat Germ Agglutinin (WGA) Alexa Fluor 488 conjugate (Thermo Fisher Scientific) was used for the live cell imaging as described previously[34]. Briefly, WGA solution (25 $\mu g.ml^{-1}$ in culture medium) was flowed through the epithelium channel for 30 min. Top channel was washed subsequently with PBS in the dark and counter-stained with DAPI to visualize nuclei. To stain acidic mucopolysaccharides within the intestinal mucus, Intestine Chips were stained with 0.1% (w/v) alcian blue solution (pH 2.5; 8GX, Sigma) in 3% acetic acid (Sigma) by flowing the solution into the microchannels at 50 $\mu L.h^{-1}$ for 12 h, and then washing with PBS.

Paracellular permeability measurements. 50 $\mu g\ ml^{-1}$ of cascade blue (5.9 kDa; ThermoFisher, C687) were introduced to the epithelium channel (60 $mL\ hr^{-1}$) and fluorescence intensity (390 nm/420 nm) of top and bottom channel effluents were measured using a multi-mode plate reader (BioTek NEO). Apical-to-basolateral flux of the paracellular marker was calculated based on the following equation: $P_{app}=(dQ/dt)/A.dC$. P_{app} ($cm\ s^{-1}$) denotes the apparent permeability coefficient, dQ/dt ($g\ s^{-1}$) is molecular flux, A (cm^2) is the total area of diffusion and dC ($mg\ mL^{-1}$) is the average gradient. In some studies, Lucifer Yellow was used instead of Cascade Blue using a previously published method[27].

Cellular toxicity. CytoTox 96 Non-Radioactive Cytotoxicity Assay (LDH; Promega, G1780) was used according to the manufacturer's instructions to measure epithelium and endothelium viability over time under aerobic and anaerobic culture conditions. In

brief, effluents were collected from top and bottom channels, mixed with LDH substrate reagent and incubated for 30 min. The enzymatic reaction was terminated using stop solution (containing acetic acid) and the absorbance at 492 nm was recorded using a multi-mode plate reader (BioTek NEO). The LDH activity was assessed using quadruplicate of each group, calculated after subtracting the background absorbance values and reported as a fold change of the total LDH values of control group.

16S rRNA sequencing analysis. Following sequencing, read counts were obtained by processing the FASTQ files using QIIME 1.0 under standard protocols and resulting joined reads were aligned to the Greengenes database. A total of 938 OTUs were identified. As one of the steps in our analyses of the 16S sequencing data, we removed OTUs that did not meet certain criteria in terms of representation across all the samples. The data were loaded into R and the phyloseq package[69] was used for further processing. Data from a sequencing control (medium only) were used to correct the count data in all of our samples. For any given OTU identified, the read counts for that OTU found in the control sample (*i.e.*, a medium sample without microbes that was run through the sequencer, allowing for the control of sequencing errors) was effectively subtracted. In the cases where the number of reads for a given OTU in a sample of interest was negative (*i.e.*, the number of reads in the control was higher than that of the sample), we listed the number of reads of that OTU as 0. After performing diversity analyses, all singletons were removed from the data set and the OTUs were summarized to the genus level, resulting in a total 42 unique OTUs, corresponding to 9 well characterized genera (34 OTUs) and 8 OTUs of unknown genus (Proteobacteria and Firmicutes phyla). Differential abundance of these genera between the two culture

conditions (*i.e.* aerobic and anaerobic) was done using the DESeq2 package[70]. OTUs showing a differential abundance with an FDR corrected p-value q < 0.05 were considered significant. The PERMANOVA test was run using in R using the adonis function in the vegan package between aerobic and anaerobic conditions, as well as between the two oxygen conditions across the different days. Comparisons to human stool microbiome was done against the Human Microbiome Project HMP1 data set (data set contains 44,740 OTUs across 4,743 samples from 18 different body sites.)

Statistical analysis. All experiments were carried out at n=3-6 (see figure captions), and results and error bars indicate mean ± standard deviation (SD). Data analysis was performed with a one-way analysis of variance (ANOVA) with Tukey HSD post hoc tests using Prism (GraphPad). Statistical analysis between two conditions was performed by an unpaired student's *t*-test. P values less than 0.05 were considered significant.

Reporting summary. Further information on research design is available in the Nature Research Reporting Summary linked to this article.

Data availability

The main data supporting the findings of this study are available within the Article and its Supplementary Information. The raw data generated in this study are available from the corresponding author upon reasonable request.

References

1. Cho, I. & Blaser, M. J. The human microbiome: at the interface of health and disease. *Nat. Rev. Genet.* **13**, 260 (2012).

2. Donaldson, G. P., Lee, S. M. & Mazmanian, S. K. Gut biogeography of the bacterial microbiota. *Nat. Rev. Microbiol.* **14**, 20–32 (2016).

3. Pickard, J. M., Zeng, M. Y., Caruso, R. & Núñez, G. Gut microbiota: Role in pathogen colonization, immune responses, and inflammatory disease. *Immunol. Rev.* **279**, 70–89 (2017).

4. Sommer, F. & Bäckhed, F. The gut microbiota — masters of host development and physiology. *Nat. Rev. Microbiol.* **11**, 227 (2013).

5. Walter, J. & Ley, R. The human gut microbiome: ecology and recent evolutionary changes. *Annu. Rev. Microbiol.* **65**, 411–429 (2011).

6. Sommer, M. O. Advancing gut microbiome research using cultivation. *Curr. Opin. Microbiol.* **27**, 127–132 (2015).

7. Eain, M. M. G. et al. Engineering Solutions for Representative Models of the Gastrointestinal Human-Microbe Interface. *Engineering* **3**, 60–65 (2017).

8. Fritz, J. V., Desai, M. S., Shah, P., Schneider, J. G. & Wilmes, P. From meta-omics to causality: experimental models for human microbiome research. *Microbiome* **1**, 14 (2013).

9. Arrieta, M.-C., Walter, J. & Finlay, B. B. Human Microbiota-Associated Mice: A Model with Challenges. *Cell Host Microbe* **19**, 575–578 (2016).

10. Nguyen, T. L. A., Vieira-Silva, S., Liston, A. & Raes, J. How informative is the mouse for human gut microbiota research? *Dis. Model. Mech.* **8**, 1–16 (2015).

11. Sadabad, M. S. et al. A simple coculture system shows mutualism between anaerobic faecalibacteria and epithelial Caco-2 cells. *Sci. Rep.* **5**, 17906 (2015).

12. Dutta, D. & Clevers, H. Organoid culture systems to study host–pathogen interactions. *Curr. Opin. Immunol.* **48**, 15–22 (2017).

13. Fatehullah, A., Tan, S. H. & Barker, N. Organoids as an in vitro model of human development and disease. *Nat. Cell Biol.* **18**, 246–254 (2016).

14. Williamson, I. A. et al. A High-Throughput Organoid Microinjection Platform to Study Gastrointestinal Microbiota and Luminal Physiology. *Cell. Mol. Gastroenterol. Hepatol.* ***6, 301–319 (2018).***

15. Bein, A. et al. Microfluidic Organ-on-a-Chip Models of Human Intestine. *Cell. Mol. Gastroenterol. Hepatol.* **5**, 659–668 (2018).

16. Abbeele, P. V. den et al. Incorporating a mucosal environment in a dynamic gut model results in a more representative colonization by lactobacilli. *Microb. Biotechnol.* **5**, 106–115 (2012).

17. Marzorati, M. et al. The HMI™ module: a new tool to study the Host-Microbiota Interaction in the human gastrointestinal tract in vitro. *BMC Microbiol.* **14**, 133 (2014).

18. Van de Wiele, T., Van den Abbeele, P., Ossieur, W., Possemiers, S. & Marzorati, M. The Simulator of the Human Intestinal Microbial Ecosystem (SHIME®). in *The Impact of Food Bioactives on Health: in vitro and ex vivo models* (eds. Verhoeckx, K. et al.) (Springer, 2015).

19. Van den Abbeele, P. et al. Microbial community development in a dynamic gut model is reproducible, colon region specific, and selective for Bacteroidetes and Clostridium cluster IX. *Appl. Environ. Microbiol.* **76**, 5237–5246 (2010).

20. Kim, H. J., Huh, D., Hamilton, G. & Ingber, D. E. Human gut-on-a-chip inhabited by microbial flora that experiences intestinal peristalsis-like motions and flow. *Lab. Chip* **12**, 2165–2174 (2012).

21. Kim, H. J., Li, H., Collins, J. J. & Ingber, D. E. Contributions of microbiome and mechanical deformation to intestinal bacterial overgrowth and inflammation in a human gut-on-a-chip. *Proc. Natl. Acad. Sci.* **113**, E7–E15 (2016).

22. Park, G.-S. et al. Emulating Host-Microbiome Ecosystem of Human Gastrointestinal Tract in Vitro. *Stem Cell Rev.* **13**, 321–334 (2017).

23. Chung, H. et al. Gut immune maturation depends on colonization with a host-specific microbiota. *Cell* **149**, 1578–1593 (2012).

24. Surana, N. K. & Kasper, D. L. Moving beyond microbiome-wide associations to causal microbe identification. *Nature* **552**, 244–247 (2017).

25. Kim, H. J., Huh, D., Hamilton, G. & Ingber, D. E. Human gut-on-a-chip inhabited by microbial flora that experiences intestinal peristalsis-like motions and flow. *Lab. Chip* **12**, 2165–2174 (2012).

26. Jalili-Firoozinezhad, S. et al. Modeling radiation injury-induced cell death and countermeasure drug responses in a human Gut-on-a-Chip. *Cell Death Dis.* **9**, 223 (2018).

27. Kasendra, M. et al. Development of a primary human Small Intestine-on-a-Chip using biopsy-derived organoids. *Sci. Rep.* **8**, 2871 (2018).

28. Zheng, L., Kelly, C. J. & Colgan, S. P. Physiologic hypoxia and oxygen homeostasis in the healthy intestine. A Review in the Theme: Cellular Responses to Hypoxia. *Am. J. Physiol. Cell Physiol.* **309**, C350-360 (2015).

29. Jiang, B. H., Semenza, G. L., Bauer, C. & Marti, H. H. Hypoxia-inducible factor 1 levels vary exponentially over a physiologically relevant range of O2 tension. *Am. J. Physiol.* **271**, C1172-1180 (1996).

30. Chilov, D. et al. Induction and nuclear translocation of hypoxia-inducible factor-1 (HIF-1): heterodimerization with ARNT is not necessary for nuclear accumulation of HIF-1alpha. *J. Cell Sci.* **112**, 1203–1212 (1999).

31. Surana, N. K. & Kasper, D. L. The yin yang of bacterial polysaccharides: lessons learned from B. fragilis PSA. *Immunol. Rev.* **245**, 13–26 (2012).

32. Patrick, S., Reid, J. H. & Larkin, M. J. The growth and survival of capsulate and non-capsulate Bacteroides fragilis in vivo and in vitro. *J. Med. Microbiol.* **17**, 237–246 (1984).

33. Hudak, J. E., Alvarez, D., Skelly, A., von Andrian, U. H. & Kasper, D. L. Illuminating vital surface molecules of symbionts in health and disease. *Nat. Microbiol.* **2**, 17099 (2017).

34. Shin, W. & Kim, H. J. Intestinal barrier dysfunction orchestrates the onset of inflammatory host–microbiome cross-talk in a human gut inflammation-on-a-chip. *Proc. Natl. Acad. Sci.* **115**, E10539–E10547 (2018).

35. Kuo, J. C.-H. et al. Detection of colorectal dysplasia using fluorescently labelled lectins. *Sci. Rep.* **6**, 24231 (2016).

36. Kim, H. J. & Ingber, D. E. Gut-on-a-Chip microenvironment induces human intestinal cells to undergo villus differentiation. *Integr. Biol. Quant. Biosci. Nano Macro* **5**, 1130–1140 (2013).

37. Rozee, K. R., Cooper, D., Lam, K. & Costerton, J. W. Microbial flora of the mouse ileum mucous layer and epithelial surface. *Appl. Environ. Microbiol.* **43**, 1451–1463 (1982).

38. Lock, J. Y., Carlson, T. L., Wang, C.-M., Chen, A. & Carrier, R. L. Acute Exposure to Commonly Ingested Emulsifiers Alters Intestinal Mucus Structure and Transport Properties. *Sci. Rep.* **8**, 10008 (2018).

39. Villmones, H. C. et al. Species Level Description of the Human Ileal Bacterial Microbiota. *Sci. Rep.* **8**, 4736 (2018).

40. The Human Microbiome Project Consortium *et al.* Structure, function and diversity of the healthy human microbiome. *Nature* **486**, 207–214 (2012).

41. Stearns, J. C. et al. Bacterial biogeography of the human digestive tract. *Sci. Rep.* **1**, 170 (2011).

42. Guarner, F. & Malagelada, J.-R. Gut flora in health and disease. *The Lancet* **361**, 512–519 (2003).

43. Wang, M., Ahrné, S., Jeppsson, B. & Molin, G. Comparison of bacterial diversity along the human intestinal tract by direct cloning and sequencing of 16S rRNA genes. *FEMS Microbiol. Ecol.* **54**, 219–231 (2005).

44. Fujio-Vejar, S. et al. The Gut Microbiota of Healthy Chilean Subjects Reveals a High Abundance of the Phylum Verrucomicrobia. *Front. Microbiol.* **8**, 1221 (2017).

45. Schneeberger, M. et al. *Akkermansia muciniphila* inversely correlates with the onset of inflammation, altered adipose tissue metabolism and metabolic disorders during obesity in mice. *Sci. Rep.* **5**, 16643 (2015).

46. Everard, A. et al. Cross-talk between Akkermansia muciniphila and intestinal epithelium controls diet-induced obesity. *Proc. Natl. Acad. Sci.* **110**, 9066–9071 (2013).

47. Shah, P. et al. A microfluidics-based *in vitro* model of the gastrointestinal human–microbe interface. *Nat. Commun.* **7**, 11535 (2016).

48. Pedicord, V. A. et al. Exploiting a host-commensal interaction to promote intestinal barrier function and enteric pathogen tolerance. *Sci. Immunol.* **1**, (2016).

49. Sheridan, W. G., Lowndes, R. H. & Young, H. L. Intraoperative tissue oximetry in the human gastrointestinal tract. *Am. J. Surg.* **159**, 314–319 (1990).

50. He, G. et al. Noninvasive measurement of anatomic structure and intraluminal oxygenation in the gastrointestinal tract of living mice with spatial and spectral EPR imaging. *Proc. Natl. Acad. Sci.* **96**, 4586–4591 (1999).

51. Ohland, C. L. & Jobin, C. Microbial Activities and Intestinal Homeostasis: A Delicate Balance Between Health and Disease. *Cell. Mol. Gastroenterol. Hepatol.* **1**, 28–40 (2015).

52. Flint, H. J., Scott, K. P., Louis, P. & Duncan, S. H. The role of the gut microbiota in nutrition and health. *Nat. Rev. Gastroenterol. Hepatol.* **9**, 577 (2012).

53. Albenberg, L. et al. Correlation Between Intraluminal Oxygen Gradient and Radial Partitioning of Intestinal Microbiota in Humans and Mice. *Gastroenterology* **147**, 1055-1063.e8 (2014).

54. Baughn, A. D. & Malamy, M. H. The strict anaerobe Bacteroides fragilis grows in and benefits from nanomolar concentrations of oxygen. *Nature* **427**, 441–444 (2004).

55. Hsiao, E. Y. et al. Microbiota modulate behavioral and physiological abnormalities associated with neurodevelopmental disorders. *Cell* **155**, 1451–1463 (2013).

56. Clemente, J. C., Ursell, L. K., Parfrey, L. W. & Knight, R. The Impact of the Gut Microbiota on Human Health: An Integrative View. *Cell* **148**, 1258–1270 (2012).

57. Shin, N.-R., Whon, T. W. & Bae, J.-W. Proteobacteria: microbial signature of dysbiosis in gut microbiota. *Trends Biotechnol.* **33**, 496–503 (2015).

58. Goodman, A. L. et al. Extensive personal human gut microbiota culture collections characterized and manipulated in gnotobiotic mice. *Proc. Natl. Acad. Sci.* **108**, 6252–6257 (2011).

59. Karhausen, J. et al. Epithelial hypoxia-inducible factor-1 is protective in murine experimental colitis. *J. Clin. Invest.* **114**, 1098–1106 (2004).

60. Manresa, M. C. & Taylor, C. T. Hypoxia Inducible Factor (HIF) Hydroxylases as Regulators of Intestinal Epithelial Barrier Function. *Cell. Mol. Gastroenterol. Hepatol.* **3**, 303–315 (2017).

61. Cirstea, M., Radisavljevic, N. & Finlay, B. B. Good Bug, Bad Bug: Breaking through Microbial Stereotypes. *Cell Host Microbe* **23**, 10–13 (2018).

62. Workman, M. J. et al. Enhanced Utilization of Induced Pluripotent Stem Cell–Derived Human Intestinal Organoids Using Microengineered Chips. *Cell. Mol. Gastroenterol. Hepatol.* **5**, 669-677.e2 (2018).

63. Kim, H. J., Li, H., Collins, J. J. & Ingber, D. E. Contributions of microbiome and mechanical deformation to intestinal bacterial overgrowth and inflammation in a human gut-on-a-chip. *Proc. Natl. Acad. Sci.* **113**, E7–E15 (2016).

64. Hooper, L. V., Littman, D. R. & Macpherson, A. J. Interactions Between the Microbiota and the Immune System. *Science* **336**, 1268–1273 (2012).

65. Rimoldi, M. et al. Intestinal immune homeostasis is regulated by the crosstalk between epithelial cells and dendritic cells. *Nat. Immunol.* **6**, 507 (2005).

66. Henry, O. Y. F. et al. Organs-on-chips with integrated electrodes for trans-epithelial electrical resistance (TEER) measurements of human epithelial barrier function. *Lab. Chip* **17**, 2264–2271 (2017).

67. Huh, D. et al. Microfabrication of human organs-on-chips. *Nat. Protoc.* **8**, 2135–2157 (2013).

68. Otsu, N. A Threshold Selection Method from Gray-Level Histograms. *IEEE Trans. Syst. Man Cybern.* **9**, 62–66 (1979).

69. McMurdie, P. J. & Holmes, S. phyloseq: An R Package for Reproducible Interactive Analysis and Graphics of Microbiome Census Data. *PLOS ONE* **8**, e61217 (2013).

70. Love, M. I., Huber, W. & Anders, S. Moderated estimation of fold change and dispersion for RNA-seq data with DESeq2. *Genome Biol.* **15**, 550 (2014).

Acknowledgements

This research was supported by the U.S. FDA grant (HHSF223201310079C), DARPA THoR grant (W911NF-16-C-0050), Bill & Melinda Gates Foundation, Wyss Institute for Biologically Inspired Engineering at Harvard University, and Fundação para a Ciência e a Tecnologia (FCT) Portugal (project PD/BD/105774/2014 to the Institute for Bioengineering and Biosciences). We thank D. E. Achatz (PreSens Precision Sensing

GmbH, Germany) for graciously providing oxygen sensing particles and her expert technical advice, and T. Ferrante for his assistance with imaging.

Author contributions

S.J-F., E.L.C., F.S.G, J.M.S.C., R.N. and D.E.I. designed the research. S.J-F, E.L.C., F.S.G., B.N., C.F., A.T., A.B., B.S., and M.C. performed experiments. S.J-F., D.M.C, E.L.C., F.S.G, B.N., D.L.K., R.N. and D.E.I. analysed and interpreted the data. K.E.G helped in preparation of infant microbiota. D.T.B established and prepared human ileal organoids. S.J-F, F.S.G, E.L.C, D.M.C., and D.E.I wrote the paper with input from B.N., O.L., J.M.S.C., and R.N.. The paper has been reviewed, discussed and edited by all authors.

Competing interests

The authors declare competing financial interests: D.E.I. holds equity in Emulate, Inc., consults to the company, and chairs its scientific advisory board.

Additional information

Supplementary information is available for this paper at https://doi.org/10.1038/s41551-01X-XXXX-X.

Reprints and permissions information is available at www.nature.com/reprints.

Correspondence and requests for materials should be addressed to D.E.I.

Publisher's note: Springer Nature remains neutral with regard to jurisdictional claims in published maps and institutional affiliations.

© The Author(s), under exclusive licence to Springer Nature Limited 2019

Supplementary Tables

Supplementary Table 1 | Media tested for microbial diversity

Sample number (Hmb or Mmb)	Media tested*
1	Stock
2	Brain Heart Infusion
3	Brucella
4	GMM[58]
5	Hemin 5 μg/ml
6	Hemin 5 μg/ml, Vitamin K1 0.5 μg/ml
7	Vitamin K10.5 μg/ml
8	Porcine mucin 1 mg/ml
9	Porcine mucin 1 mg/ml, Apple pectin 1 mg/ml
10	Porcine mucin 1 mg/ml, Hemin 5 μg/ml, Vitamin K1 0.5 μg/ml
11	Porcine mucin 1 mg/ml, Hemin 5 μg/ml, apple pectin 1 mg/ml Vitamin K1 0.5 μg/ml
12	Thioglycolate
13	Wilkins-Chalgren
14	YPG Yeast 20 mg/ml, NaCl 5mg/ml, K_2HPO_4 5 mg/ml, Proteose 5 mg/ml, Glucose 5 mg/ml, L-cysteine 1 mg/ml, Hemin 5 μg/ml, Vitamin K1 0.5 μg/ml

*Dissolved in DMEM 20% FBS 1% glutamax

Supplementary Table 2 | Analysis of the diversity of stool microbiome co-cultured in primary Intestine Chips.

Ileum sample (day 5)	Observed richness	Shannon diversity
36 wk infant	122	0.32
36 wk infant	118	0.34
36 wk infant	121	0.31
30 wk infant	135	1.10

Supplementary Figures

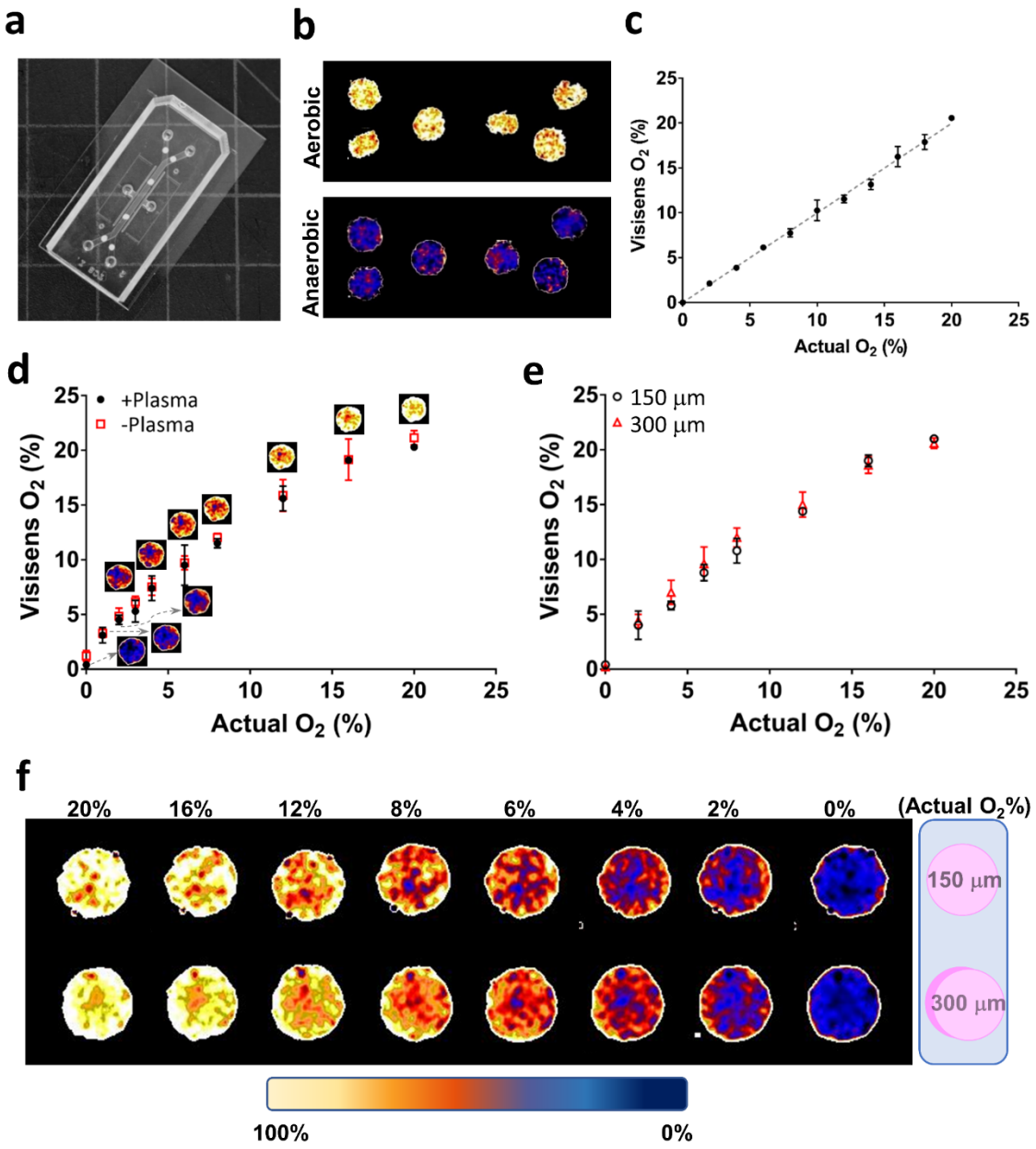

Supplementary Figure 1. (**a**) Representative optical image of an oxygen sensing Intestine Chip and (**b**) pseudocolor image of the Intestine Chip oxygen distribution under aerobic (top, yellow) and anaerobic (bottom, blue) culture conditions. (**c**) Accuracy analysis of oxygen detection by the sensor spots located in the Intestine Chip in response to defined, standard oxygen concentrations. Oxygen levels measured by the Intestine Chip sensor spots were validated by measuring levels before and after plasma treatment (**d**), which altered thickness (150 µm vs. 300 µm) of the spots (**e**). (**f**) Representative pseudocolor images of the spots when varying oxygen concentrations from 20% to 0% oxygen, or aerobic (yellow) to anaerobic (blue) conditions.

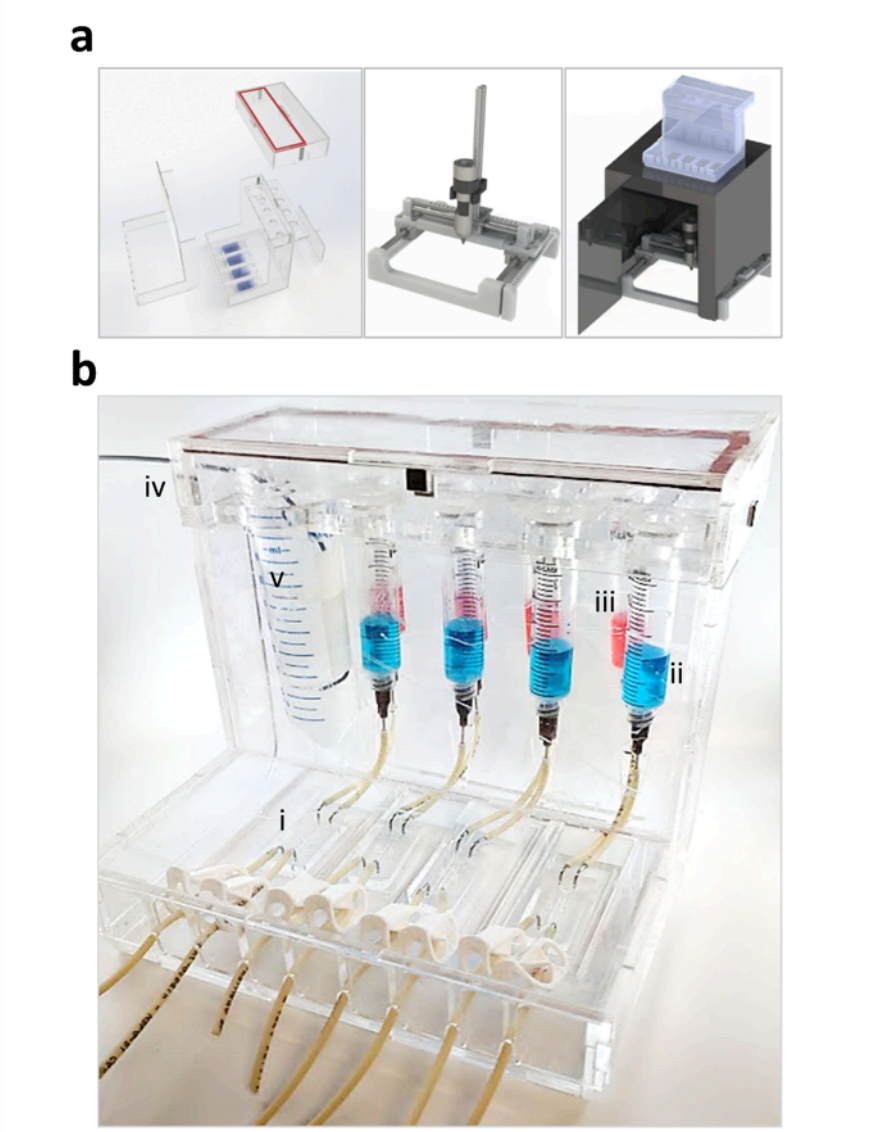

Supplementary Figure 2. (**a**) Exploded views of the anaerobic chamber (left); linear positioning system for indexed motions of the camera to any sensor spot along the chip or between the chips (middle); and rendering of hypoxic farm on imaging stand for monitoring of sensors without removing chips from anaerobic chamber (right). (**b**) Photograph of an anaerobic chamber while in use. Chips (i) are placed in the hypoxic region of the chamber and medium is flowed through epithelial channels (ii, blue) and exposed low to oxygen levels. The medium reservoirs for the vascular channels are placed outside the anaerobic chamber (iii, red) are exposed to room air and thereby, maintained under normoxia conditions. The chamber is purged with N_2 flow (iv) through a bubbler (v).

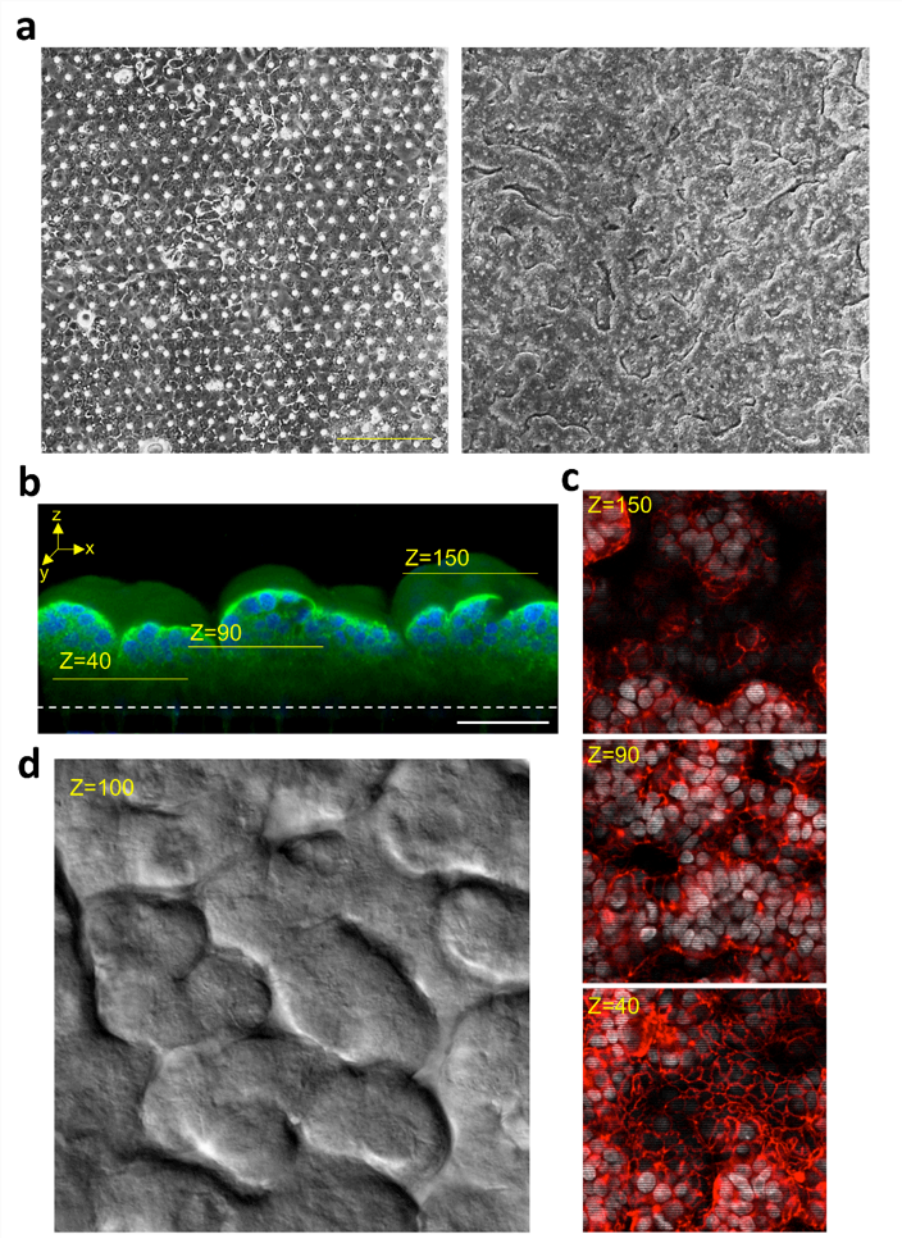

Supplementary Figure 3. (**a**) Phase contrast images of Caco2 epithelium at Day 1 (left) and 7 (right) of culture in the Intestine Chip. (**b**) Representative vertical cross-sectional, confocal micrographic views through the intestinal epithelium-membrane interface of the Intestine Chip at day 7 of culture, when immunostained for villin (green) and nuclei with DAPI (blue) (white dashed lines indicated upper surface of the porous matrix-coated membrane; bar, 100 μm). (**c**) Microscopic views showing the villus morphology of the human Caco-2 intestinal epithelium cultured for 7 days in the Intestine Chip when viewed from above by immunofluorescence staining for the tight junction protein, ZO-1, at different heights or by (**d**) DIC imaging at z=100 μm. (bar, 100 μm).

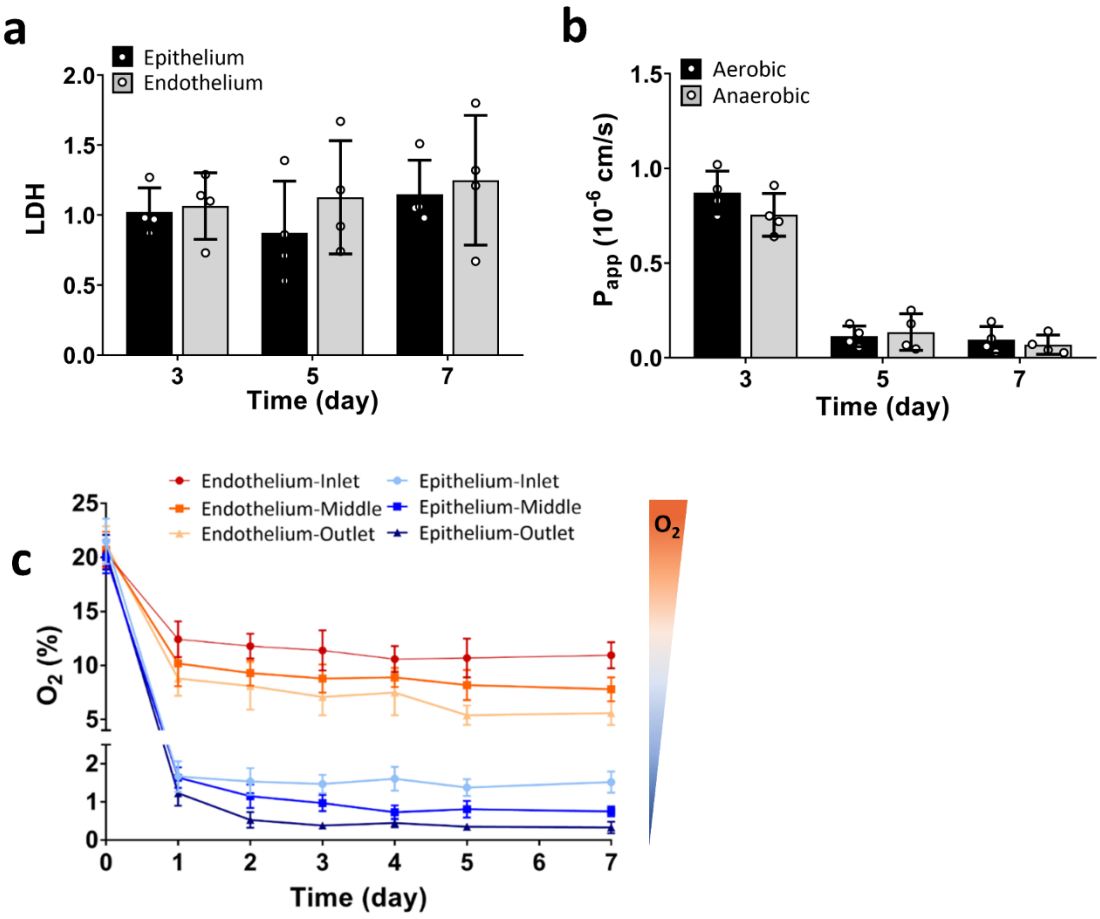

Supplementary Figure 4. (**a**) Graph showing effects of anaerobic culture on viability of intestinal epithelium and vascular endothelium, as assessed by quantifying LDH released from cells (data are presented as fold change in LDH levels relative to the aerobic control chips; n=4). (**b**) Changes in apparent permeability (P_{app}) measured by quantitating cascade blue transport across the tissue-tissue interface within the Intestine Chips cultured aerobically or anaerobically (n=4). (**c**) Radial and longitudinal oxygen profiles within anaerobically-cultured Intestine Chips during 7 days of culture. Schematic colors indicate average oxygen concentration in more aerobic (orange) versus anaerobic (blue) regions of both the epithelial and endothelial channels.

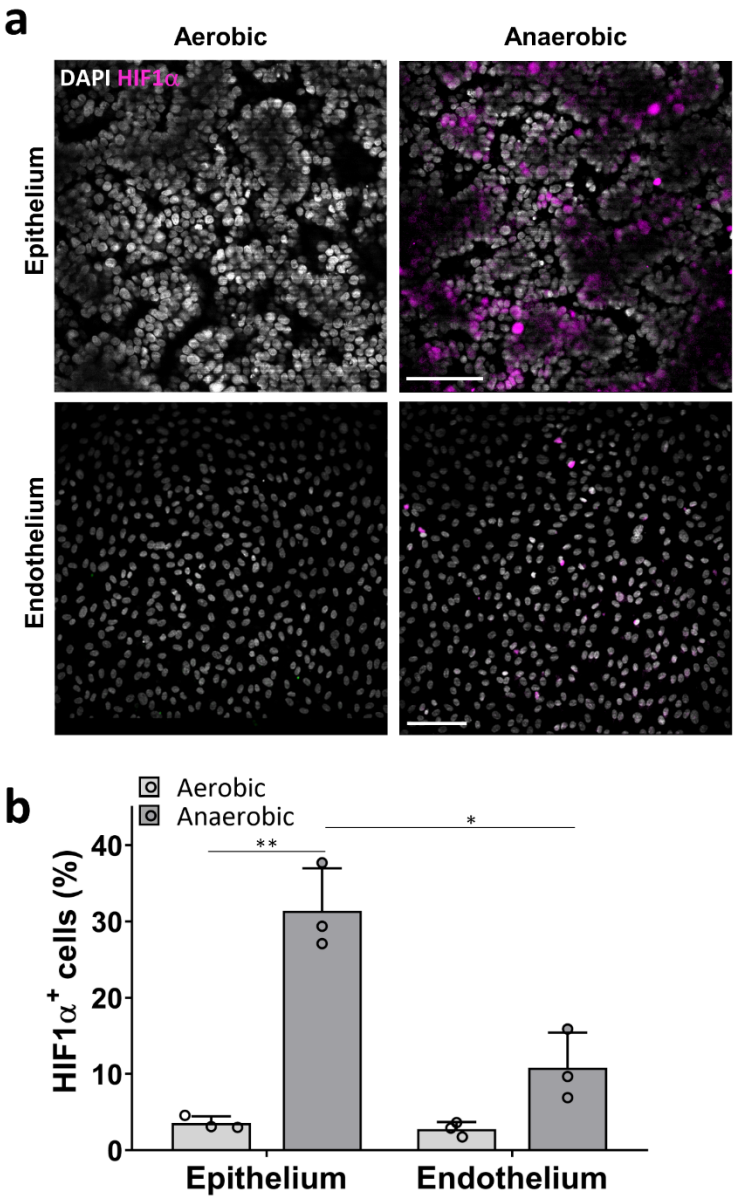

Supplementary Figure 5. (**a**) Representative images (from the middle of the chip) of immunofluorescence staining for nuclei with DAPI (white) and HIF1-α (magenta) in human intestinal epithelial cells and endothelial cells cultured aerobically and anaerobically (bar, 100 μm). (**b**) Graph showing the quantification of the percentage of epithelial and endothelial cells that expressed HIF1-α (HIF1-α^+ cells) after exposure to the conditions shown in **a** (n=3; *, P<0.05; **, P<0.01).

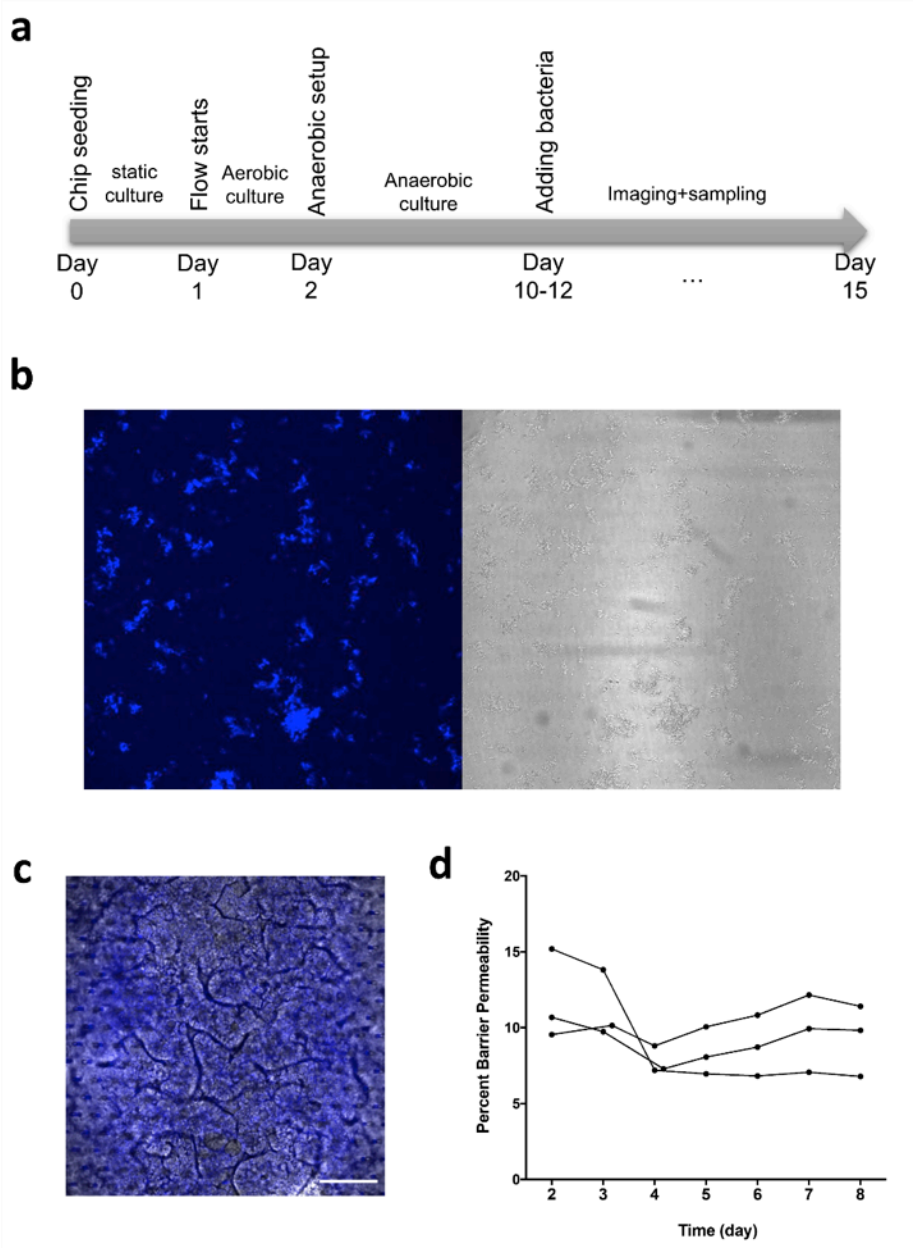

Supplementary Figure 6. (**a**) Diagram of the experimental timeline used for Intestine Chip co-culture studies. (**b**) Fluorescenc microscopic images of *B. fragilis* bacteria labeled with HADA (blue; left) and corresponding brightfield image (right) before they were added to the chips. (**c**) Representative immunofluorescence micrograph with simultaneous phase contrast imaging of a co-culture of HADA-labeled *Bacteroides fragilis* (blue) in the Intestine Chip showing the bacteria distributed over the top surface of the intestinal villi (viewed from above; bar, 50 μm). (**d**) Barrier permeability of Caco2 Intestine Chips cultured with *B. fragilis* under anaerobic conditions measured over time, represented by the percent of Lucifer yellow translocated from the apical channel. This panel represents data from 3 independent chip experiments normalized relative to control bacteria-free chip cultures.

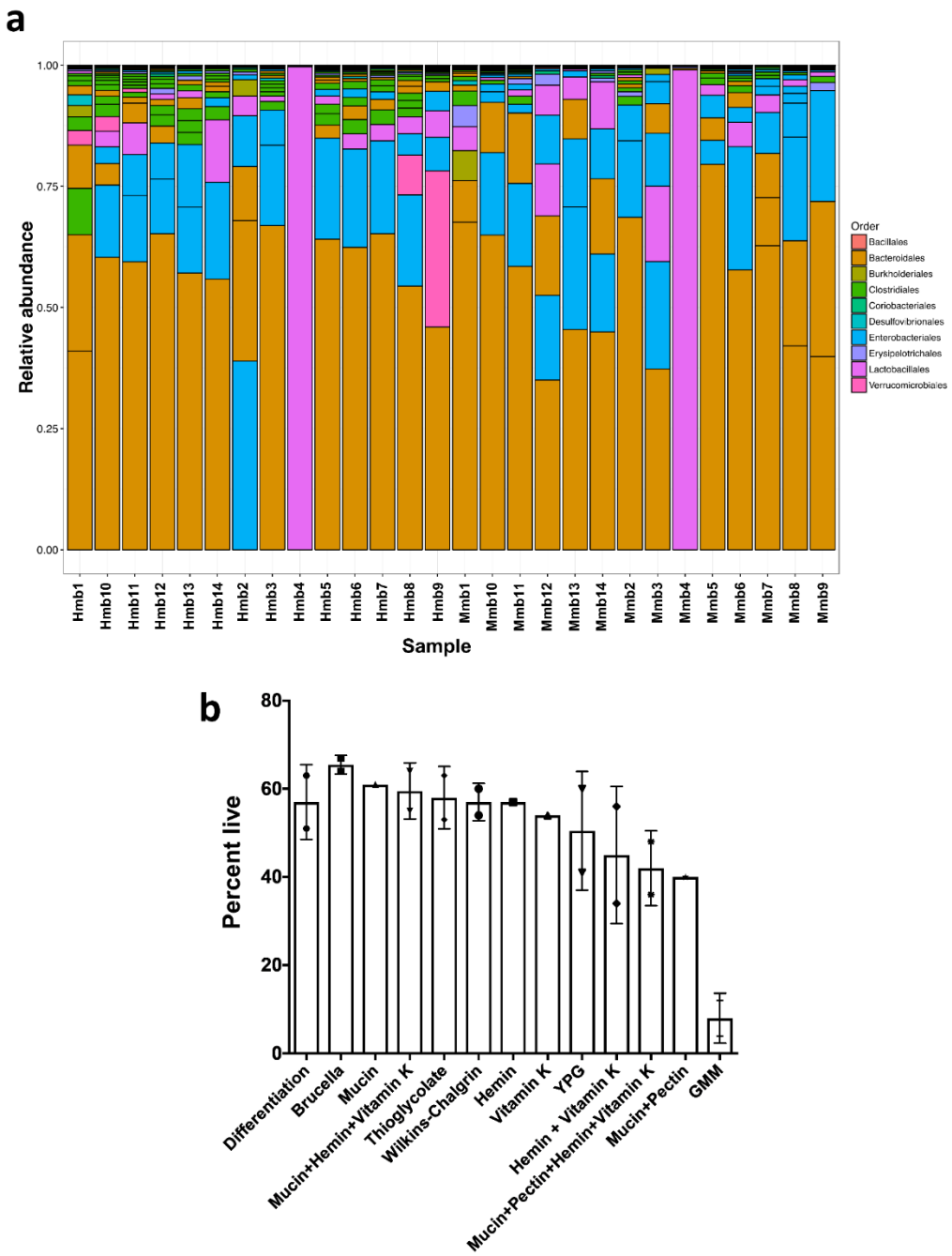

Supplementary Figure 7. (**a**) Relative abundance of identified OTUs of Hmb stock cultured in 13 different medium conditions, summarized to Phylum level. (**b**) Caco-2 viability in 13 different types of medium used for defining optimized growth of the human gut microbiome (see **Supplementary Table 1** for the composition of the various culture media tested).

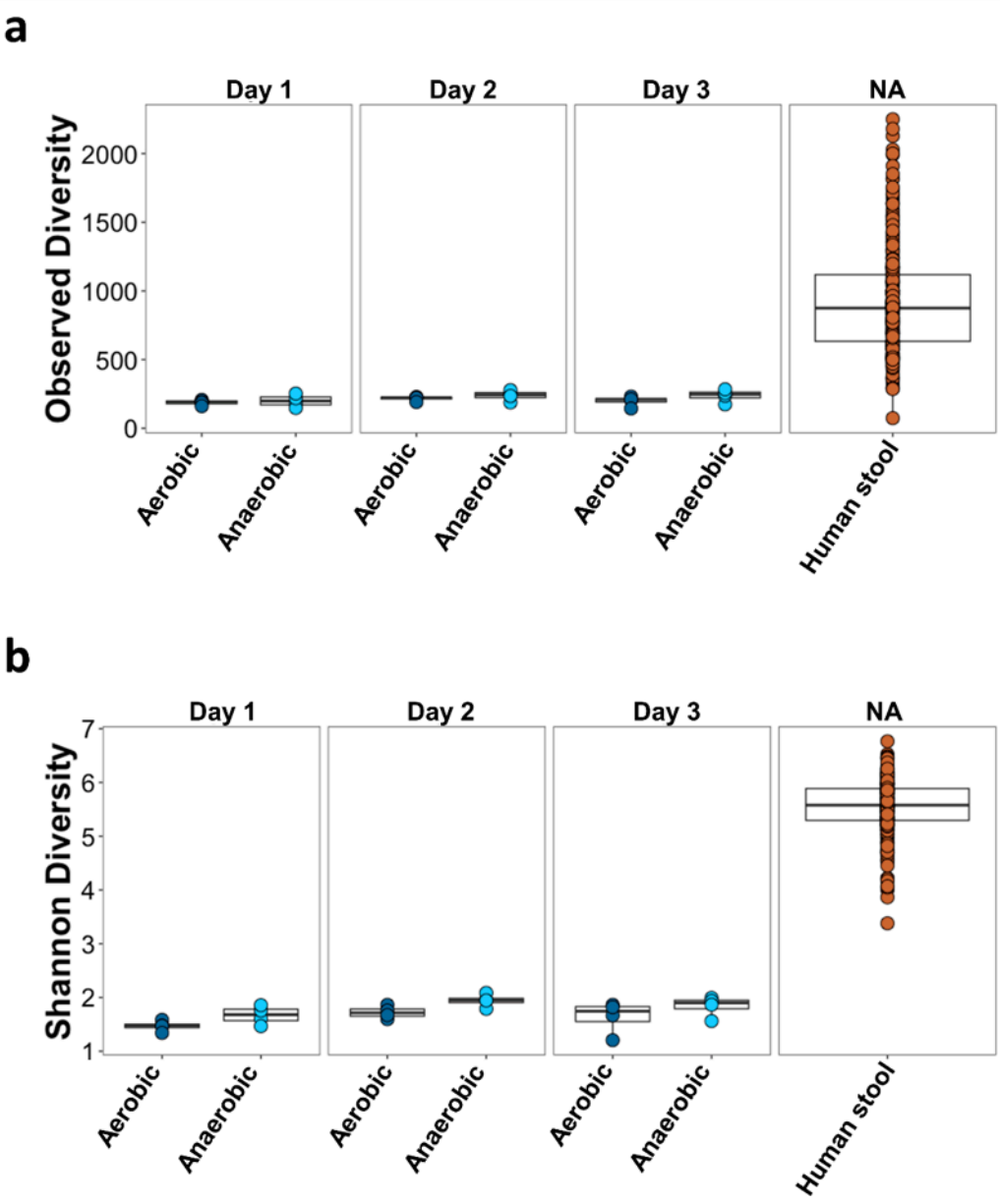

Supplementary Figure 8. (**a**) Observed alpha diversity (richness) and (**b**) Shannon diversity between the Intestine-Chip samples on either condition and the human microbiome stool sample (from HMP).

a

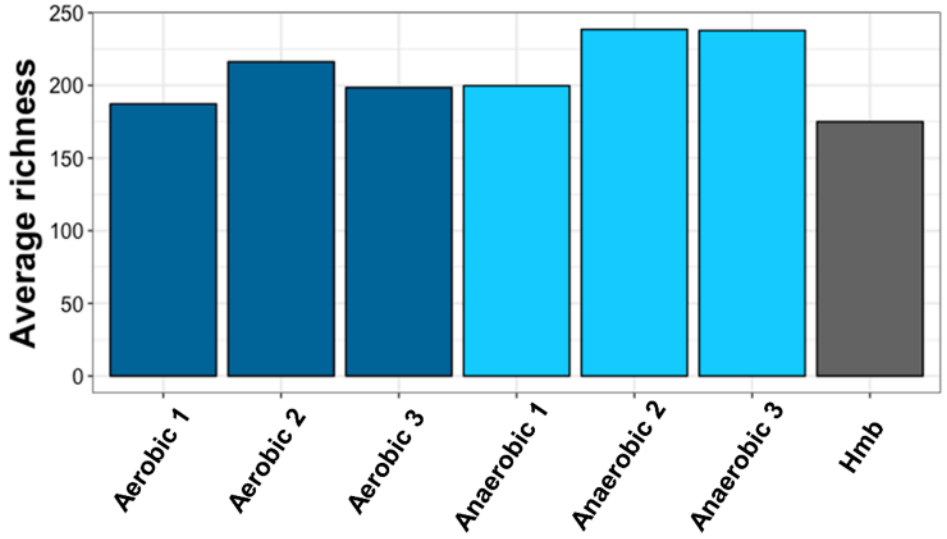

b

Sample	Mean	SD
Starting culture	175	NA
Aerobic, day 1	187	19.7
Aerobic, day 2	216	17.1
Aerobic, day 3	198	37.7
Anaerobic, day 1	200	45.9
Anaerobic, day 2	238	38
Anaerobic, day 3	238	46.7

Supplementary Figure 9. (**a**) Observed alpha diversity (richness) for the aerobic or anaerobic chips, as well as the original (starter) microbiome culture. (**b**) Table shows the mean and standard deviation of this population richness metric across all groups.

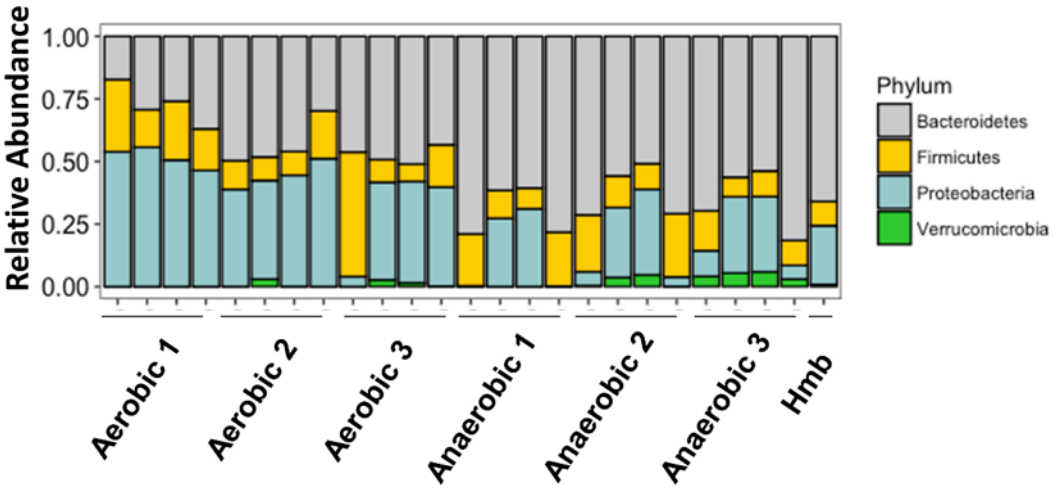

Suplementary Figure 10. Relative abundance of identified OTUs under aerobic or anaerobic conditions, summarized to Phylum level. The 4 bars presented for each of the 3 replicates cultured under aerobic or anaerobic conditions represent results at days 0, 1, 2 and 3 days of culture (left to right, respectively); Hmb stock indicates phyla abundance in the complex microbiome stock at time 0.

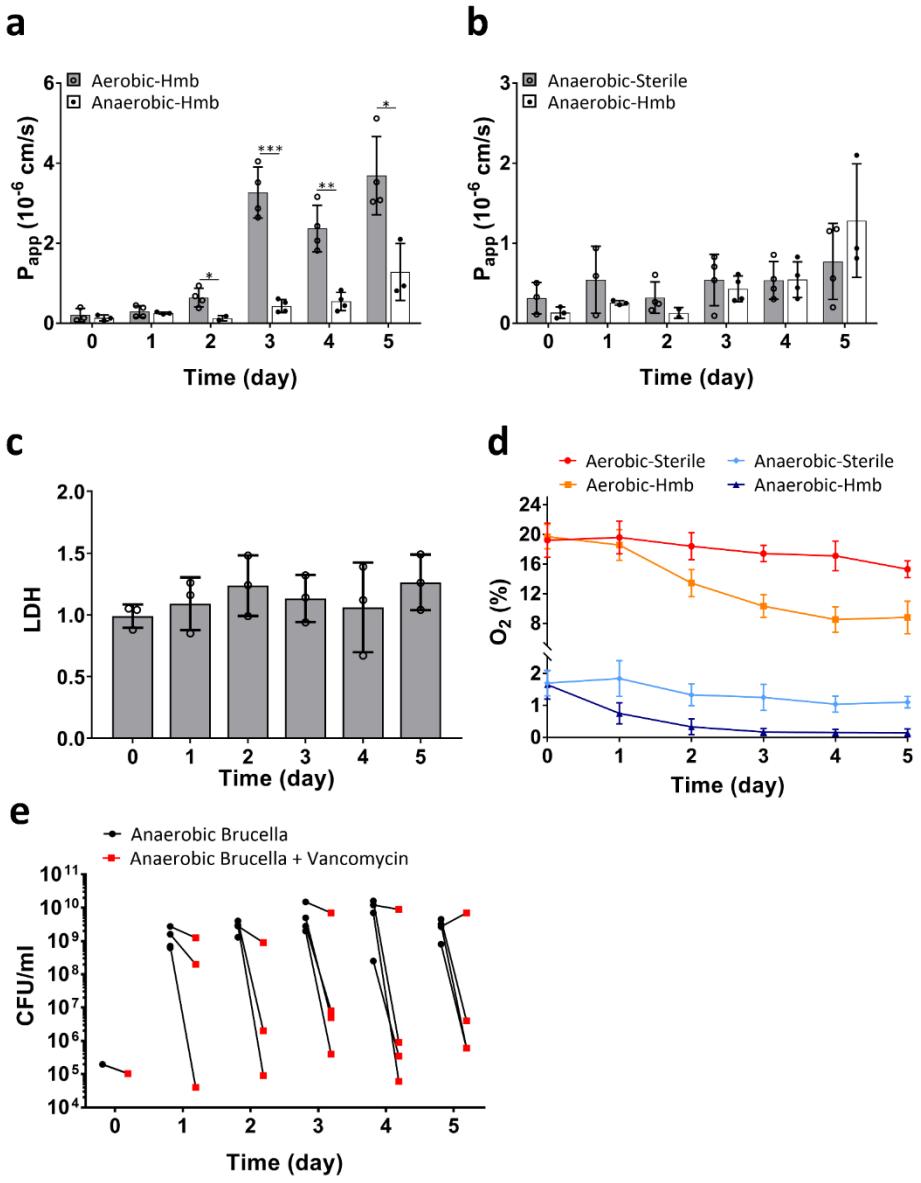

Supplementary Figure 11. Changes in apparent paracellular permeability (Papp) measured by quantifying cascade blue transport across the tissue-tissue interface within aerobic or anaerobic Intestine Chips co-cultured for 1 to 5 days with complex Hmb gut microbiome (**a**) or over a similar timecourse in anaerobic Intestine Chips cultured with or without (sterile) microbiome (**b**) (n=4; *P<0.05, **<0.01, ***P<0.001). (**c**) Graph showing effects of complex microbiome co-culture on viability of intestinal epithelium, as assessed by quantifying LDH released from cells (data are presented as fold change in LDH levels relative to the sterile control chips; n=3). (**d**) Oxygen concentration profiles measured in sterile aerobic and anaerobic Intestine Chips and similar Intestine Chips co-cultured with complex microbiome for 5 days. (**e**) CFU/ ml measured within effluent samples flushed from the epithelial microchannel anaerobic chips, as determined by plating serial dilutions on Brucella culture plates in the presence or absence of vancomycin and grown in the anaerobic chamber at 37°C.

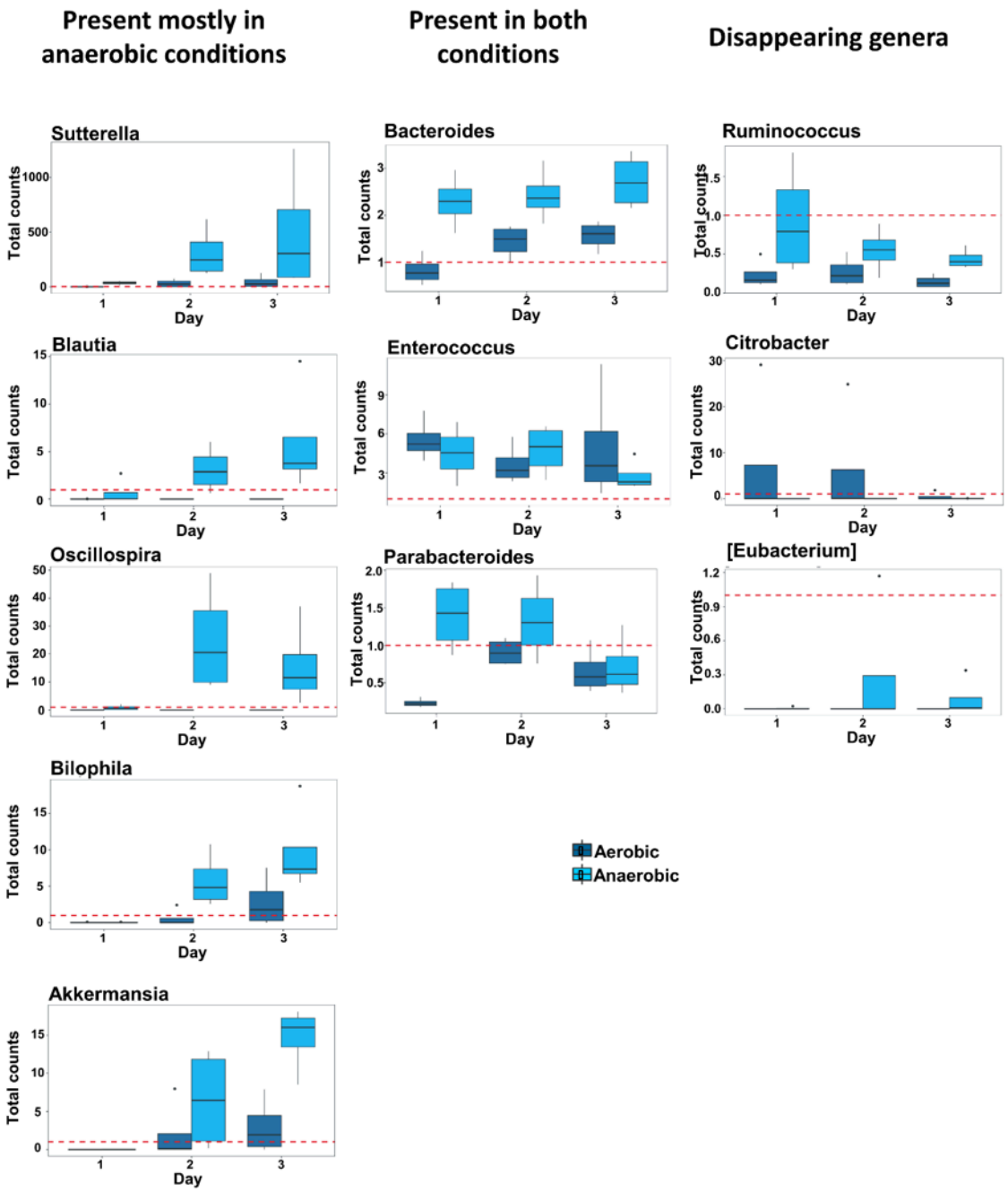

Supplementary Figure 12. Total counts of genera detected in Caco2 Intestine Chips over 1 to 3 days of co-culture with Hmb microbiome. For comparison, the dashed red line represents the number of counts identified in the anaerobic liquid culture sample.

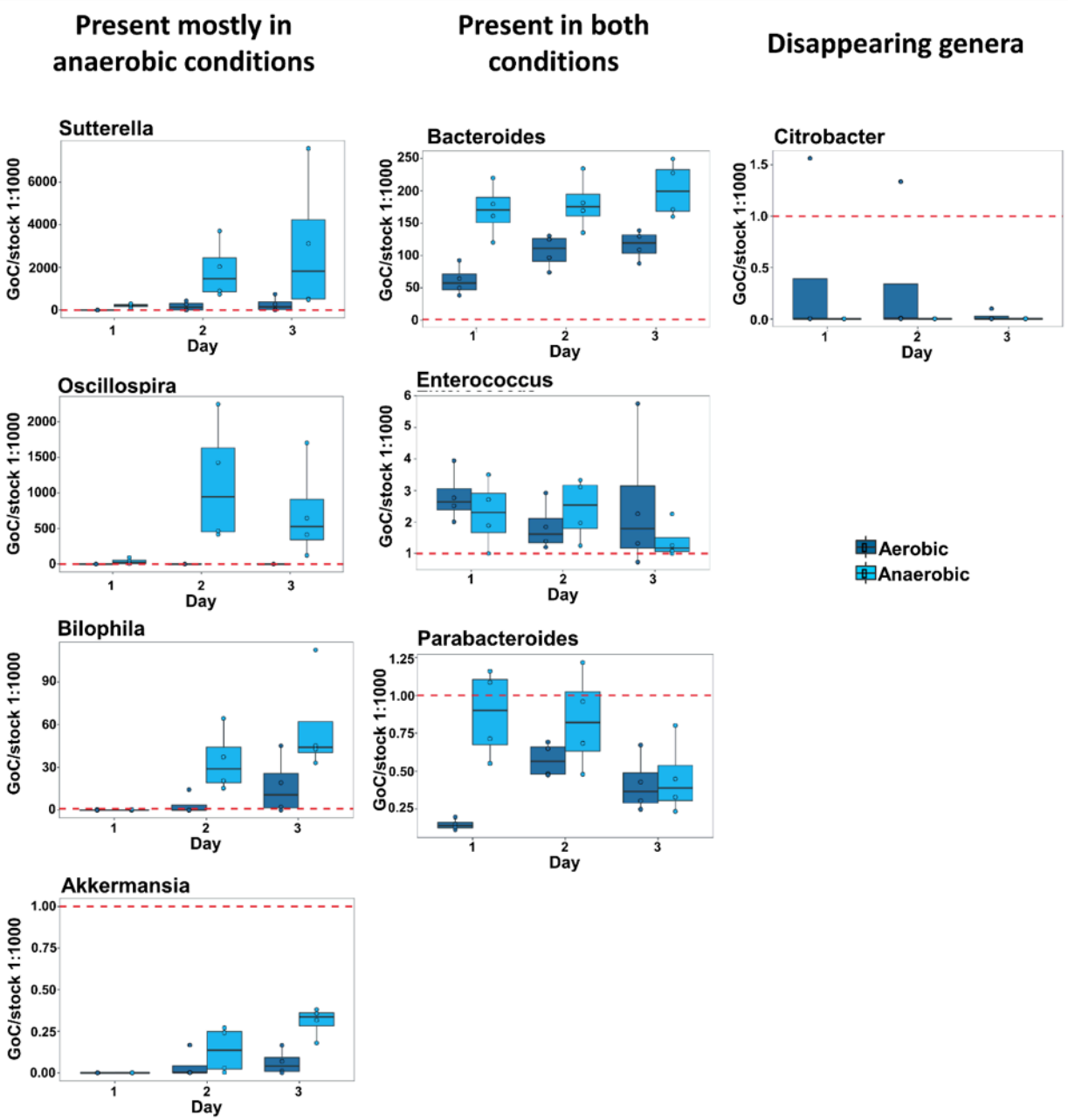

Supplementary Figure 13. Normalized counts of genera detected the in Intestine Chips over 1 to 3 days of co-culture with microbiome, compared to the starting human Hmb microbiome stock. The counts measured in both the aerobic and anaerobic chips are normalized to the total number of reads of that genus in the human stock. The dashed red line represents the normalized counts for the human stock. When a genus is not present in the stock, its line is set to 0 and the plot represents total counts of the genus in the chips.

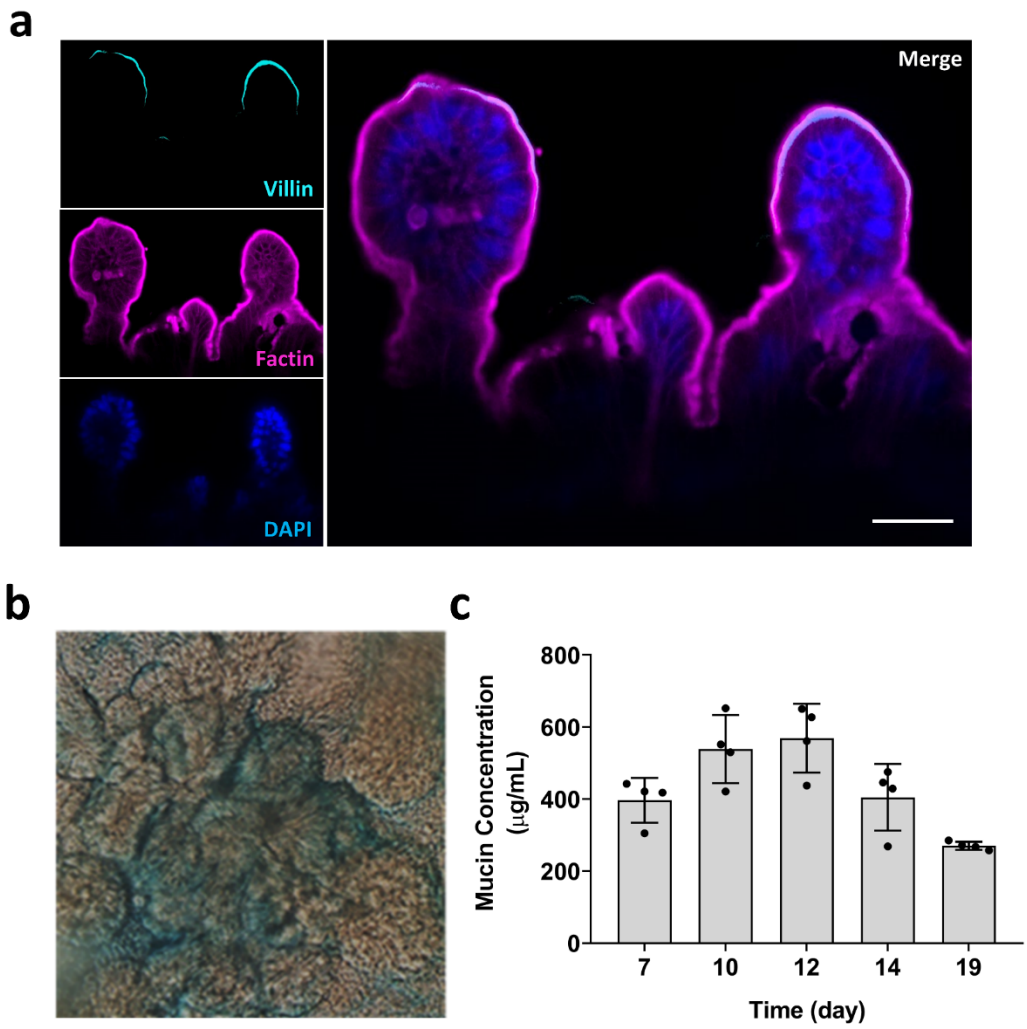

Supplementary Figure 14. (**a**) Confocal fluorescence microscopic views showing the villus morphology of the primary ileal epithelium stained for villin (cyan), F-actin (magenta) and DAPI (blue) (bar, 50μm). (**b**) Phase contrast views of ileum chips stained with alcian blue. (**c**) Quantitation of alcian blue staining in cultures shown in **b**.

V. Chapter 5

Conclusions and Future Directions

Exposure to ionizing γ-radiation, whether therapeutic or accidental, may result in acute radiation syndrome that is associated with potentially life-threatening gastrointestinal disturbances. As exposing healthy people to radiation for clinical trials would be unethical, efforts to identify mechanisms underlying radiation damage or drugs that can mitigate the effects of radiation exposure have been limited to animal studies, which are notoriously poor predictors of how a given drug will behave in humans. Ethical issues related to animal high-dose radiation exposure also present a considerable hurdle, particularly when it relates to studies on primates. As a result, the mechanisms underlying the radiation-induced gastrointestinal syndrome remain unclear, and this represents a major challenge with regards to discovery of new medical countermeasure drugs (MCMs). Understanding of radiation-induced intestinal injury could be greatly facilitated by the availability of experimental *in vitro* models that recapitulate human cell and tissue responses to radiation; unfortunately, this has not been possible using existing culture systems as they limited in mimicking the complexity of human intestine.

Using Intestine Chip microfluidic culture system, we developed a model of the gut lined by human intestinal epithelium interfaced with vascular endothelum, which simulated radiation-induced intestinal injury at a radiation dose of 8 Gray (Gy), which is known to cause gastrointestinal effects in humans. We observed increases in several markers of cell damage in both the endothelium and epithelium. These included increased apoptosis, generation of reactive oxygen species (ROS), double-stranded DNA breaks, degradation of membrane lipids, and loss of microvilli structure, as well as disruption of cell-cell junctions that form the barrier that protects the intestinal wall from bacteria and toxins. While intestinal stem cells have always been assumed to be the major mediator

of intestinal radiation damage, recent studies suggest that apoptosis within the microvascular endothelium may be a key mediator of radiation damage that, in turn, leads to stem cell dysfunction. So, unlike past radiation models, we incorporated vascular endothelium in the Intestine Chip to unravel the role of endothelial cells in radiation response. We showed that the endothelial cells in the vascular channel exhibited a stronger response to radiation than the epithelial cells in terms of ROS generation, lipid degradation, DNA fragmentation and apoptosis. Interestingly, when we repeated the on-chip experiments without endothelial cells, irradiated intestinal cells did not express their typical response to radiation, suggesting that endothelial cells serve as mediators of radiation-induced intestinal dysfunction. We also validated a potential radioprotective drug, dimethyloxaloylglycine (DMOG) for the first time *in vitro*. We confirmed that DMOG significantly reduced apoptosis, intestinal permeability, and microvillus injury of intestinal epithelial cells, as well as ROS generation and lipid degradation in both endothelium and intestinal epithelium, a result that has never been demonstrated in previous experimental models. While Caco-2 Intestine Chip can recapitulate many features of the human ileum, since it is a tumor cell line it might differ in sensitivity to radiation. So we recapitulated radiation-induced intestinal injury using human primary Intestine Chip with cells isolated from patient biopsies. This approach provides us with the opportunity to evaluate patient-specific responses to radiation as well.

Commensal microbiome that are present within the intestinal microenvironment are believed to play a pivotal role in intestinal radiation toxicity *in vivo*, yet no method is available to sustain these complex microbial communities in direct contact with living

human intestinal cells for more than a few hours to a day *in vitro*. To recapitulate human host-microbiome interactions on-chip, we recently developed methods to co-culture of living human intestinal epithelium in Organ Chips in direct contact with stable communities of aerobic and anaerobic microbiota derived from human stool specimens under a hypoxia gradient similar to that observed *in vivo*. Our model accurately recapitulates *in vivo* behaviors, including the maintenance of an abundance of obligate anaerobic bacteria with ratios of Firmicutes and Bacteroidetes similar to those observed in human feces. Although we did not study the effects of radiation on intestinal epithelium and endothelium in presence of human complex microbiome, our model could be harnessed to unravel functional links between intestinal epithelial cells and gut microbes to understand mechanisms of human radiation disease, discover new MCMs, and advance personalized medicine to save lives of cancer patients, astronauts, or civilians who are accidentally exposed to radiation.

In summary, we believe that human Intestine Chip model, comprising human intestinal epithelium, endothelium and complex microbiome, offers a potentially powerful tool for studying the mechanisms that underlie radiation-induced injury in humans, and that it offers a way to recapitulate human-level responses far better than any animal model.